Project JKM 5A11:

Renewable Energy Applications

A Major Qualifying Project

Submitted to the Faculty

of

WORCESTER POLYTECHNIC INSTITUTE

in partial fulfillment of the requirements for the

Degree of Bachelor of Science

in Electrical and Computer Engineering

by

Anthony Ducimo

Kurt Snieckus

Nathaniel VerLee

Date: April 13, 2012

Approved:

Professor John A. McNeill

Abstract

Sustainability is a widely discussed topic in engineering disciplines with the concept of renewable energy often serving as a focal point. The desire of many is to arrive at an optimal solution for the accumulation and distribution of renewable energy sources. When considering solar amongst the many resources for energy production there are many different hardware options that can be tested for their ability to transduce sunlight into electrical power or in their efficiency in converting electrical power for storage. A solar energy harvesting board was designed and built for efficiently collecting and storing energy in batteries, with an emphasis placed on measurement and testing capabilities. The final product allows for maximum power extraction from solar panels up to 250W, implementation of battery management algorithms, and may work in tandem with other units to charge battery banks. The system will serve as a foundation for hardware testing and future solar energy projects at WPI. By developing accurate measurement circuitry and power converter topologies, variances in solar panel and converter designs can be scrutinized while providing data about the system's energy flow. Recorded data can be utilized to infer which hardware configuration offers the best solution and study system performance based on meteorological conditions.

Executive Summary

The original focus of this project was to create a system to be featured in the lobby of Atwater Kent as a "21st Century Power Panel" to augment or supplement the old power panel originally installed in the lounge. After the existing power panel was moved to a new location, there was much consideration over what type of a system should be installed and what the project should focus on. Many different ideas were discussed, including wind and solar energy sources, systems for storing and displaying renewable energy data, a renewable energy site surveying device for determining the feasibility of a renewable energy system, repurposing and reusing currently available resources, and the installation of new renewable energy sources. Existing installations on the roof were surveyed and previous research and reports were considered for their findings. A cost and benefit analysis of each of the possible options was conducted. Ultimately, it was determined that the wind turbine was a poor resource and that the installation of solar panels and an appropriately designed power system for the panels was the best option.

After making the decision to construct a solar energy system, discussion of design of the system and then location for the panels began. Through Professor Looft, the ECE department head, contact was made with Jim Dunn, who runs a business called Future Solar LCC. The team discussed with Jim how different panels have different behaviors and characteristics such as their response to temperature, direct versus indirect sunlight, performance over age and so on. Jim offered ideas and donated six solar panels of three different models so the team could compare different kinds of technologies.

Atwater Kent was surveyed for the best roof site with a tool called a solar pathfinder that provides a shade analysis of buildings and trees conflicting with a particular site. The central area of the roof was picked as the best location. Two of the six panels are currently placed on the roof and ballasted with ballast pans that hold the panels down with paver stones. The pans are placed on top of non-slip mats to help prevent the pans from moving and from damaging the roofing material if they do shift. Additional ballast pans and solar panels are available to groups for future experimentation and research. Over the course of the winter and spring, the setup was surveyed occasionally and no obvious hazards arose.

The core of the project was a system that would take energy from the solar panels and use it to charge batteries and drive DC loads such as lighting, radios, computer systems, and sensors. The basic solar energy harvester has a DC input from the solar panels and a DC output to a battery. Voltage and current are measured at both the input and the output, and a converter between the input and the output allows the voltage to be stepped down. Loads can be connected to the battery through a mechanism to protect from overcurrent and shut off the load if the battery is depleted. Because solar panels have a unique V-I characteristic, specific power electronics and control algorithms are needed to extract power from a solar panel at its maximum potential, known as the maximum power point. This power point is a dynamic point of the V-I curve that must be determined by making changes in the systems and then measuring how those changes affect the power extraction. The point can be affected by the amount of sunlight and the ambient temperature. In order to operate at the power point, voltage and current are measured on the input side of the system. Voltage and current measurement on the output side determines the state of charge of the batteries. The efficiency of the system can be determined using both the input and output measurements.

System architecture, voltage measurement, current measurement, and converter topologies needed were discussed in detail. Precise current and voltage measurements were necessary to measure the efficiency of the converter effectively. The system was designed to handle in excess of 230W, 45V, and 9A to take input from all three different types of panels. A Hall Effect sensor was chosen to measure current, a differential amplifier was chosen to measure voltage, and a buck converter was chosen as the converter topology. A 16-bit ADC was used to digitize the measurements and an MSP430 was chosen to be the system's microcontroller. After producing and testing a first revision of the populated printed circuit board with the aforementioned hardware, a second revision was created that included 12V, 5V, 3.3V, and -5V rails in order to power all parts of the system. The rails can derive power either from the system battery itself or from and external source. I2C and RS232 isolated communication ports were also added so that multiple harvesters could communicate with each other to work together and with a computer for collecting data and information.

The completed product is a highly integrated piece of hardware that can serve many purposes on both the experimental level as well as in real world applications. The board is engineered for precise measurements in order to allow its users to make better assessments of the efficiency of the system. It is designed to be connected to a computer and allow for collection of data over time to study trends and performance. The system can also function on its own in real world applications such as providing renewable energy lighting or power in developing nations, energy harvesting for solar vehicles, or power for instrumentation or radios in remote, inaccessible locations. This hardware ultimately represents a body of work that will enable future projects at WPI to continue to make strides in innovation and address and study issues in the solar renewable energy field.

Contents

Figures

Tables

1 Introduction

The primary objective was to develop a "21st Century Power Panel," to supplant the 1800s era power panel on display in the Atwater Kent (AK) Laboratories lobby on the Worcester Polytechnic Institute (WPI) campus. The project as originally proposed to applicants was to develop a system to harness wind and/or solar energy and display information about the renewable energy generated. The system concept was to include an interactive control and include display of data about the power consumption both alongside the "power panel" and on the World Wide Web.

1.1 Report Overview

Initial research included reviewing available resources, previous MQPs and Interactive Qualifying Projects (IQPs) related to renewable energy harvesting. Ideas were developed into eight different project elements that posed an intellectual challenge and then combined to produce a system level design. Elements were grouped into three different possible MQP opportunities and the advantages and disadvantages of each were compared. After meeting with the project advisor, Professor John McNeill, and the Electrical and Computer Engineering (ECE) Department Head, Professor Fred Looft, a consensus on which project opportunity to pursue was reached.

1.2 Existing Resources

In 2008, a SWIFT Wind Energy System was donated and installed on Atwater Kent Laboratories by National Grid, a local electrical utility company. The intentions of the ECE Department faculty were that the turbine would foster more renewable energy research. Several projects have since been conducted related to its use.

1.3 Previous WPI Projects

Prior to this project, several MQPs and IQPs were conducted in the domain of renewable energy. These projects focused on monitoring potential locations for renewable energy harvesting, the instrumentation of renewable energy systems, and monitoring power consumption of various campus locations. Each of these previous projects set out to complete one or more of the tasks defined in this project. This project to be proposed intends to build on these outcomes of these previous projects.

Photovoltaization of WPI

This IQP studied various locations on the WPI campus and assessed the feasibility and potential output of a solar panel installation at each location [**1**]. This IQP was valuable for the development and installation of monitoring units that measure the wind and solar irradiance characteristics of potential locations.

Instrumentation of the Atwater Kent Wind Turbine

Upon completion of this MQP, a peripheral system to monitor and use the power output of the Swift Wind Energy System installed on the Atwater Kent roof was developed. The project disconnected the turbine from the grid-tie inverter and instead used the power output from turbine to charge batteries. The project also included voltage and current monitoring on the turbine output and made these measurements available on the ECE department webpage [**2**].

Monitoring Electricity Consumption on the WPI Campus

The intention of this IQP was to characterize the current power consumption monitoring capabilities in place on the WPI campus. It also suggested new solutions to upgrade the current system. Because the power metering equipment on the WPI campus was incomplete, the report included energy consumption information of only certain buildings on campus. Group members also recommended the installation of a data collection system to monitor all campus buildings, citing several other campuses having installed such systems and reporting significant reduction in energy usage as a direct resultant [**3**].

2 Project Conceptualization

Initially the definition of the MQP was flexible, that is, one of the major goals was to define project outcomes. With many areas of focus within the renewable energy umbrella, the three major categories were explored: system installation/integration, energy auditing, and renewable energy hardware. Additional subcategories were investigated, defined and discussed. It was then decided to combine these project elements into three pursuable MQPs.

2.1 Project Elements

When developing ideas for this project, they were viewed as building blocks of a renewable energy system. For this reason the ideas are presented as project elements, several of which would comprise a renewable energy system suitable for development by an MQP. Furthermore, these ideas were developed under the impression that collaboration would take place with another MQP team who would also be contributing project elements for an eventual system. The following details the eight final ideas developed.

2.1.1 Solar Energy System

The goals of this element were to install and instrument solar panels atop AK, with capabilities of driving a load and monitoring the energy production. A block diagram of this system can be seen in Figure 1.

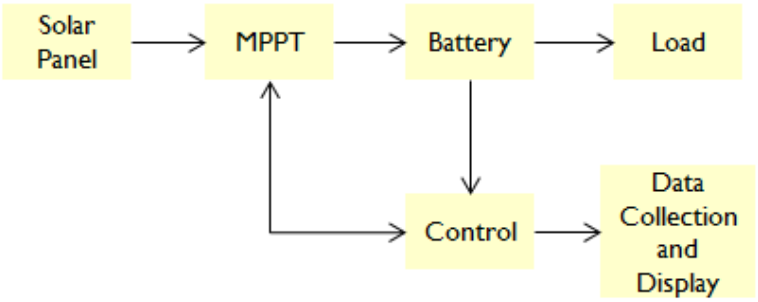

FIGURE 1: SOLAR ENERGY SYSTEM BLOCK DIAGRAM

This project component would involve the purchase or donation of suitable solar panels, installation of the solar panels on the roof of Atwater Kent, the development of a maximum power point tracking (MPPT) converter to extract the maximum amount of power out of the solar panels and the measurement of the power consumption from the panels. The preliminary cost estimate of this system was based in the thousands of dollars. Existing resources for this project include lead acid batteries and a previous MQP involving the development of an MPPT system. Considerations for this project would involve obtaining funding, mounting the solar panels, evaluating the effectiveness of solar panels on the roof of AK, and the installation of wiring to power any loads within AK.

2.1.2 Wind Turbine Relocation

Because the wind turbine (as installed at the time of this report) was not generating an appreciable amount of energy, the goal of this project idea was to move the existing wind turbine to a location with an appreciable amount of wind. A block diagram of the system associated with the wind turbine is depicted in Figure 2.

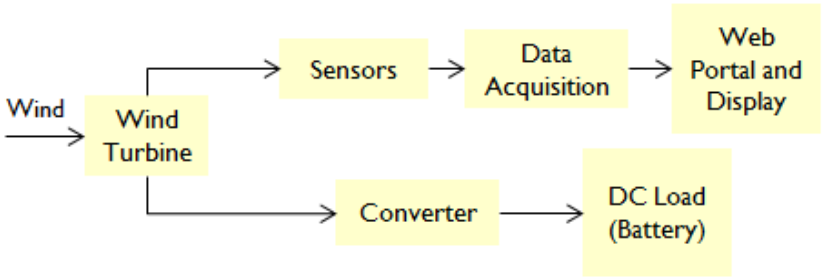

FIGURE 2: WIND TURBINE BLOCK DIAGRAM

This block diagram was adopted from the Instrumentation of the Atwater Kent Wind Turbine project **[2]**. This project idea proposed that the entire system be moved to another location after monitoring various locations for wind characteristics. A new monitoring system would also be implemented on the relocated turbine so that the amount of power generated could be displayed.

A rough cost estimate of this project was based in the thousands of dollars, aside from the cost of resources to move the turbine along with other project components required to create a system display interface. Some concerns with this project involved WPI policy regulations, building codes, and zoning laws governing the movement of the turbine to an ideal location. Other considerations would have to be made when deciding on an adequate period to monitor prospective locations and finally pooling resources needed to move the wind turbine.

2.1.3 Hybrid Source Energy System

The goal of this idea was to interface multiple renewable energy systems with one another to drive various AC and DC loads while meeting safety regulations. Figure 3 depicts the block diagram of this system.

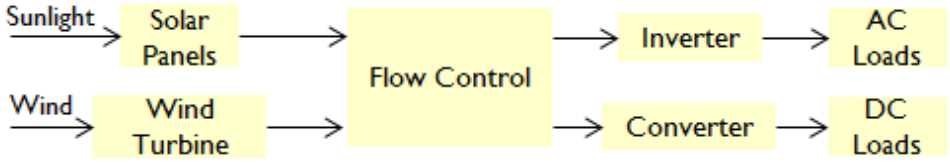

FIGURE 3: HYBRID SOURCE ENERGY SYSTEM BLOCK DIAGRAM

This system would involve developing a unit to combine the power outputs of solar and wind renewable energy systems, and use the combined power to drive one or more AC or DC loads using a control system to allow the power from both sources to be used simultaneously.

The estimated cost of this project was based in the hundreds of dollars. Available resources included lead acid batteries to implement as an energy storage device, previous MQP designs of a battery charge controller, the wind turbine and inverter unit. Some considerations included the installation of wiring to drive intended loads and the design of a module for different sizes and types of renewable energy systems.

2.1.4 Universal Grid Tie

Similar to the previous project idea, the goal of this project was to develop a system that could combine the outputs of multiple renewable energy sources and deliver that energy to the electrical distribution grid while meeting standard safety regulations for grid connections and grid connected equipment. A block diagram for this idea can be seen in Figure 4.

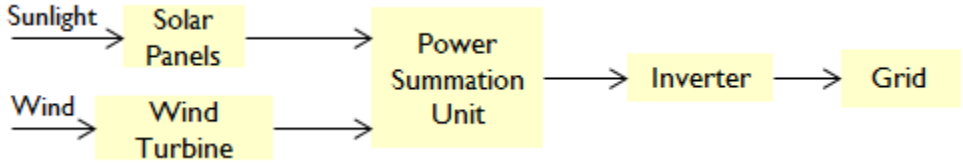

FIGURE 4: UNIVERSAL GRID TIE BLOCK DIAGRAM

This system would combine the power generated by solar and wind renewable energy systems, invert the DC to AC and deliver the power to the grid.

The cost of this idea was estimated to be in the hundreds of dollars. Previous MQP reports document example AC inverter designs that can be used in the development of such a system. It was also found that a design has been previously developed for a universal grid interface [**4**]. Considerations for this project involved the installation of electrical conduits if necessary and sizing the system for different renewable energy systems as well as regulations and codes associated with grid-tie systems.

2.1.5 AK Energy Monitoring

The system intended to monitor the energy consumed by the entire Atwater Kent building or individual distribution systems within AK and provide this information for display. A system block diagram of this idea is depicted in Figure 5.

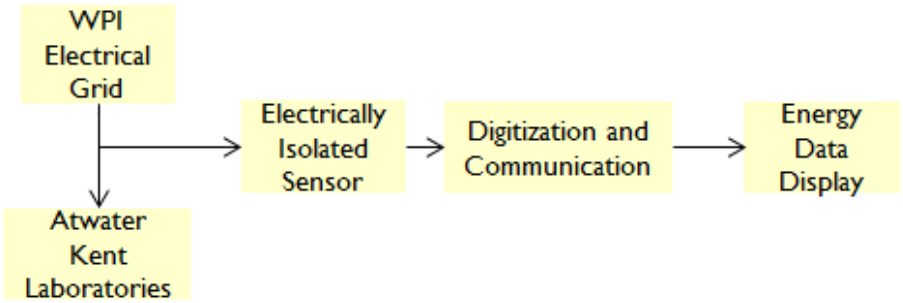

FIGURE 5: AK ENERGY MONITORING SYSTEM BLOCK DIAGRAM

This idea involved developing a system to measure one or more power distribution points in AK. The devices would be designed to be electrically safe and non-invasive to allow for service of the distribution system when required. These measurements would then be stored and displayed by to the public by another system.

The cost of this idea was estimated to be within hundreds of dollars. Considerations for this project would involve working with WPI electricians regarding the installation of the monitoring devices and the necessary communications system to get the monitoring data to a display system.

2.1.6 Energy Data Display

The endeavor constituted the development of a flexible system to display real-time data and information about potential and current renewable energy generation systems as well as energy consumption on the WPI campus. This display system would be located in the Atwater Kent Laboratories lobby as well as be available on the World Wide Web and would display the collected energy generation and consumption data to the public in an interactive and understandable manner. Figure 6 depicts the block diagram for this system.

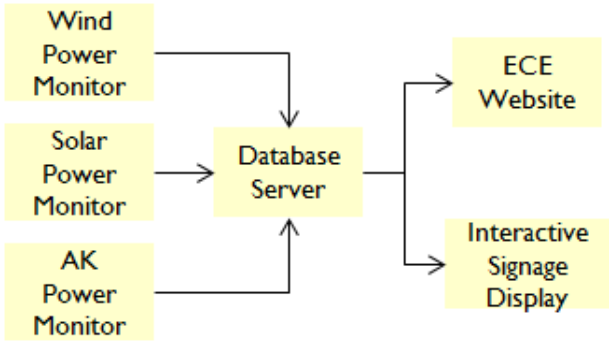

FIGURE 6: ENERGY DATA DISPLAY SYSTEM BLOCK DIAGRAM

This system would monitor the energy outputs of the wind turbine and a prospective solar system along with the energy being delivered to loads within AK. The data collected would be sent to a database server and then displayed on both the ECE website and an LCD display in the building.

The cost range of this project was estimated to be within the range of hundreds of dollars. Existing resources included an LCD display, a department hosted website, a spare computer for data storage, and existing energy data resultant of previous MQPs. One thing to consider when executing this project would be the achievement of a critical mass of data.

2.1.7 Energy Usage Exhibit

The goal of this concept was to develop a museum style exhibit related to the energy production of a renewable energy system. A concept diagram of the exhibit design is shown in Figure 7. Upon user interaction, the exhibit would equate the energy produced by a renewable energy system over several different lapses in time.

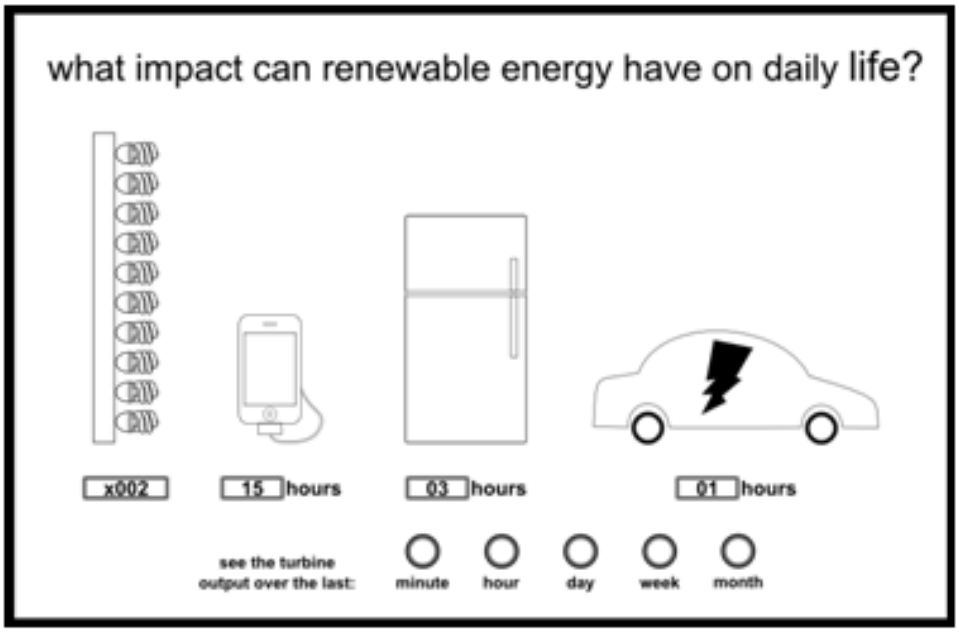

FIGURE 7: ENERGY USAGE EXHIBIT DESIGN

The cost of such an exhibit was estimated to be in the hundreds of dollars. Existing resources include the wind turbine energy data gathered as a resultant of a previous MQP [**2**]. Considerations would include seeking approval to install such an exhibit and the need for an appreciable amount of energy production to highlight the benefits of renewable energy harvesting.

2.1.8 Weather Assessment Modules

The goal of this project element was to develop devices to measure weather characteristics of prospective renewable energy sites. The data would be collected and used to estimate outputs of sized renewable energy systems if they were installed. The device would be self-sufficient, durable, and capable of communicating with a remote data server. Once developed the system would be installed in several locations on the WPI campus. A system block diagram is depicted in Figure 8.

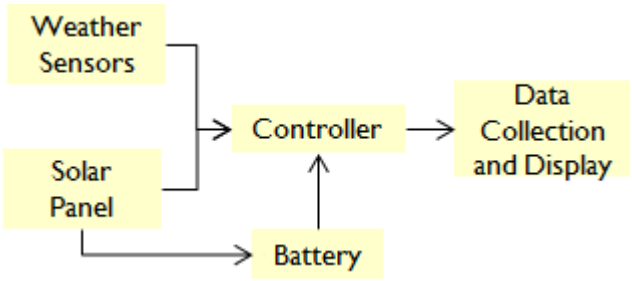

FIGURE 8: WEATHER ASSESSMENT MODULE SYSTEM BLOCK DIAGRAM

This module would measure solar irradiance and wind speed amongst other weather characteristics. Solar panels would also be used to provide power to the system making it self-sufficient. The module would transmit the data recorded to a remote server for display. The display aspect was intended to educate the public about what renewable energy opportunities could be explored on the WPI campus.

The cost of this idea was estimated in the range of hundreds of dollars per unit. Existing resources included a weather measurement station which could be used a foundation for prototyping. Considerations for this project include developing a reliable system for communication between units and the data display system, the permissions required to install these devices on campus buildings, the determination of appropriate site locations, and the time required to make multiple units.

2.2 Project Ideas Discussion

After developing a platform to evaluate each idea they were presented to Professor John McNeill, the project advisor, and the MQP team potentially collaborating with this project to discuss and evaluate all of the available ideas. It was found that the other MQP would most likely be developing a display system separate from a renewable energy system in the AK lobby. Realizing that the other MQP could use data from the proposed project, or possibly serve as a load for the project, it was decided to concentrate on combining aspects of the aforementioned ideas into three possible projects independent of the other MQP team's work.

2.3 Project Possibilities

The following sections set out to describe the three projects, as compilations of one or more of the project ideas previously discussed. Each one of these projects was evaluated with respect to cost, pros, cons, and best and worst case scenarios.

2.3.1 Solar Monitoring and Display

Proposal

The purpose of this project would be to install solar panels on the roof of AK, have it drive a load, and monitor its output characteristics. The measurements would be compared to data collected regarding to the power usage by the entire AK building. The comparison of power generated versus power distributed would be displayed for the public to see. Weather information gathered at the site of the solar arrays would also be acquired in an attempt to correlate weather characteristics with the arrays power output. Figure 9 depicts the block diagram of the Solar Monitoring and Display system.

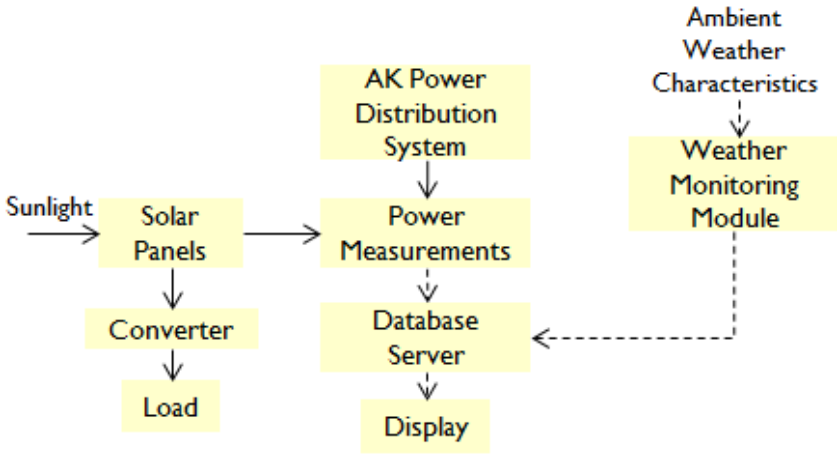

FIGURE 9: SOLAR SYSTEM MONITORING AND DISPLAY BLOCK DIAGRAM

Anticipated Outcomes

Ideally, this project would entail the installation of a solar panel array that would power display system under construction by the other MQP group. The solar system would implement maximum power point tracking to extract the power from the solar array efficiently. Monitoring equipment would be designed to measure the energy characteristics of the solar system and the AK distribution point. Another monitoring unit would either be designed to monitor the weather conditions of the solar array site. The other MQP team's display unit could have been used as the display medium for the collected data, it would be developed to interface with the monitoring systems and descriptively quantify the power consumed and produced in terms that any member of the public could understand. The data would also be made available on the ECE website. The display would allow for real time presentation of data along with data trends over an elapsed time. Weather characteristic trends would also be displayed alongside of the power outputted by the solar system allowing the public to infer correlations between the data sets.

Cost

The main component cost of this endeavor would involve the installation of a solar system. An installation quote was estimated at $14,300 for a minimum size of a 2000W system (see appendix for solar calculator input parameters) **[5]**. Another option was an 850W system with other accessories that needed additional mounting hardware to mount the panels to the roof the system alone was $4,560 **[6]**. The individual panels of the system (along with some undesired accessories) could be purchased at $480 per 85-watt panel **[6]**. Individual solar panels were found to be cheaper if bought online. Table I summarizes the costs of solar panels that could be purchased through online distributors **[7,8,9,10]**

Panel	W	$/W	Note	Power, Cost (# Panels)	
Sharp	240W	$1.87/W	Poly	480W, $900 (2)	960W, $1800 (4)
Sanyo	225W	$2.66/W	Hybrid	450W, $1200 (2)	900W, $2400 (4)
Solyndra	200W	$3.50/W	Thin Film Tube	400W, $1400 (2)	800W, $2800 (4)
HQRP	85W	$3.23/W	Poly	510W, $1650 (6)	680W, $2,200 (8)

TABLE I: SOLAR PANEL COST COMPARISON

Sharp solar panels offer the best deal with considerations to cost and system size. In purchasing the panels alone, additional mounting hardware would be required to install the panels. It was advised that the installation require no direct anchoring to the roof of the AK. Therefore, a ballasting system, which mounts the panels to a rack and the racking unit itself is weighed down was chosen to be an alternative type of installation. A conservative estimate of the racking system was priced around $200 **[11]**.

Another component of this system would pertain to power storage. It would be desired that the system charge batteries, which would drive a load when there is little or no sunlight. Table 2 lists the cost of power storage depending battery type and power capacity specifications [**12**,**13**].

Battery	WHr	$/WHr	Capacity, Cost (# Batteries)		
BB Battery BP40-12	480Wrs	$0.195/ Whr	1,920WHr $376 (4)	2880W, $564 (6)	3840W, $ 752 (8)
UPG UB12500	600WHrs	$0.151/ Whr	2400WHr, $364 (4)	3600WHr, $546 (6)	4800WHr, $728 (8)

TABLE 2: BATTERY COST COMPARISON

In this competitive analysis, the UPG model offers a larger capacity at less of a cost. After compiling all of this preliminary cost information, a conservative overall cost for this endeavor was calculated at $4000 allotting additional funding to fulfill the remainder of the project's objectives

Pros

Implementing such a system would provide a concrete demonstration of harnessing and utilizing renewable energy. If it were able to power the LED wall, it would show how a green energy system could efficiently drive DC loads in an uncomplicated manner. The system would also allow correlations to be drawn between weather characteristics and the energy harnessed by a renewable energy system via user interaction with the display unit.

Cons

Once installed, the solar array would need eventual servicing. Insufficient designs in the display and the monitoring system would also increase the need for system service. This could have posed future maintenance costs for the system after its implementation. The display may have required some facilitation to encourage interactive use. The solar system would provide an unregulated power output because its dependency on sunlight so loads would have to be driven intermittently.

Challenges

Possible areas of concern involved insufficient funding for the installation of solar panels that would bring the project to an immediate halt. Upon inspecting the roof of Atwater Kent, there existed only a limited space to mount a solar panel array. In order to power the LED wall, conduits would have to be installed to route the electrical conductors needed. The installation costs of conduits from the roof to the lounge could inhibit powering the LED wall. If insufficient power were generated by the solar array, displaying the data regarding the system's output would be frivolous. Difficulties could arise when attempting to develop a monitoring system that also properly interfaces with the display aspect of the project. Constant monitoring of AK's power distribution may stir up some issues of legality and practicality to the point that it may not be possible to monitor it continuously. In addition, the time it takes to perform one or more of the desired tasks may leave little or no time to complete the rest of the tasks in the duration of one MQP.

2.3.2 Wind Turbine Monitoring and Display

Proposal

The purpose of this project was to survey prospective locations for a wind energy system, move the turbine atop of AK to a better location, and monitor its output. The output characteristics would be compared to the power delivered by a distribution point in AK. The comparison of power generated versus power consumed would be made visual via a display module. Weather characteristics of the site of the turbine would be collected and displayed to draw correlations between the weather and the power output of the turbine. The block diagram of this system is depicted in Figure 10.

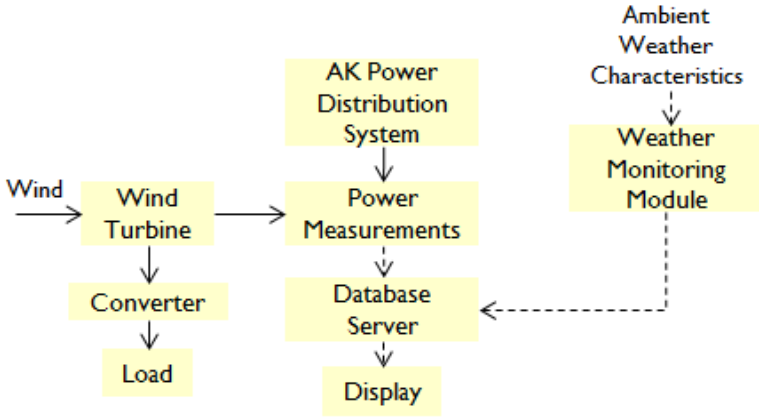

FIGURE 10: WIND TURBINE MONITORING AND DISPLAY SYSTEM BLOCK DIAGRAM

Anticipated Outcomes

The execution of this would assess prospective sites for the harvesting of wind energy. This could be used for future renewable wind-energy system installations about campus. Another desired goal of this project would revolve around the movement of the wind turbine to a location with an appreciable amount of wind. The wind turbine would be configured to either drive a load or interface with the electrical grid. A monitoring system would be implemented to communicate remotely with a server allowing for the display of real time information regarding the power output of the system and its ambient weather conditions. An AK power distribution point would be measured and the data collected would be used to compare energy consumed within AK to the energy produced by the wind turbine. The energy would be quantified into units that the public would find relatable. Ideally, the data collected would be displayed utilizing the interactive display system under development by another MQP group; it would also be made available on the ECE website.

Cost

It proved to be difficult to estimate the cost of moving the wind turbine. Most of the services listed online dealt primarily with large, commercial scale wind turbine installations, not with smaller residential installations. After consulting Professor James O'Rourke and Professor Alexander Emanuel, it was found that the cost of the original installation was around $10,000 [**14**]. It was also advised the cost of the installation did not accurately reflect the cost of such a procedure. It was revealed that the installation of the wind turbine was executed with a coordinated effort of members of the WPI facilities department, members of the ECE department, and members of the National Grid workforce not by a

professional installer. It was relayed that the cost of a professional installation could be twice that of the above amount [**15**]. Being conservative, the cost of the project was estimated at $20,000+.

Pros

Implementation of this system would demonstrate real use of alternative energy via the display its power output. Moving the wind turbine repurposes an underutilized resource, as the turbine, upon playful observation, was not in a prime location. If moved to a more visible location on the campus the wind turbine could serve as an icon to WPI's initiative to move towards a greener future. The use of a wind turbine allows for a more frequent and regulated harnessing of power since it can operate at all hours of the day. One of the existing resources available is a grid tie supplied with the turbine therefore interfacing it with the electrical grid is a plausible goal.

Cons

Other aspects of this project may have undesired corollaries associated with it. Since the wind turbine may be grid connected, there will be no way to present a visible load driven by a green energy system to the public. Reinstalling the wind turbine involves construction, management, and their associated costs. Moving the wind turbine removes a renewable energy icon from the Atwater Kent Building. If the system were to be implemented it would need some intermittent service to keep the system running. Again, the display apparatus may require some facilitation to encourage system interaction.

Challenges

Issues that may arise when pursuing this idea include an insufficient period to monitor prospective sites. Limited observation time could result in insufficient data generation possibly imposing a wrongful decision being made concerning the movement of the turbine. Another possible scenario is that resources may not exist to move the wind turbine. One undesirable facet of this project is that the power generated by the wind turbine may be too insufficient to display in real time or over short windows of time. There is also a possibility that the monitoring system, once in place, has issues communicating with the display module. Alternatively, the monitoring unit developed may not be adequate for use or interface with the display unit. Interfacing this system with the peripheral display system might be out of the question depending upon the other MQP groups design.

2.3.3 Site Monitoring and Display

Proposal

This MQP would involve developing multiple weather monitoring units and installing them at prospective locations for renewable energy harvesting across campus. The data collected would be used to approximate power outputs of sized renewable energy systems located at each site. These calculations would then be compared with the power delivered by a distribution point within AK. The energy characteristics would then be displayed for public viewing. Figure 11 shows a block diagram of the system.

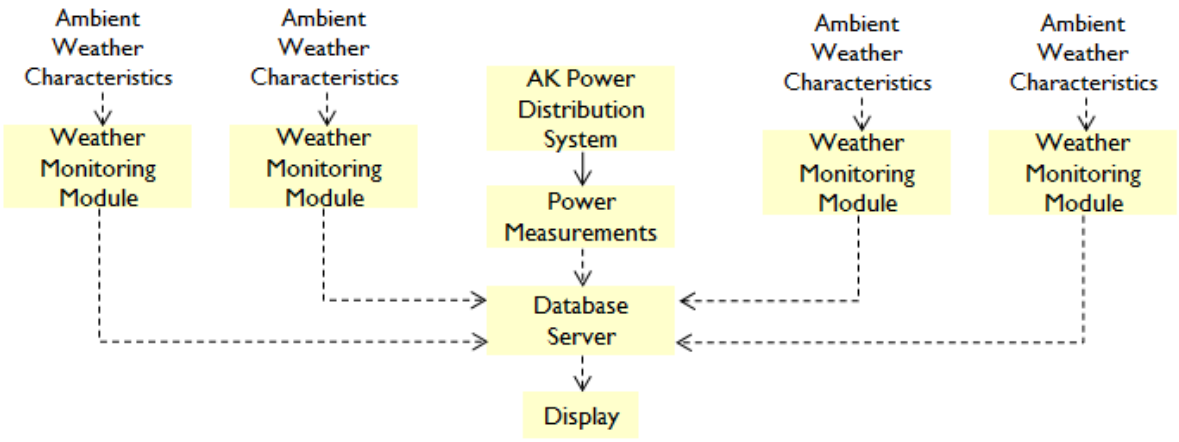

FIGURE 11: SITE MONITORING AND DISPLAY SYSTEM BLOCK DIAGRAM

Anticipated Outcomes

Ideally, the project would involve the development of multiple durable, self-powered, monitoring units designed to have no moving parts and measure weather characteristics such as wind speed, solar irradiance, barometric pressure, etc. A separate monitoring unit would be developed to measure a power distribution to AK from the grid. Each of these units would be capable of transmitting data to a central server for further use. The data would be used to compare possible power production of a sized renewable energy system with current power consumption of a facet of AK both in real time and over specific time intervals. The quantification of energy would be displayed in a qualitative manner, easily understood by the public. The display medium desired would be the interactive display previously mentioned.

Cost

An estimate was put together to price out a per-unit cost for each weather monitoring module. It was reasoned that the weather instrumentation would cost around $100. The printed circuit board (PCB), assorted circuit components, and weatherproof enclosures were priced at $180. A wireless communication module would cost about $40. The irradiance measuring solar panel would run a cost near $90. Lead acid batteries used as a power storage unit for each module would cost approximately $25. The mounting hardware, which would vary depending upon installation location, was estimated to cost $40. Accounting for the possibility of additional needed componentry the per-module cost of this endeavor ranged between $400 and $600 [**16**].

Pros

The development of this system raises awareness in the public as to renewable energy potentials that could but have not been implemented at the current time. This system would create some political pressure to generate funding for the installation of various renewable energy systems. Self-sufficient monitoring modules would emanate the use of renewable energy by harvesting it to power system components. The system as conceptualized by the group would be wireless and require no complexities involving installation of these units.

Cons

Developing multiple monitoring units utilizes a considerable amount of resources with one of those resources being time. The system may need to be routinely serviced especially in severe weather conditions. The fact that there may be many locations to manage and certain locations may have issues with ease of facility access. This would create additional costs for the ECE department to handle. It is possible that these units could backfire in the desired green energy initiative. If the modules were inaccurate, calculations would not reflect the actual amount of energy that could be harvested. On the other hand, it could be that the prospective sites are not as ideal as once perceived. The system may possess a yearly downtime due to winter weather conditions. In addition, the display module may require some facilitation to encourage public interaction with the exhibit.

Challenges

While pursuing this project several issues may arise, one of them being the denial of approval to install these monitoring units across campus. An inability to transmit the data would bring most of the project to a halt. If the monitoring devices are not self-sufficient, it may detract from the nature of the system to promote harvesting renewable energy. Restrictions regarding the locations possible install locations may limit the number of monitoring modules being put into place. Display interface issues may arise when trying to communicate with the modules. The weather data (mainly irradiance or wind speed) when manipulated to estimate power delivered a sized renewable energy system may theoretically produce insufficient amounts of power, making display purposes frivolous.

2.4 Project Discussion and Decision

Once the final three MQP project ideas were defined, explored, and estimated for cost, they were presented to Professor Looft, the ECE department head. Once presented, a brief discussion about the feasibility of each project took place. Each idea was carefully considered by the team to determine which project would be the best choice. Factors considered were economic and technical feasibility, impact of the overall outcome, challenges presented by the projects, available resources, and possible pitfalls. Table 3 summarizes the findings of the discussion.

Project:	Goals:	Advantages/Disadvantages:	Decision Factors:
Solar System	• Install Solar Panels • Harvest and Utilize Green Energy • Monitor Energy Production and Consumption	+ Utilizes Green Energy + Displays Useful Data + Moderate Cost - Installation Concerns - Intermittent Intervals of Sunlight	• Completion of MQP in One Year • Desire to Make Use of Green Energy • Idea Non-Intrusive to WPI Policies
Wind System	• Relocate/Install Wind Turbine • Harvest and Utilize Green Energy • Monitor Energy Production and Consumption	+ Increases Green Energy Production + Displays Useful Data - Large Cost - Need Additional Resources/Manpower - Possible Insufficient Power Production	• Limited Manpower • Limited Available Resources on Campus
Site Monitoring System	• Monitor Weather at Separate Site Locations • Monitor Prospective Energy Production • Monitor Energy Consumption	+ Calculates Prospective Energy + Displays Potential Data Characteristics + Low Cost - Installation Concerns - Maintenance and Service Difficulties - Does Not Harvest Renewable Energy - System Communication Challenges	• Limited Budget • Allocation of Space for Testing • Project Sustainability After Completion • Impact of Project After Completion

TABLE 3: PROJECT SUMMARIES

Judging each of these project's pros and cons against MQP priorities and other factors it was deemed that the wind turbine project was too costly when weighing the necessary finances, resources, and labor to execute the project. One of the major concerns was the feasibility to complete such a project in one academic year, considering it would take a substantial amount of time for WPI's upper management to approve such an endeavor. The site-monitoring project was ultimately discarded because it would take a considerable amount of time to locate and seek approval to install theses apparatuses about the campus. The project would also not provide a concrete example of renewable energy usage as it would only report the green energy potential of the site. Beyond that, this project would strain the resources of the ECE department when system maintenance was required. It was finally decided to pursue the solar system project as it met the demands of a Major Qualifying Project while satisfying the majority of the decision factors. Modifications made to the scope of the solar project are discussed in the following chapter.

3 Proposed System Design

Once the solar energy harvesting and information display project was chosen, the system could be designed and implemented. The subsequent sections briefly discuss systems in existence similar to the prospective project and details functionality of the system to be developed along with the work necessary to complete the project.

3.1 Related Systems

Currently there are technologies and practices in place that furnish and install solar systems and auxiliary equipment that measures the electrical characteristics of the system. This subsection of this report discusses a couple of practices already in existence.

Solectria Renewables

One company, Solectria Renewables LLC, develops products specifically dealing with solar systems. It also offers various types of system monitoring. Solectria designs and manufactures inverters, which convert the DC output of a solar array to AC power to interface with the electrical grid. In addition, they also manufacture string combiners that combine arrays of solar panels for various system configurations. Solectria offers monitoring packages that include informational displays local to system equipment or various subsystems and on-site data display kiosks. Information is viewable online utilizing web based monitoring. Data is periodically updated and stored and trends can be observed over given time intervals [**17**]. A more detailed monitoring system is realized and reviewed in the next subsection.

Sanyo Kasai Green Energy Park

In Japan, Sanyo has constructed a green energy park, a corporate facility harvesting solar energy on a massive scale utilizing the technologies that are designed and developed within the complex. The park employs an energy monitoring system that measures the energy consumption, the production of renewable energy from the solar system installed, and equates the renewable energy produced to the reduction of carbon emissions [**18**]. The monitoring display kiosk is shown in Figure 12.

FIGURE 12: SANYO GREEN ENERGY PARK ENERGY MONITORING DISPLAY

Our project plans to be a hybrid of the aforementioned systems, displaying the solar system's electrical characteristics from both a system level of abstraction and a subsystem level. It will report on not only the overall system outputs but will reveal data on the equipment used to comprise the system. The data

will have a detailed and understandable display medium to educate all those who enter the Atwater Kent Building and visitors to the ECE department's website. The information will also be used to extract information critical to the devices involved with the conversion and storage of solar energy.

3.2 Functional System Description

The final proposed system involved the installation of six solar panels atop the roof of the Atwater Kent building; the precise location was determined by a solar path analysis discussed in a later section of this report. Each panel had conductors leading from the panel, and terminated at an overcurrent protection device located in room AK317. The six solar panels consisted of two identical solar panels each from one of three manufacturers. In this way, each panel was compared to another identical solar panels as well as panels from other manufacturers.

Separate maximum power point, DC-DC converters were developed to convert the power outputted by each panel and either charge batteries or drive a DC load. The converter would find the maximum power point using a perturb and observe algorithm.

The converter would continually take measurements of the power it outputted, comparing one measurement with a previous measurement and adjust the duty cycle of the switching circuit performing the conversion to output optimal power. The maximum power point converter was embedded within a power management subsystem designed for a single solar panel. Figure 13 depicts the block diagram of the panel management circuitry.

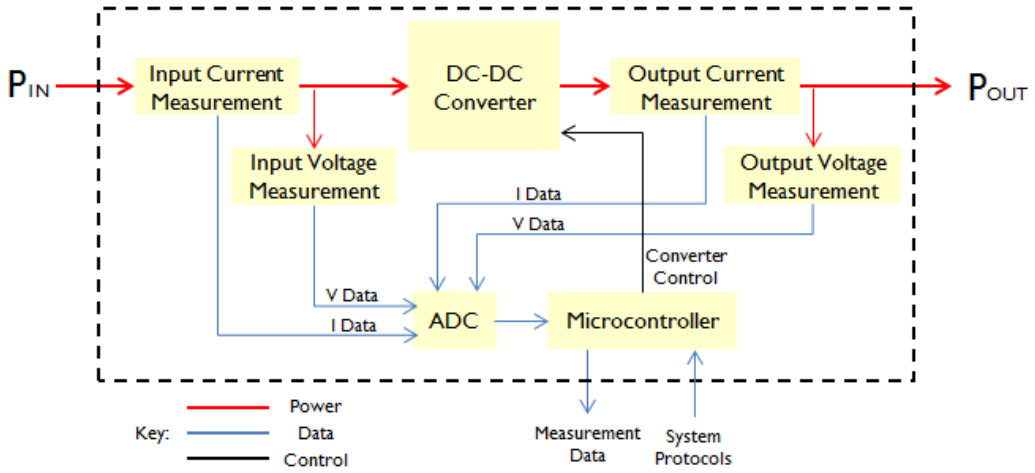

FIGURE 13: SOLAR ENERGY HARVESTER BLOCK DIAGRAM

The Solar Energy Harvester actually consists of three separate blocks working as one. The DC-DC converter is controlled by a local microcontroller that runs the maximum power point algorithm based on measurements taken from the measurement blocks and adjusts the converter circuitry accordingly. Measurement apparatuses would be designed and built to measure the output of the panel and the output of the converter. Specifically, the measurement devices would measure the voltage and current values at each point in the system. The local microcontroller would poll an analog to digital converter for the voltage and current values measured, adjust the converter operation, and send the data to a system "master" microcontroller where it will be processed. This local "slave" microcontroller could

also receive information from the master microcontroller and adjust the converter operation accordingly. A system block diagram is depicted in Figure 14.

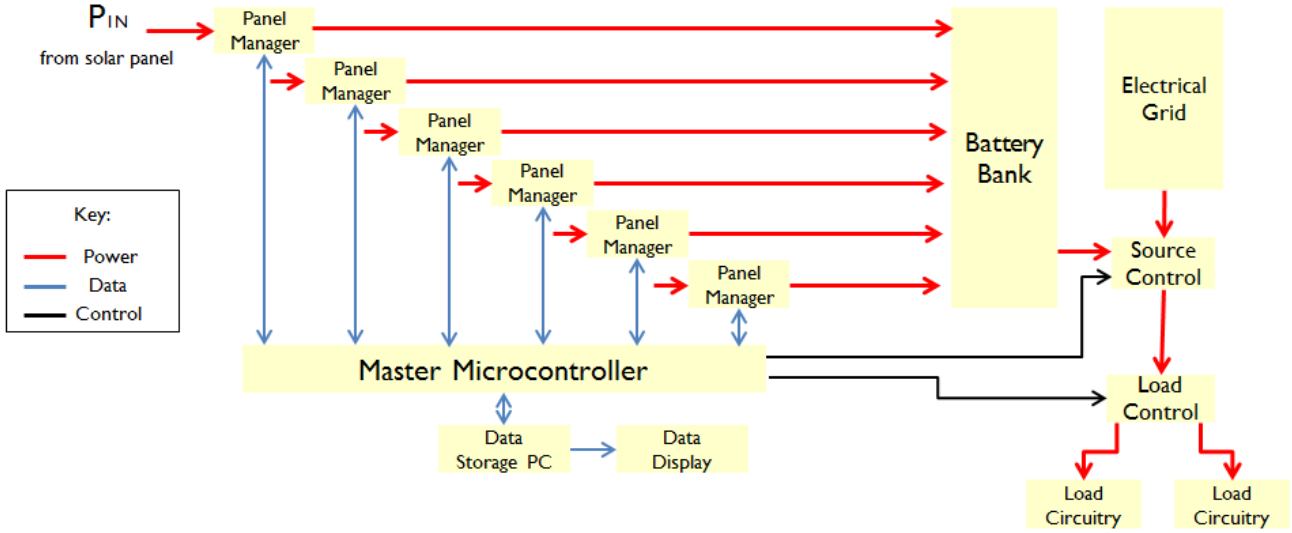

FIGURE 14: SYSTEM BLOCK DIAGRAM

The slave microcontroller of each panel management circuit sends data to a master microcontroller, which in turn transmits the data to a PC. The stored data would then be processed and displayed online and on an LCD monitor in the lounge area of the Atwater Kent building. From these measurements, additional electrical characteristics such as power are calculated and displayed. By measuring the converter input and output, the efficiency of the converter can be calculated. The conditions of the batteries designed to store the converted solar energy are also monitored by voltage measuring circuits. The master microcontroller receives data relevant to the battery and either continues charging the battery or diverts power to DC loads. The master microcontroller would also send information to the panel manager blocks and alter converter operation. The control decisions made by the master microcontroller are summarized in a flow chart in Figure 15.

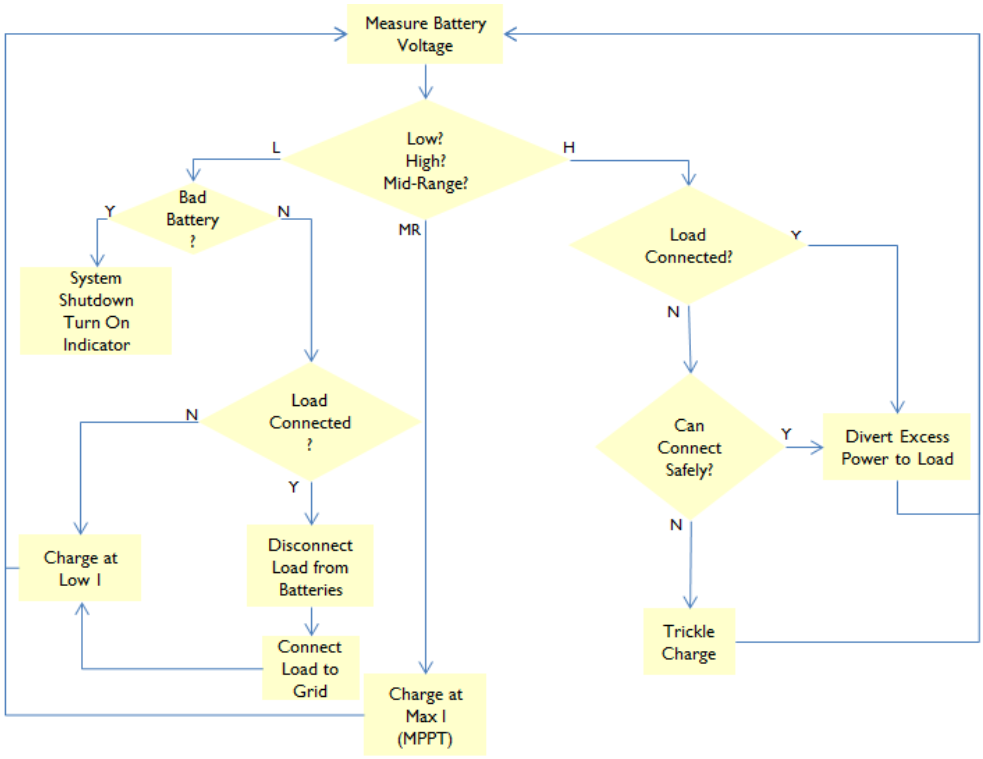

FIGURE 15: SYSTEM CONTROL DECISION FLOW DIAGRAM

As a safety feature, the master microcontroller had the ability to cease system operation if any hazardous conditions were detected. Using the battery-monitoring feature, the master microcontroller would decide what source would be used to drive the DC loads. If the batteries possessed enough charge, the system would drive the loads from the battery banks, if the charge in the battery bank was depleted, the electrical grid would drive the loads whilst the solar panels would charge the batteries. If the batteries were fully charged, and sufficient power was still being output by the panels, the system would divert power directly to the DC loads.

Another optional avenue was to include a user-controlled aspect to the project. Using a display medium such as an LCD touch panel a user would be able to interactively turn on and turn off DC loads. The system would incorporate its own automatic override if user interaction would jeopardize the integrity of the system. Ultimately, the progress made in the development of other subsystems would decide whether to pursue this option.

4 Detailed Design

This section of the report will address the decisions made in the design process of the project in three separate categories: solar panel installation, circuit design, and system integration and interface. The research and experimentation to arrive at such decisions will also be covered.

4.1 Solar Panel Installation

This subsection of the report discusses the research, consultation, experimentation, and execution of solar panel installation.

4.1.1 Site Location

Many factors were taken into consideration when deciding where to install the solar panels. The length of cable that would need to be run, the visibility of the panels, the amount of solar energy a given area is exposed to, the susceptibility to damage that the panels were exposed to along with how the installation may damage the surrounding area and the roofing materials were the top concerns of the group. Initial research was conducted to calculate the potential amount of solar irradiation collected by the panels under various conditions. Next, three sites were chosen based on the natural and artificial surroundings of the site and the public visibility of the panels. The site locations are marked in the Figure 16.

FIGURE 16: ATWATER KENT BUILDING ROOF W/ INSTALLATION SITE LOCATIONS [**19**]

Site 1 was chosen to address the possibility of mounting the solar panels such that they would hang over the lip of the roof of the building. Making the panels visible to the public by mounting them in such a will reflect WPI's initiative for a greener future. Site 2 minimizes the shading created by surrounding structures. Site 3 would minimize the amount of shading the panels would be exposed to and decrease the conductor length needed to connect the panels to a load. As mentioned before the cabling would enter the building via an opening beneath the base of the wind turbine.

After determining the sites, the path the sun would take over an hourly and monthly basis was analyzed serving as one of the deciding factors in which site was finally chosen.

Insolation Data

Insolation is a measurement of the amount of solar energy a specific area receives per day. It is based on many different factors, most importantly the latitude line that the area of interest is on. The

instantaneous solar radiation is expressed in $\frac{W}{m^2}$, while solar radiation for a single day can be measured in $\frac{kWh}{(m^2*day)}$ or the amount of work produced by a square meter solar panel of ideal efficiency each day.

Reliable insolation data is available from the NASA Atmospheric Science Data Center [**20**]. This data provides information about the amount of sunlight energy delivered relative to a specific latitude and longitude for a specific month. Several different measurements are made based on tilts relative to horizontal and relative to the equator. Table 4 is a series of measurements for each month averaged over a 22-year period based on different types of angles and measurements at a latitude specific to Worcester, Massachusetts.

Position	Jan	Feb	Mar	Apr	May	Jun	Jul	Aug	Sep	Oct	Nov	Dec	Total
Direct	3.31	4.07	4.33	4.29	4.50	4.65	5.18	4.87	4.64	4.05	3.14	2.95	4.17
0°	1.80	2.62	3.61	4.46	5.13	5.49	5.61	4.99	4.04	2.93	1.89	1.54	3.68
27°	2.82	3.59	4.32	4.73	5.09	5.23	5.48	5.15	4.64	3.84	2.80	2.50	4.19
42°	3.19	3.88	4.42	4.57	4.73	4.78	5.04	4.89	4.65	4.08	3.10	2.86	4.18
57°	3.37	3.95	4.29	4.20	4.17	4.14	4.38	4.41	4.42	4.09	3.23	3.06	3.97
90°	3.09	3.35	3.26	2.80	2.54	2.45	2.57	2.79	3.19	3.37	2.89	2.86	2.93
Optimum Angle	3.39	3.95	4.42	4.74	5.21	5.51	5.66	5.19	4.68	4.11	3.24	3.09	4.43

TABLE 4: MONTHLY INSOLATION DATA

Insolation measured in $\frac{kWh}{(m^2*day)}$ is tabulated by month based on a panel pointed normal to the equator tilted at a specified angle. A direct measurement of insolation with a panel pointed normal to the sun (tracking the movement of the sun) is given as well as the optimum angle, the ideal tilt angle of a panel specific to the month. For the scope of this project, tracking the sun with the panel normal to the sun is not feasible. Instead, an ideal fixed angle will need to be chosen with consideration to the data available, the mounting method used, and the site chosen.

While it may seem logical to choose the angle that produces the highest annual insolation numbers, when considering a graph of each different angle over the months (see Figure 17) more about the availability of energy is revealed. While certain angles will produce higher annual values, others will produce energy at a steadier rate through the seasons. The angle the panels are currently mounted at is fixed because of the nature of the panel mounting system currently used that was donated to the project. Future mounting systems may make it possible to experiment with different angles.

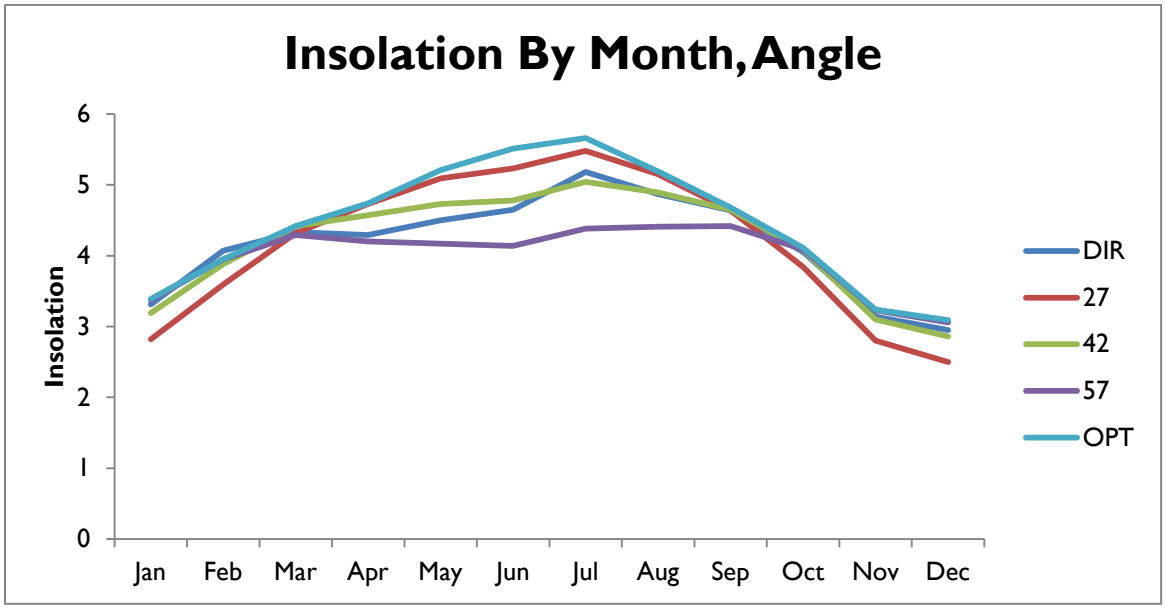

FIGURE 17: MONTHLY INSOLATION RATINGS PER ANGLE OF TILT

Solar Path Finder Measurements and Results

With the three sites chosen, data was collected about the path the sun would take on a daily basis over different seasons of the year. A device known as a solar pathfinder was used to map out how the surroundings of the site would cast shadows over a daily basis throughout the year. The solar pathfinder apparatus (see Figure A-1) was oriented to compensate for the tilt of the earth's axis, the latitude and longitude of the site, and the fact that the true north is off from the magnetic north measured by a compass (magnetic declination). A dome would be placed over a shade analysis grid and any object that would cast shade over the location would be reflected in the dome. The outlines of these reflections were traced and used to interpret percentages of the sunlight seen by a solar panel installed at this location. An example of a filled shade analysis grid is depicted in Figure 18.

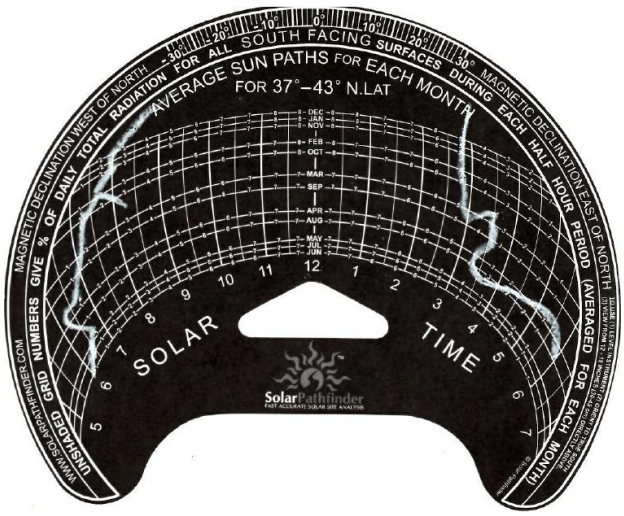

FIGURE 18: SOLAR PATH FINDER EXAMPLE SHADE ANALYSIS CHART

The outline of the reflected objects covers up portions of the chart beginning at the perimeter of the chart itself. The grid on the chart marks percentages of the total daily sunlight spread out over each half-hour of the day from the approximate sunrise to the approximate sunset (5am to 7pm). Adding up the percentages on a particular horizontal curve (month) not covered up by the reflection trace provides the total daily percentage of sunlight exposure. The varying amount of daylight in each month is compensated by the curvature of the horizontal axes and the change in the half-hourly percentages along these axes [**21**]. Each of the sites was analyzed twice and the monthly percentages of sunlight exposure were computed. For a better view of the shade analysis charts see Figure A-2 through Figure A-7 in the appendix. The results are listed in Table 5.

Month	Sun Exposure Percentages [%]					
	Site 1		Site 2		Site 3	
	Measurement 1	Measurement 2	Measurement 1	Measurement 2	Measurement 1	Measurement 2
January	84	84	90	88	93	90
February	82	76	94	94	93	87
March	80	87	91	89	89	93
April	88	100	94	96	99	99
May	99	100	100	100	99	100
June	99	100	99	99	99	99
July	100	100	100	100	99	100
August	91	100	95	98	99	99
September	91	91	94	91	96	96
October	82	80	94	94	91	89
November	82	76	88	89	91	88
December	81	81	90	86	93	84
Average	88.25	89.58	94.08	93.67	95.08	93.67

TABLE 5: SOLAR PANEL SUNLIGHT EXPOSURE PERCENTAGES

The data reflected that the optimal location for installing the solar panels would be Site 3. Site 3 also offered the benefit of a shorter conductor run from panel to the eventual load. In addition, the installation of panels at Site 1 would have required additional hardware to make the panels directly visible to the public; it would have also introduced additional liability concerns. Because of the mounting system used, Site 2 served as the best compromise between conductor length and shading percentage.

4.1.2 Initial Installation

The solar panel mounting procedure involved bolting down the solar panels to a metal structure known as a pan. These pans are bolted together one behind another to form multiple columns of solar panels. These columns are placed adjacent to each other to maximize the roof space. The mounting hardware is secured to the roof by weighing down each pan with a series of paver stones. This procedure is illustrated in Figure 19.

FIGURE 19: TYPICAL SOLAR INSTALLATION BY FUTURE SOLAR SYSTEM LLC [**22**]

This installation procedure provides a non-invasive alternative to typical solar panel installations. To prevent damage to the roofing material, anti-slip matting is placed between the metal installation hardware and the roofing material.

The solar panels installed were donated by a Jim Dunn, a WPI alum and President of Future Solar Systems LLC. The six solar panels consisted of two 215W Sun Power Panels (SPR-215-BLK-U), two 230W Sun Power Panels (SPR-230-WHT-U), and two 230W Canadian Solar Panels (CS6P-230P). One of each type of Sun Power Panels was mounted on the roof initially and eventually, through coordination with WPI's facilities staff and the ECE department staff, the remainder of the solar panels would eventually be installed.

4.2 Solar Panel and Energy Harvesting Theory

Before getting into the details of the system operation, it was important to understand the panel from a circuit modeling perspective. In doing this, the specifications and end goals of the energy harvesting system could be defined.

4.2.1 Solar Panel Theory

Solar panels are comprised of strings of individual solar cells, a semiconductor device typically fabricated out of silicon. A solar cell is modeled as a constant current source up to a specific voltage, at which point the current falls off exponentially. This cell voltage is typically around 0.6V-0.7V for a silicon cell, but varies based on the cell's chemical composition and manufacturing processes. The voltage of a cell is inversely proportional to temperature governed by the thermal voltage of the semiconductor material. The current produced by a solar cell is directly proportional to the intensity of light at the wavelengths the cell responds too, and directly scales based on the size of the cell, so a cell with twice the area will produce twice the current. Figure 20 shows the circuit equivalent of a single solar cell.

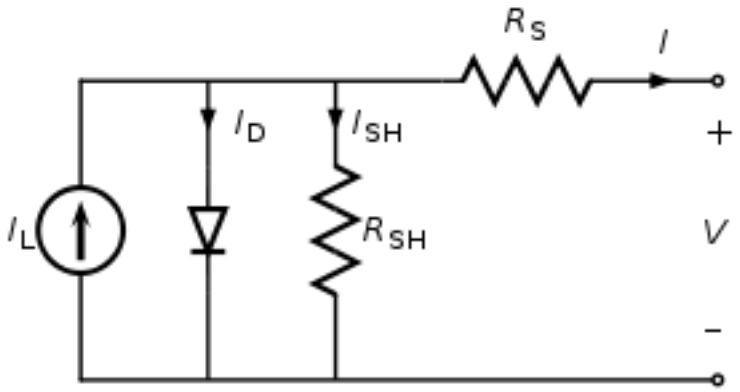

FIGURE 20: SOLAR CELL CIRCUIT EQUIVALENT [**23**]

The current source, a direct function of sunlight, has some series and parallel resistance, R_S and R_{SH} respectively. These resistances are due to the natural resistive properties of the silicon. The output current and voltage of the cell are defined by the equations:

$$V = V_{CELL} - I \cdot R_S$$

$$I = I_L - I_D - I_{SH}$$

where V_{CELL} is the voltage across the model's current source. These equations are linked by the V-I characteristic of the diode (Shockley's diode equation):

$$I_D = I_S \left(e^{\frac{qV_{CELL}}{nkT}} - 1\right)$$

The temperature dependence of the panel is reflected in the equation - the thermal voltage of the diode contributes to the variations in the output voltage based on ambient temperature. The ability of a solar cell to produce power is measurably decreased in the summer and increased in the winter. Taken directly from the datasheet of one of the solar panels, Figure 21 reflects the general shape of the voltage and current relationships for this circuit model.

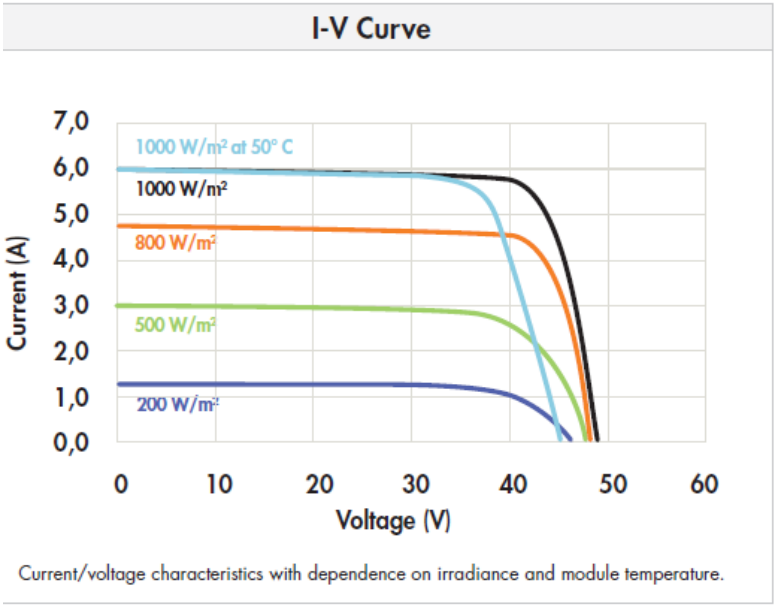

FIGURE 21: SOLAR PANEL V-I CURVES [**24**]

The falling exponential shape of the graph is largely defined by the exponential characteristic of the diode in the circuit model. The series and shunt resistance also give a slope to the approximately constant current and constant voltage sections of the graph. As power is the product of voltage or current, there is a point on the curve where the maximum power of the cell can be extracted.

Solar panels, as previously mentioned, are composed of many solar cells connected together. Cells can be connected in series, parallel, or combinations thereof, but large panels in excess of 100W are nearly always connected in one series string because of the I^2R losses associated with parallel connections. Series connected cells produce V-I characteristics with the same output current as a single cell at a much higher cell voltage. The only drawback is that a single cell being blocked from light will appear as a resistance to all other cells in the panel. Various strategies can be used to mitigate these effects, such as bypass diodes every few cells.

In order to maximize the effectiveness of a solar panel, energy should be extracted at the maximum power point, where the effective impedance of a load connected to the panel must be directly matched to absorb power at the current and voltage corresponding to the maximum power that the panel can produce. Because the current varies with illumination and the voltage varies with temperature, this point can change dramatically based on the current conditions and must be "tracked" by a load that can change its apparent impedance. While loads with relatively constant impedance such as a battery or LED can be connected directly to a solar panel, it is in the interest of efficiency that a more intelligent energy conversion system is implemented to use the panel effectively. This is accomplished with a circuit such as a DC-DC or DC-AC converter capable of changing the Input-Output transfer characteristic alongside a measurement and control system capable of finding the most efficient power point. This technique is known as "maximum power point tracking".

4.2.2 Maximum Power Point Tracking

Because the location and magnitude of the maximum power point varies widely based on environmental conditions and the type and characteristics of a solar panel, it is necessary to "track" this point. Essentially any given point on the V-I curve of a solar panel under specific conditions has an associated load resistance which, when attached, will power from the panel at that specific point. Note that there are multiple pairs of points that have the same associate power, but different associated load resistances. In order to draw power from a panel at the maximum power point, a system must be able to find that point by either having previous knowledge of the panels characteristics or by "experimenting" with different loads until the one that extracts the most power is found.

Most loads attached to a solar system will be nonlinear in nature, such as batteries that are a relatively constant voltage with a small series resistance. For this project, a buck converter was chosen (discussed later in 4.3.1), which exhibits the input output voltage relationship:

$$D = \frac{V_O}{V_I}$$

This relatively simple relationship links the expressions for the solar panel and the battery. Essentially, the converter exchanges voltage for current and current for voltage at some efficiency, which allows us to "pick" points on the solar panels V-I curve by changing the apparent resistance of the battery. This is controlled by changing the duty cycle, D of the converter.

By making measurements of the power flowing into the converter, we can keep track of which duty cycle produces the most power and operates at that point until the maximum power point moves elsewhere, at which point the duty cycle is changed again until optimum conditions are found. This technique, and flow diagram of which can be seen in Figure 22, is known as a simple "Perturb and Observe" algorithm for finding the maximum power point. While there are many different ways to implement this algorithm, all of them involve either making changes and observing or having records or knowledge of the panel characteristics.

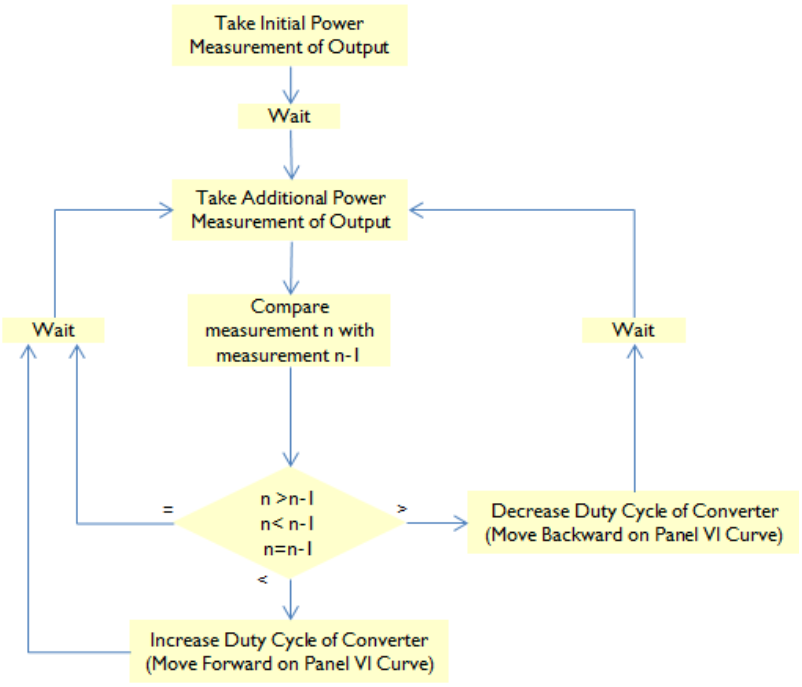

FIGURE 22: MAXIMUM POWER POINT ALGORITHM

4.3 Circuit Design

The measurement and converter module was the focus of this project. This module involved the design of a DC-DC converter, accurate voltage and current measurement and digitization, and a digital control system with feedback. The result of this design is a circuit that converts DC power from the solar panel to a level usable by standard DC loads such as a battery or lighting system. Additionally, the module is designed to output the current and voltage measurements at both the both input and output of the converter in a manner accurate enough to determine the efficiency of the entire module. A block diagram that details the connection of each of the major parts of the module can be seen in Figure 23.

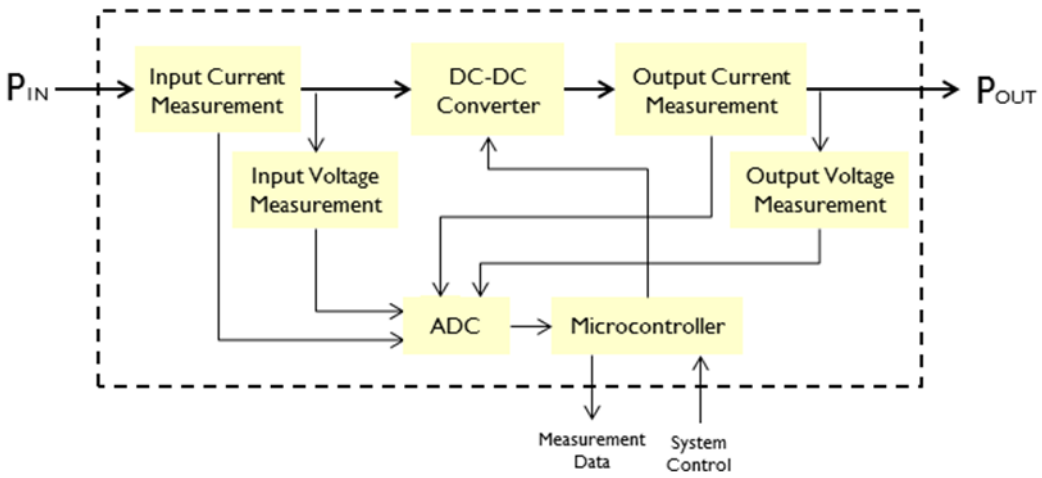

FIGURE 23: SOLAR ENERGY HARVESTER BLOCK DIAGRAM

The following sections describe the major parts in detail.

4.3.1 Converter Design

The DC-DC converter in the system couples the output of the solar panel to the battery in a manner that allows the apparent resistance of the battery from the perspective of the panel to "match" the maximum power point of the panel. Table 6 lists the general specifications chosen based on the panels that were donated, battery chemistries, converter controller options and the desired system voltages, currents, and power.

Criteria:	Input:	Output:
Voltage	0V-50V	0A-25V
Operating Voltage	18V-50V	8V-15V
Current	0A-9A	0A-26A
Power (max)	250W	250W

TABLE 6: CONVERTER SPECIFICATIONS

Based on these specifications, all three types of panels donated could be utilized in addition to other panels meeting the input specifications. The non-isolated buck topology was chosen due to its simplicity and wide number of controllers available for converter implementation. Ultimately, the Texas Instruments TPS40170 was chosen to control the buck converter. The TPS40170 had many features and settings that were chosen for the specific needs of the solar application. The synchronous switching buck converter drives low and high side MOSFETs, has bootstrap high side gate drive configuration, and is powered from VIN by an 8V regulator for the MOSFET gate drive and a 3.3V regulator for internal analog and digital controls, a 600mV reference for the feedback error amplifier when used as a constant voltage regulator [**25**].

Switching Frequency and RT

After studying various application notes and frequencies for various different applications, a frequency of 250KHz was chosen for a good balance between switching losses and inductor and capacitor size. The equation for timing resistance yields 38KΩ:

$$R_{RT} = \left(\left(\frac{10^4}{f_{SW}(KHz)}\right) - 2\right) * (K\Omega)$$

Undervoltage Lockout

The under voltage lockout disables the converter when the input voltage is below a threshold set by a voltage divider on the UVLO pin. A voltage of 18V was chosen as the upper turn on threshold and 16V as the lower turn off threshold.

Master / Slave Select

While the M/S pin allows the TPS40170 to be clock synchronized with other controllers as a master or a slave either in 0° or 180° phase synchronization, it was only used in master mode for this application. The pin was broken out to allow for experimentation but in most applications should be tied to VIN for Master mode. The sync pin, which is used in conjunction with the M/S select, can be used as a clock output for triggering when taking oscilloscope waveforms.

Enable

The enable pin on the TPS40170 allows the converter to be turned on or shut down into a low power mode. The enable pin is connected to a jumper than forces the converter on in one position and allows the microcontroller to enable or disable the converter in the other position.

PGOOD

The PGOOD pin from the controller indicates when the converter is running properly, internal regulators and temperature are within normal range. This pin is an open drain which is normally pulled up to VDD. The pin is connected to the microcontroller in order to determine if a fault condition is present.

Inductor and Capacitor Selection

The inductor and capacitor values were computed by executing the recommended calculations in the TPS40170 data sheet. A total bulk capacitance C_{IN}=120uF and C_{OUT}=180uF were needed. A combination of X5R 100V ceramic capacitors and 63V Nichicon aluminum polymer organic capacitors were used to keep the equivalent series resistance low. A 10uH SER2918H Coilcraft inductor with an equivalent series resistance of 2.86mΩ gives a loss of 1.93W under maximum load.

MOSFET Selection

The "PowerPak" Type MOSFET was used for it small size, low on resistance and superior power dissipation. The MOSFETs need to be able to withstand currents up to at least 30A and voltages up to at least 50V. The Vishay SiR826DP MOSFET exceeds these ratings at 60A, 80V. Two MOSFETs can be placed on the PCB for both the high and low side for better conduction losses. Conduction losses with the 5mΩ MOSFETs are 3.52W at the full 250W load. The losses are halved to 1.76W when to FETs are used in parallel.

The switching losses can be approximated based on the maximum rise and fall times of the MOSFETs. The total high side and low side switching losses were calculated at 5.72W, for a total FET loss of 7.48W at full load, and total FET + Inductor loss of 9.41W and a theoretical efficiency of 96%.

Input Voltage

In a typical application, the TPS40170 uses a "voltage feed forward" topology to nearly instantaneously respond to change in the input voltage, resulting in much faster response times for supply voltage variation. This feature is unnecessary for the system and may even have negative consequences. The voltage feed forward creates a ramp voltage with an amplitude 1/15th the voltage of the input voltage, with a small roughly 0.9V bias. This voltage ramp is then compared to the error amplifiers compare voltage, which synthesizes the PWM signal to drive the MOSFET gates. See the following figure for a block diagram of the controller.

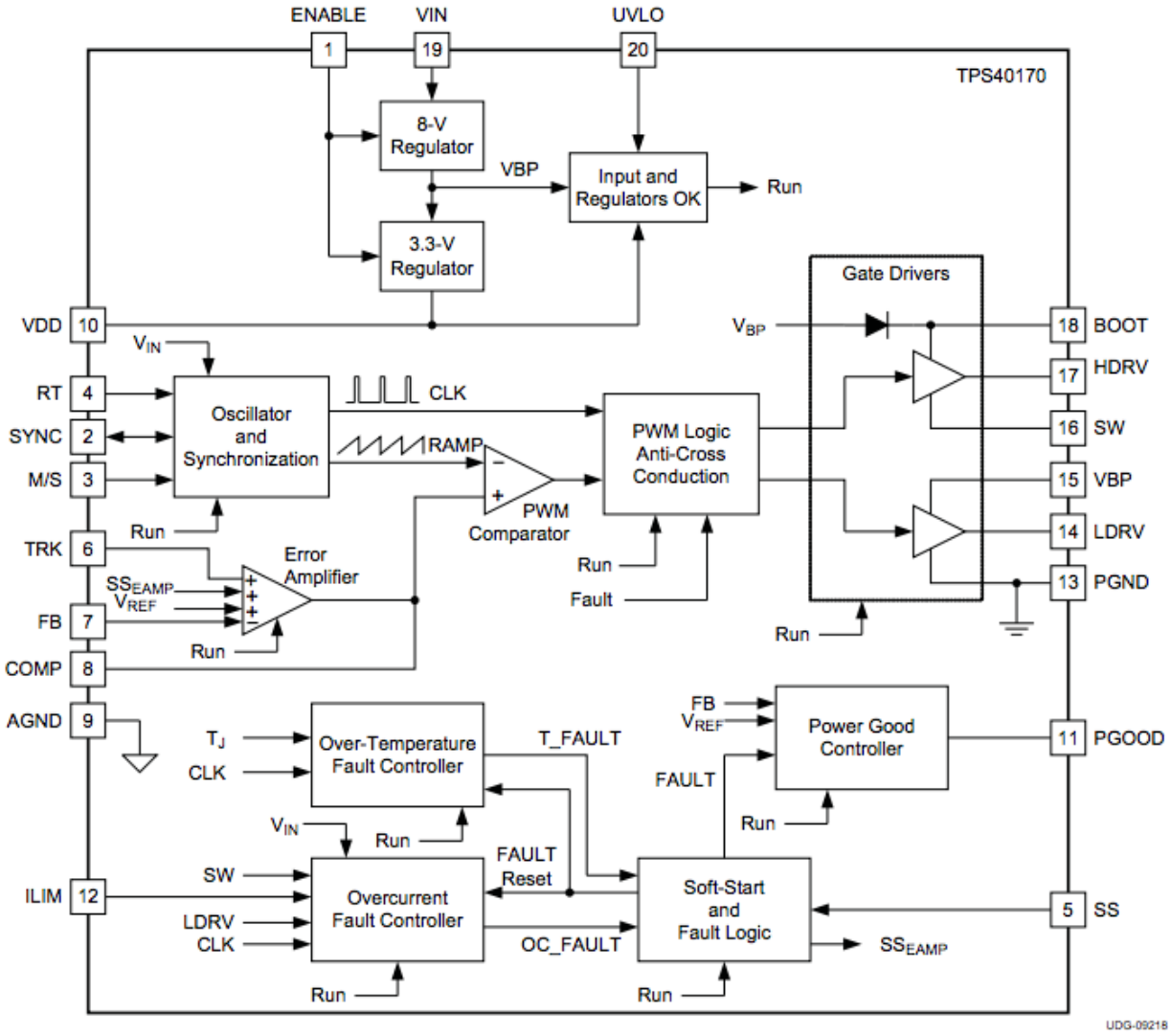

FIGURE 24: BUCK CONTROLLER BLOCK DIAGRAM [**25**]

In order to disable the voltage feed forward, V_{IN} is connected to a fixed 12V power supply so that the resulting ramp voltage is constant and predictable. This is critical when controlling the system from the DAC in the microcontroller and allows the microcontroller to directly augment the duty cycle of the converter.

Duty Cycle Control with DAC

The duty cycle of the converter is directly controlled from the DAC voltage output. When VIN is connected to a fixed input voltage, the RAMP voltage slews between 0.947V to 1.87V. The resulting equation defines the compare voltage to duty cycle relationship:

$$D = 1.10 \cdot V_{COMP} - 1.06$$

The converter can then be controlled using this equation to map the 0-3.3V output of the DAC to the 0.947-1.87V input needed to cover all ranges of duty cycle. Three resistors are used between the FB

node, one to COMP, one to GND and one to V_{DAC}. The voltage at the FB node will always be 0.6V, so the values of the resistor to GND is chosen based on the desired current. The DAC and COMP resistors can be selected by solving the system of equations:

$$\begin{cases} V_{COMPLO} = 0.6V\left(I_{RGND} - \dfrac{V_{DACHI}}{R_{COM}}\right)R_{FB} \\ V_{COMPH} = 0.6V\left(I_{RGND} - \dfrac{V_{DACLO}}{R_{COMP}}\right)R_{FB} \end{cases}$$

4.3.2 Measurement Circuitry

This section details the development of the voltage and current measurement circuitry, from the theoretical equations governing the circuit design to the design implementation. It will detail plausible design options and the weight factors assessed when choosing an optimal design configuration.

Preliminary Measurement Error Analysis

It was realized that both the voltage and current measurements would produce error relative to the true currents and voltages being measured. The error was modeled by attributing offset and gain parameters to the true values. Gain error terms characterize the difference between an ideal value and the measured value as the ideal value being measured increases. Offset errors reflect the difference between the ideal value and the measured value when the ideal value is zero. This is modeled mathematically in the following equations where ε_{VT} and ε_{IT} are the gain errors and I_{TOS} and V_{TOS} are the offset errors in the measurement circuits.

$$V_{Panel\ Measured} = V_{Panel}\,(1 + \varepsilon_{VT}) + V_{TOS}$$

$$I_{Panel\ Measured} = I_{Panel}\,(1 + \varepsilon_{IT}) + I_{TOS}$$

Depending on how the measurement circuits are constructed, error terms can be additive or destructive to one another. The remainder of this section characterizes how the error in the voltage and current measurement propagate though other calculations made by the system beginning with the power calculation:

$$\begin{aligned} P_{Panel\ Measured} &= V_{Panel\ Measured} * I_{Panel\ Measured} \\ &= [V_{Panel}\,(1 + \varepsilon_{VT}) + V_{TOS}] * [\,I_{Panel}\,(1 + \varepsilon_{IT}) + I_{TOS}] \\ &= [V_{Panel} + \varepsilon_{VT}V_{Panel} + V_{TOS}] * [I_{Panel} + \varepsilon_{IT}I_{Panel} + I_{TOS}] \\ &= V_{Panel}I_{Panel} + \varepsilon_{IT}V_{Panel}I_{Panel} + \varepsilon_{VT}V_{Panel}I_{Panel} + V_{Panel}I_{TOS} + I_{Panel}V_{TOS} \\ &+ \varepsilon_{VT}\varepsilon_{IT}V_{Panel}I_{Panel} + \varepsilon_{VT}V_{Panel}I_{TOS} + \varepsilon_{IT}I_{Panel}V_{TOS} + V_{TOS}I_{TOS} \\ &= V_{Panel}I_{Panel}(1 + \varepsilon_{IT} + \varepsilon_{VT} + \varepsilon_{VT}\varepsilon_{IT}) + V_{Panel}(I_{TOS} + \varepsilon_{VT}I_{TOS}) \\ &+ I_{Panel}(V_{TOS} + \varepsilon_{IT}V_{TOS}) + V_{TOS}I_{TOS} \end{aligned}$$

Since it was designed to keep error terms as small as possible, second order error terms can effectively be truncated. A second order error term results from the multiplication of two first order error terms. The simplification due to the truncation of second order error terms is as follows:

$$P_{Panel\ Measured} \approx V_{Panel}I_{Panel}(1 + \varepsilon_{IT} + \varepsilon_{VT} + \cancel{\varepsilon_{VT}\varepsilon_{IT}}) + V_{Panel}(I_{TOS} + \cancel{\varepsilon_{VT}I_{TOS}})$$
$$+ I_{Panel}(V_{TOS} + \cancel{\varepsilon_{IT}V_{TOS}}) + \cancel{V_{TOS}I_{TOS}}$$
$$\approx V_{Panel}I_{Panel}(1 + \varepsilon_{IT} + \varepsilon_{VT}) + V_{Panel}I_{TOS} + I_{Panel}V_{TOS}$$

Redefining the remaining error terms in the equation for simpler future derivations results in:

$$P_{Panel\ Measured} \equiv P_{Panel}(1 + \varepsilon_P) + P_{OS}$$

Where:

$$P_{Panel} = V_{Panel}I_{Panel}$$
$$\varepsilon_P = \varepsilon_{IT} + \varepsilon_{VT}$$
$$P_{OS} = V_{Panel}I_{TOS} + I_{Panel}V_{TOS}$$

The final calculation made by the system would be the efficiency of the converter, which calculates the power outputted by the converter as a percentage of the power inputted to the converter. The efficiency measurement derivation is as follows:

$$\eta_{Converter\ Measured} = \frac{P_{OUT}(1 + \varepsilon_{P\ Out}) + P_{OS\ Out}}{P_{IN}(1 + \varepsilon_{P\ In}) + P_{OS\ In}}$$
$$= \frac{P_{OUT}}{P_{IN}} \frac{\left(1 + \varepsilon_{P\ Out} + \frac{P_{OS\ Out}}{P_{OUT}}\right)}{\left(1 + \varepsilon_{P\ In} + \frac{P_{OS\ In}}{P_{IN}}\right)}$$

To simplify derivations, the following formulaic relation was used:

$$\frac{1}{1+\epsilon} \approx 1 - \epsilon \qquad (for\ small\ values\ of \epsilon)$$

Implementing the approximation, the efficiency derivations simplify to:

$$\eta_{Converter\ Measured} = \frac{P_{OUT}}{P_{IN}}\left(1 + \varepsilon_{P\ Out} + \frac{P_{OS\ Out}}{P_{OUT}}\right)\left(1 - \varepsilon_{P\ In} - \frac{P_{OS\ In}}{P_{IN}}\right)$$

$$= \frac{P_{OUT}}{P_{IN}}\left(1 + \varepsilon_{P\,Out} - \varepsilon_{P\,In} - \varepsilon_{P\,Out}\varepsilon_{P\,In} + \frac{P_{OS\,Out}}{P_{OUT}} - \varepsilon_{P\,In}\frac{P_{OS\,Out}}{P_{OUT}} - \frac{P_{OS\,In}}{P_{IN}} - \varepsilon_{P\,Out}\frac{P_{OS\,In}}{P_{IN}} - \frac{P_{OS\,Out}}{P_{OUT}}\frac{P_{OS\,In}}{P_{IN}}\right)$$

$$= \frac{P_{OUT}}{P_{IN}}\left(1 + \varepsilon_{P\,Out} - \varepsilon_{P\,In} - \varepsilon_{P\,Out}\varepsilon_{P\,In} + \frac{1}{P_{OUT}}(P_{OS\,Out} - \varepsilon_{P\,In}P_{OS\,Out}) - \frac{1}{P_{IN}}(P_{OS\,In} + \varepsilon_{P\,Out}P_{OS\,In}) - \frac{P_{OS\,Out}}{P_{OUT}}\frac{P_{OS\,In}}{P_{IN}}\right)$$

Truncating second order error terms yields:

$$\approx \frac{P_{OUT}}{P_{IN}}\left(1 + \varepsilon_{P\,Out} - \varepsilon_{P\,In} \cancel{- \varepsilon_{P\,Out}\varepsilon_{P\,In}} + \frac{1}{P_{OUT}}(P_{OS\,Out} \cancel{- \varepsilon_{P\,In}P_{OS\,Out}}) - \frac{1}{P_{IN}}(P_{OS\,In} \cancel{+ \varepsilon_{P\,Out}P_{OS\,In}}) \cancel{- \frac{P_{OS\,Out}}{P_{OUT}}\frac{P_{OS\,In}}{P_{IN}}}\right)$$

$$\approx \frac{P_{OUT}}{P_{IN}}\left(1 + \varepsilon_{P\,Out} - \varepsilon_{P\,In} + \frac{P_{OS\,Out}}{P_{OUT}} - \frac{P_{OS\,In}}{P_{IN}}\right)$$

$$\approx \frac{P_{OUT}}{P_{IN}}(1 + \varepsilon_{P\,Out} - \varepsilon_{P\,In}) + \frac{P_{OS\,Out}}{P_{IN}} - \frac{P_{OUT}P_{OS\,In}}{P_{IN}^2}$$

It was noted that the mathematical model for the error revealed that the offset error terms would dominate when the power being measured approached zero. Another observation made was that error terms in the input measurement are subtracted from error terms in the output measurement, thus the overall error could be significantly reduced if the same circuitry (possessing the same error terms) were used to make the measurements. It was impossible to use the same circuit to measure current and voltage in two different locations at the same time, especially if the ranges in what was to be measured varied. The circuits could be closely matched to one another but the error terms can vary. One way to reduce the overall error was be to use the same analog to digital converter when digitizing the input and output measurements. Digitizing the measurement values introduced some error in the measurement and was unavoidable if signals were to be processed by a microcontroller. In this way, the ADC would introduce the same error in the input measurement and output measurement. This would only reduce parts of the total error in the two measurements but these parts would effectively cancel one another out in the efficiency calculation.

Voltage Measurement and Analysis

Originally, the voltage measurement circuit was designed as a voltage divider circuit with a signal buffer to the ADC (see Figure 25).

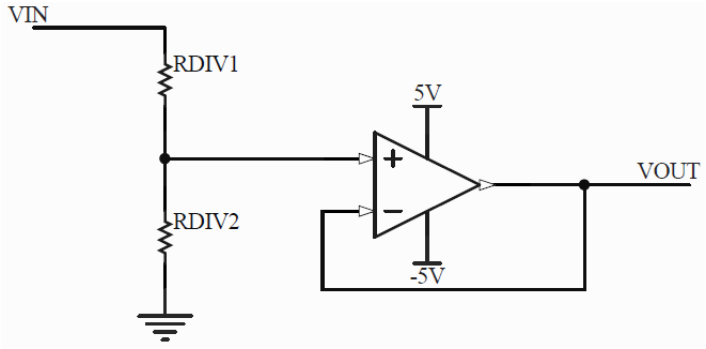

FIGURE 25: VOLTAGE MEASUREMENT CIRCUIT DESIGN 1

A resistor network would be sized to scale the measured voltages (ranging from 0V-50V), and map it to the range of voltages that can be measured by the ADC (ranging from 0V-4.096V) and an operational amplifier would serve to buffer the input signal. One major downfall of this circuit configuration would be the introduction of noise via ground loops. The accuracy of a measurement can be affected by ground loops present in adjacent circuitry. The common conductor in all electric circuitry is referred to as the ground (or common) conductor. In an ideal circuit is seen in Figure 26.

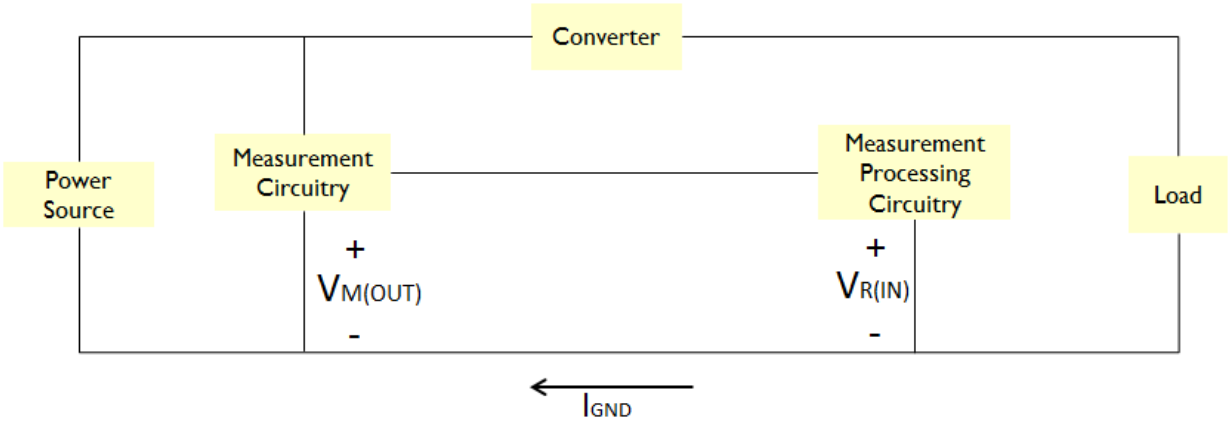

FIGURE 26: IDEAL ELECTRICAL SYSTEM W/ EMBEDDED MEASUREMENT CIRCUITRY

The ground conductor is the connection shared by most if not all elements that comprise a circuit. A converter would also have a ground connection, but this connection is left out of the figure for clarity. Ideally, this ground conductor has no losses attributed by the current flowing through it. By Kirchhoff's Voltage Law:

$$V_{R(IN)} = V_{M(OUT)}$$

In reality, there are losses in both conductors. However if the input impedance of the measurement processing circuitry is orders of magnitude larger than the impedance of the conductor between the measurement circuitry and the processing circuitry, the recorded value of the measurement will not be effected too much if at all. The real problem occurs when other circuitry shares the same ground conductor. Current flowing through the ground conductor, which has non-ideal impedances associated with it, produces a noise voltage on the conductor (see Figure 27).

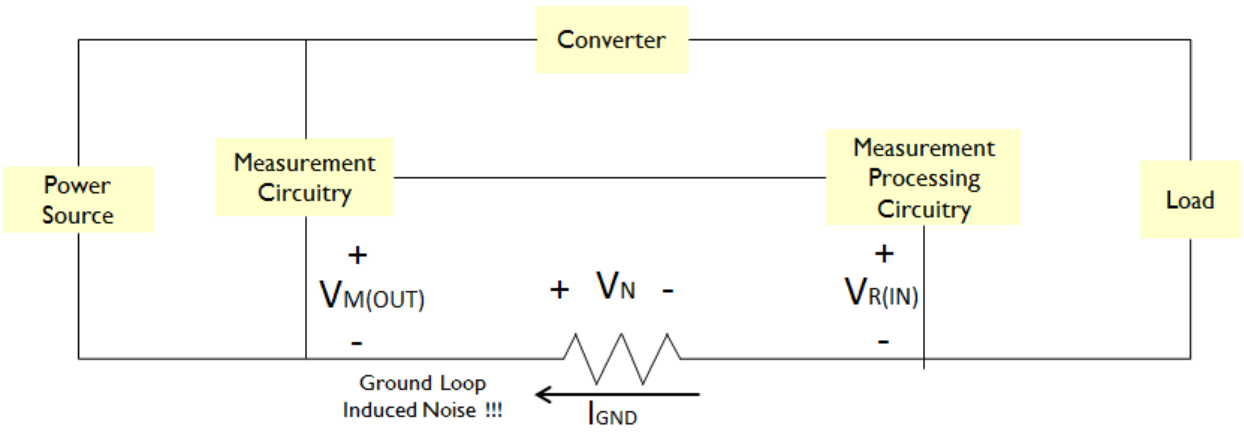

FIGURE 27: ACTUAL EMBEDDED MEASUREMENT CIRCUITRY

The measurement processing circuitry is picking up noise in addition to the output of the measurement circuitry. Applying Kirchhoff's Voltage Law around the loop reveals:

$$V_{R(IN)} = V_{M(OUT)} + V_N$$

In this configuration, the impedance of the ground conductor and ground current directly affect the measurement recorded. A DC-DC converter produces an output ripple current making the noise voltage vary with time. This ground loop would appear in both the input and output measurements.

One method to overcome the ground loop noise is to implement isolation. Isolating between circuits involves transmitting analog or digital signals over an isolation barrier from one circuit to another **[26]**. Isolation, when implemented correctly offers additional benefits, one of them being an increase in measurement accuracy. Isolation techniques are used to eliminate ground loops between power level and signal level componentry by allowing the different levels to have their own separate grounds. An isolation topology is depicted in Figure 28.

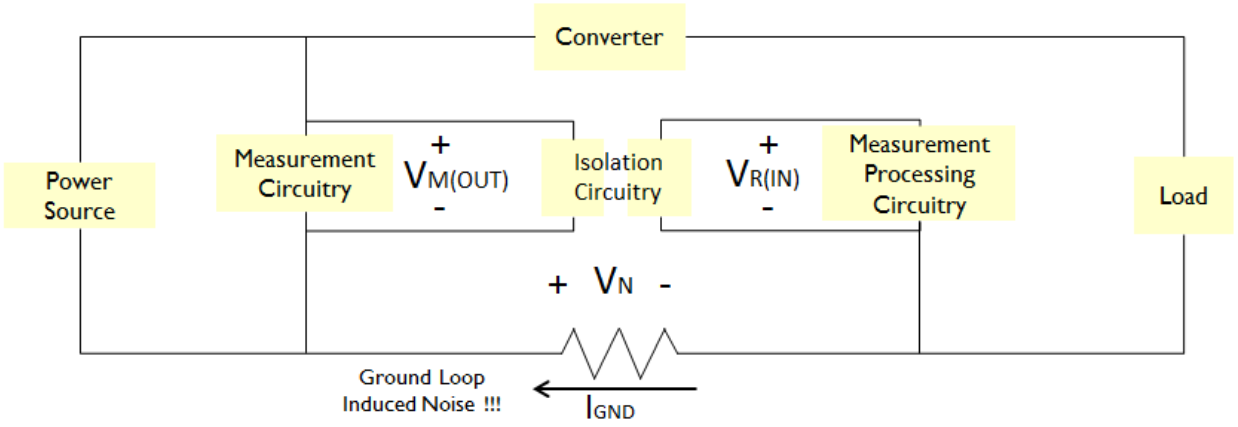

FIGURE 28: EMBEDDED MEASUREMENT CIRCUITRY USING ISOLATION

The loop between the measurement circuitry and the measurement processing circuitry is broken, $V_{R(IN)}$ is dependent upon the transmission and reception of $V_{M(OUT)}$ over the isolation barrier.

One particular method of isolation involves using optics. Optical isolation allows communication between two physically separated circuits by transducing a voltage level into a specific light intensity with one circuit and then converting it back into a voltage level with another circuit. The isolation barrier is overcome by transmitting and receiving light and mapping it to specific voltage values. For example, an LED can be implemented in the first circuit and the desired measurement will drive the LED to emit light. The light is then transduced into a current by a photodiode within the second circuit **[26]**.

A linear optocoupler performs the above optical isolation. The linear optocoupler uses an LED to emit light waves and two photodiodes to sense the intensity of the light output by the LED. One photodiode is used to transduce the light intensity into a current related to the voltage input driving the LED. A second photodiode is to be configured to provide negative feedback for the circuit driving the LED. This feedback is required to overcome the non-linearity of the LED over time and temperature **[27]**. Using a trans-conductance circuit, the current produced by first photodiode can be translated back into a voltage level linearly related to the input voltage measurement **[28]**. An example circuit configuration can be seen in Figure 29.

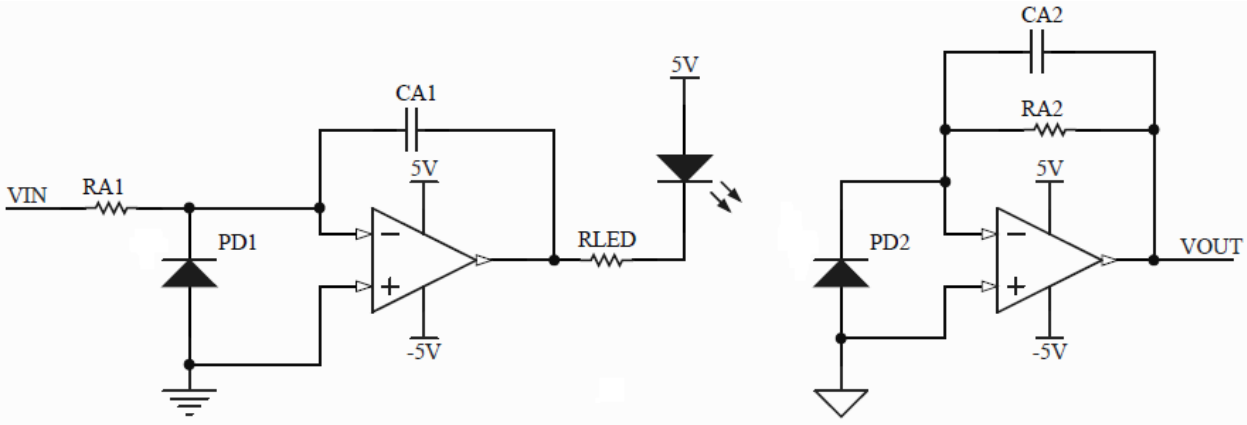

FIGURE 29: OPTOCOUPLER APPLICATION CIRCUIT [**29**]

Adopted from Avago Industries optocoupler applications circuit, the photodiodes PD1, PD2, and the LED are contained within the same integrated circuit **[29]**. The op-amp on the left is used with the photodiode PD1 to keep the LED light intensity linear with the voltage input from the solar panel. Photodiode PD2 is used to transduce the light intensity output by the LED into a current. The second op-amp is configured as a trans-conductance amplifier to convert the current output of PD2 into a voltage. Notice that the ground on the input and output sides of this optocoupler application circuit are at different potentials. In this configuration, there is no electrical path for the currents of the input circuit to couple noise into the measurement. In this schematic, the resistors R_{A1} and R_{A2} are used to scale the panel voltage, while R_{LED} is used to limit the LED current. The capacitors C_{A1} and C_{A2} are used to keep the system stable. The system is governed by the following equation:

$$V_{OUT} = \frac{R_{A2}}{R_{A1}} \frac{K_2}{K_1} V_{IN}$$

Where K1 is the proportionality constant between the current in PD1 and the LED current and K2 is the proportionality constant between the current in PD2 and the LED current.

One added benefit to implementing isolation is that it would prevent the conduction of any large currents from the power level circuits into the signal level circuitry [**26**]. This would be desired since the voltages and currents from the panel are much larger than the voltages and currents of the ADC and microcontrollers.

Another way to eliminate ground loop noise is to reject it as a common mode voltage. That is, if the noise voltage is common to two inputs of a balanced circuit it is then subtracted from itself (rejected). One method of balancing involves using a differential amplifier (see Figure 30).

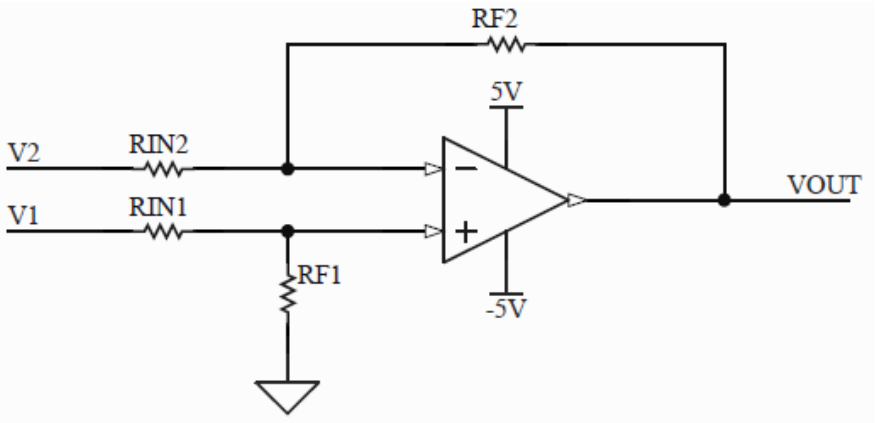

FIGURE 30: DIFFERENTIAL AMPLIFIER CIRCUIT

The differencing op-amp configuration outputs a scaled version of the difference at its voltage inputs. The equation governing the output of this circuit is as follows:

$$V_{OUT} = \frac{R_{IN2} + R_{F2}}{R_{IN1} + R_{F1}} * \frac{R_{F1}}{R_{IN2}} V_1 - \frac{R_{F2}}{R_{IN2}} V_2$$

The formula simplifies when $R_{F1} = R_{F2} \equiv R_F$ and $R_{IN1} = R_{IN2} \equiv R_{IN}$ to:

$$V_{OUT} = \frac{R_F}{R_{IN}} (V_2 - V_1)$$

In this configuration, only the difference between the two input voltages will be attenuated or amplified. Figure 31 inserts this into the embedded measurement design.

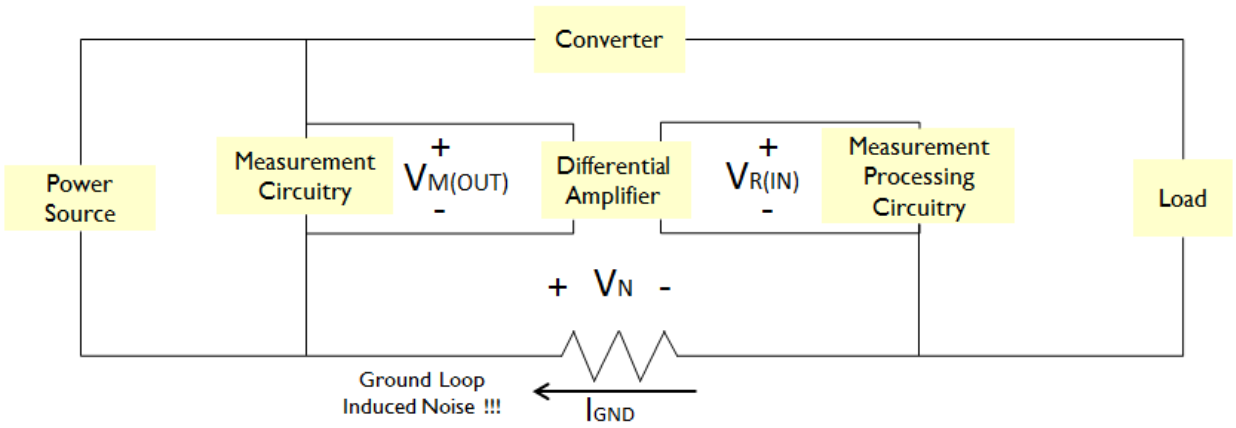

FIGURE 31: EMBEDDED MEASUREMENT CIRCUITY USING DIFFERENCE AMPLIFICATION

Taking the difference amplifier's ground reference to be the signal ground of the measurement processing circuitry will increase the accuracy of the measurement. The ground loop noise voltage is common to both inputs of the op-amp and an op-amp inherently rejects the common mode. The measurement circuitry will only see the scaled version of the difference at the input. It should be noted that this circuitry does not provide any galvanic isolation between the power and signal level circuits.

Optical isolation and circuit balancing/common mode rejection both have their advantages and disadvantages. Optical isolation provides additional protection for the signal level circuitry while the difference amplifier configuration does not. Optical isolation would introduce additional error compared to the circuit balancing technique due to the additional circuitry needed to optimize isolation. Further analysis was conducted to investigate the difference between the proposed error introduction by the differential amplifier circuit and the optocoupler measurement circuit (see Table A-1in Appendix).

The circuits in Figure 29 and Figure 30 were configured to map the 0V-50V output of the panel to the 0V-4.096V input of the analog to digital converter. Sweeping the input of each circuit configuration from 0V-50V, the outputs were measured to see how well each circuit maps the voltage levels. Utilizing this range of inputs would characterize the error more precisely because the voltage measurements vary more widely at the output of the panel. Lines of best fit were used to model circuit calibration; the errors between the measurements made by each circuit following calibration are plotted in Figure 32.

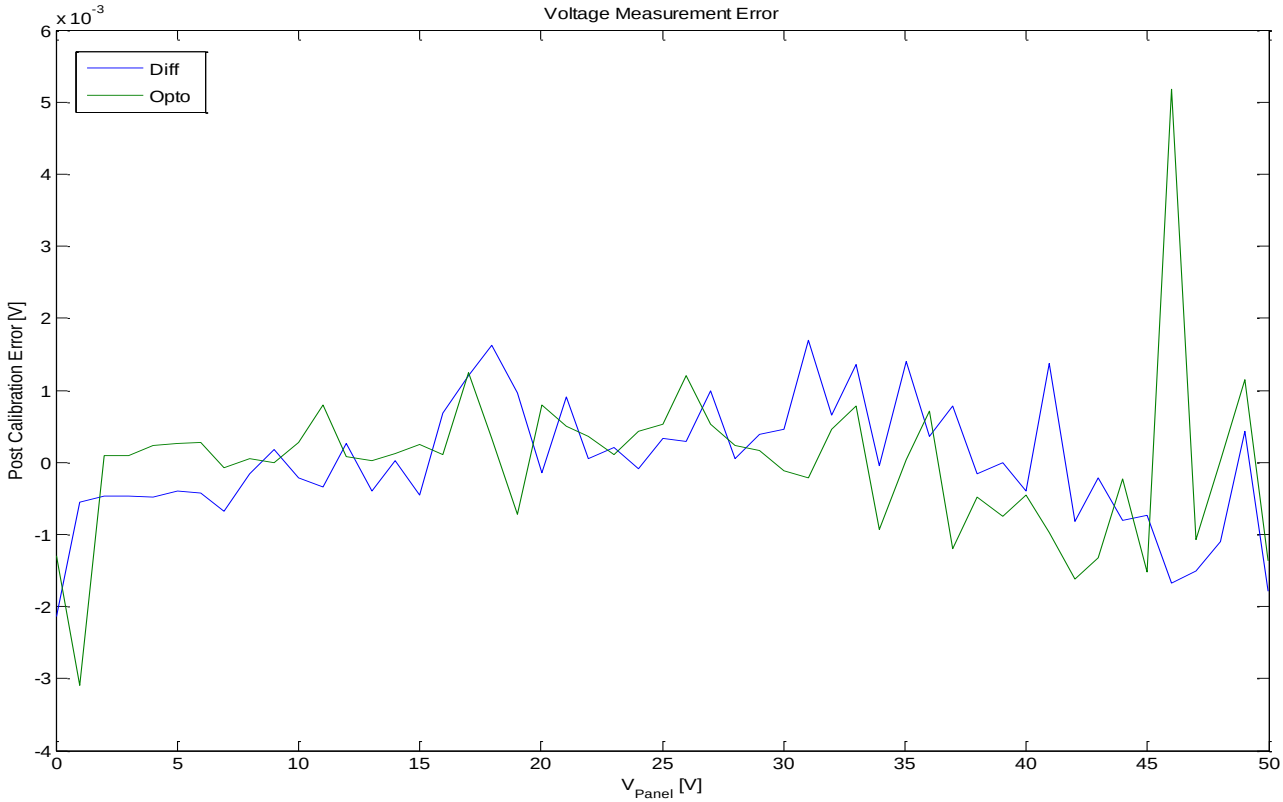

FIGURE 32: VOLTAGE MEASUREMENT ERROR ANALYSIS 1

It was observed that the error in the differential amplifier circuitry and the error in the optical isolation circuitry were bounded within approximately the same range except at one point. Attributing this spike to possible errors made in measurement (such as a copy error) and noting only one occurrence of this spike in error, it was removed from the data set. Figure 33 plots the data without this one data point.

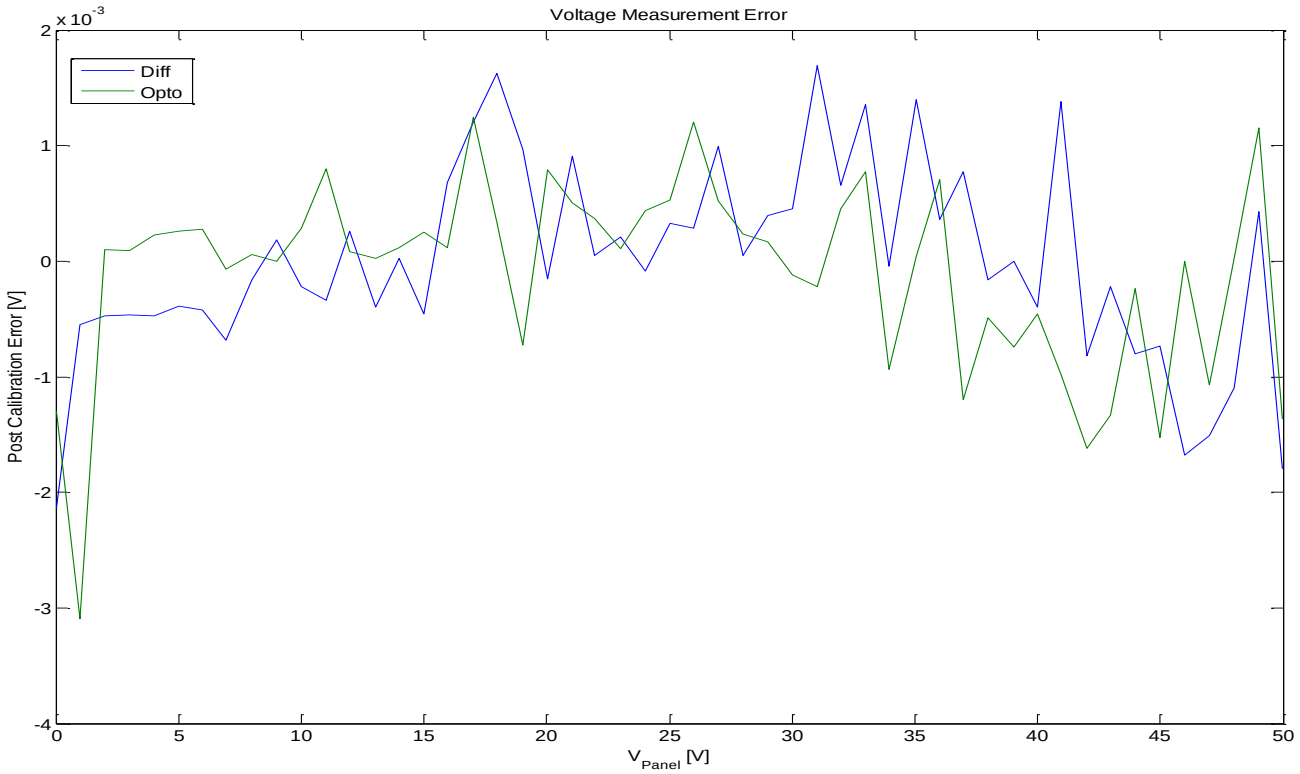

FIGURE 33: VOLTAGE MEASUREMENT ERROR ANALYSIS 2

Removing the one outlying data point, the errors in both circuit topologies were observed to be relatively the same with the largest errors occurring at low voltage inputs. This could be due to the offset voltages of the operational amplifiers used in the circuit topologies. Also interpreted from the plot is an overall nonlinearity in the error as the input voltage increases possibly a resultant of the non-linearity in the digital multi-meter used to record the measurements. Further analysis was needed to eliminate the possibility of the multi-meters non-linear contribution to the errors recorded. In the interest of time, the difference amplifier topology was implemented to make voltage measurements on both the input and output sides of the converter.

Current Measurement and Analysis

Direct Current can be measured through a variety of techniques ranging in complexity and accuracy. One of the simplest and most common is the current shunt, which uses a small resistance in series with the current being measured. The voltage drop across the resistance can be measured and then using ohms law and the resistance value, a current value can be calculated. This technique however causes several problems; first, a special differential amplifier circuit must be designed that can measure a small difference in voltage that is up to 50 volts from the system ground, second the resistance causes an energy loss that is dissipated through heat, reducing the efficiency in a system where the highest efficiency possible is a design goal.

A second option that was considered utilizes a Hall-Effect sensor, of which the project sponsor, Allegro Microsystems, had several product offerings. These types of current sensors use the voltage produced by the Hall Effect created when the magnetic field produced by a current in a nearby conductor passes

through a semiconductor. Hall Effect sensors do not require an electrical contact to the conductor, eliminating the issue with the current shunt sensor. The Hall Effect sensor only requires being next to a conductor carrying the current, eliminating most power losses cause by the current shunt. It also provides galvanic isolation between the actual current measured and the current measurement signal. The only remaining concerns were the accuracy of such a configuration, as very small hall voltages must be amplified before being digitized. Because of the sponsorship by Allegro Microsystems, and Allegro's reputation in Hall Effect current sensors, the ACS71X line of Hall Effect sensors were chosen to measure the current into and out of the module. The ACS71X line includes sensors in the 0-50A range, suitable for our project, without extra unnecessary logic [**30**]. Several ACS712 evaluation boards were obtained from Allegro and used in the prototype designs.

The op-amp circuitry as seen in Figure 34 was designed to map the output of the Hall Effect sensor to the input range of the ADC.

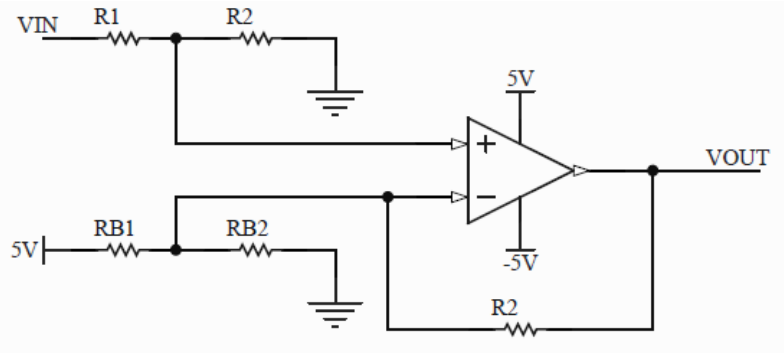

FIGURE 34: ACS712 CURRENT MAPPING CIRCUITRY

By creating a bias at the inverting input of the operational amplifier, it will be subtracted from V_{IN}. Figure 35depicts the same circuit using Thévenin's theorem.

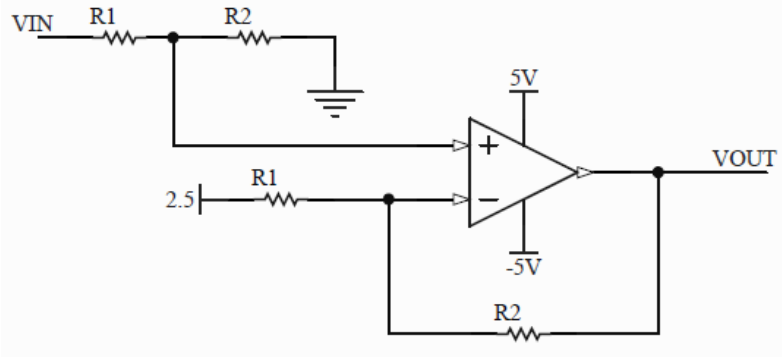

FIGURE 35: SIMPLIFIED CURRENT MAPPING CIRCUIT

Under the condition where $R_{B1} = R_{B2} \equiv 2R_1$ the bias circuit's Thévenin voltage computes to 2.5 V and the Thévenin resistance of this bias circuit becomes R_1. At low frequencies, the transfer function of this circuit equates to the following:

$$V_{OUT} = \frac{R_2}{R_1}(V_{IN} - 2.5)$$

4.3.3 Analog to Digital Converter

An analog to digital converter (ADC) was necessary to convert the voltage signals from the buffer amplifiers to a digital value usable by the microcontroller. Several different constraints were required for the ADC selected.

The first requirement was precision. As detailed in the previous measurement circuitry section, the measurement system needs to be accurate enough to allow comparison of the converter efficiency between systems. From these requirements, we calculated that the ADC should have at least 16-bits of accuracy. The next requirement was sampling rate. In order to update the maximum power point algorithm at a rate of at most 100Hz we need a sampling rate of at least 400Hz because there are four channels to sample for each iteration of the algorithm. The final requirement is a 0-5v voltage input range to accommodate the 0-5v output of the Hall Effect current sensor.

From these requirements, the Analog Devices AD7689 was chosen for analog to digital conversions. This part features eight separate channels multiplexed to a successive approximation register ADC. It includes an onboard 4.096V reference and a SPI interface. This part was also attractive because of the relationship the laboratory has with Analog Devices, granting access to evaluation boards and part samples.

4.3.4 Microcontroller Selection

The microcontroller in the solar energy harvester serves- many different purposes, including:

- Communication with ADC including sample triggering
- Computation of the maximum power point tracking algorithm at 100 Hz
- DAC output control the duty cycle of the DC-DC converter
- Monitoring converter status
- Communication with PC for data reporting and control
- Communication with other identical solar converters over I2C bus
- Battery status monitoring and control
- External load control for correct discharge of connected batteries

The microcontroller selected for the converter module needed to perform all these functions with as little external hardware as possible. Because of the team's familiarity with the MSP430 series of microcontrollers from Texas Instruments, the MSP430F2616 microcontroller was chosen. This microcontroller has 4 universal serial communication interfaces, two supporting standard serial communication needed for RS-485 communication over long distances and PC serial port communication, and two support SPI and I2C communication necessary for interfacing with the Analog Devices ADC over SPI and communicating with other identical converts via an I2C bus. In addition to the multitude of communication interfaces supported, this device contains two digital to analog converter channels suitable for control of the DC-DC converter duty cycle required for maximum power point tracking.

4.3.5 Circuit Power Supplies

The solar energy harvester board needed several different voltages in order to operate each of the different subsystems. The first revision of the PCB was be powered externally, while the second revision

possessed onboard power rails. These voltages are 12V, 5V, -3.3V, and -5V. An approximate power budget for each of the loads and the total power provided by the sources are listed in Table 7.

Rail:	Circuit:	Current Draw:	Power Draw:
12V	Converter	40mA	480mW
	Off board Relays (2)	60mA	720mW
	Total	**100A**	**1.2W**
5V	Hall Effect Sensors	20mA (2)	100mW (2)
	Op Amps	2mA (2)	10mW (2)
	ADC	2mA	10mW
	Total	**44mA**	**230mW**
3.3V	Microcontroller	60mA	198mW
	ADC	5mA	165mW
	I2C Isolator	3mA	9.9mW
	RS232	3mA	9.9mW
	Total	**71mA**	**234mW**
-5V	Op Amps	2mA (2)	10mW (2)
	Total	**4mA**	**20mW**

TABLE 7: POWER BUDGETING DATA

The 12V, 3.3V and -5V supplies all feed off the 5V supply. It is assumed that each of these systems would have an efficiency of 80% in a worst-case scenario per the part data sheet. Based on this merit, the worst-case current power draw of the system is calculated as follows:

$$Max\ System\ Power\ Draw = \frac{1}{0.8}\left(\frac{1}{0.8}\cdot 1.2W + \frac{1}{0.8}\cdot 0.234W + \frac{1}{0.8}\cdot 0.01W\right) + \frac{1}{0.8}\cdot 0.230W$$

$$= 2.54W$$

The 12V Rail was a non-isolated boost converter based on the National Semiconductor LMR62014. The converter boosts the 5V-regulated rail up to 12V. The rail is designed for 200mA, twice the specified power draw. The part selection was completed based on the national semiconductor WeBench design tool as well as the recommended values in the datasheet for the input and output capacitances, feedback resistors, inductor and recirculating diode.

The 5V Rail is a non-isolated buck converter based on the National Semiconductor LMZ14201 power module with integrated synchronous FETs and inductor. The module is capable of supplying 1A of output current, nearly twice the 508mA worst case draw of the 5V loads and the 12V, 3.3V and -5V power supplies. The input to this supply is a diode-OR between the output of the main solar buck converter that charges the batteries or an isolated external wall adapter. The external auxiliary input must be an isolated topology and cannot be shared with other converter boards unless it is isolated from them in order to prevent undesirable ground loops. The diode OR allows the board to rely on external power only when the battery voltage is low, ideally a 12V supply would be used as the fully charged lead acid batteries' float voltage is between 12-14V. The board can be forced to use the external power supply by using a higher voltage power supply such as a 24V supply. In any case, the

external supply should be capable of supplying at least 2.5W. The part selections for this converter were taken from the recommended values in the data sheet. Resistors values were calculated for an under-voltage lockout of 8V, at which point the converter will shut down, causing all other systems on the board to shut down. This will only occur if an external auxiliary power source is not connected and the battery use is improperly managed by the microcontroller.

The 3.3V Rail is a buck converter based on the National Semiconductor LM3670 buck converter with integrated recirculating diode and switching FET. The module only has and input and output capacitor and an inductor. The part values were based on the recommendations and calculations in the data sheet. The rail is designed to supply up to 200mA, nearly three times the worst-case current draw.

The -5V Rail is charge pump based on the TPS60402, 50 kHz controllers. Using only three 3.3uF capacitors, this unregulated charge pump relies on the pre-regulated voltage of the 5V rail to supply up to 60mA of output current, well in excess of the op-amps current needs.

4.3.6 Isolation

There are many situations where different parts of a system need to be electrically isolated between their respective power and ground rails in order to prevent interference and stray ground currents. Because the currents running between the panel and the battery may be in excess of 20A, relatively high voltage drops due to the small resistance of the PCB copper will appear across ground and power planes on the order of a few hundred millivolts. As the converter switches on and off, these voltage drops across a given plan will change with the switching of the converter, an undesired effect commonly known as "ground bounce" in the ground plane. If other components are in the path of these high currents, there ground reference will change relative to other components causing errors in readings. In addition, should there be any ground that travel off board and eventually meet battery or panel ground terminals, high stray currents may flow through these conductors, creating the possibility of significant losses, overheating of unrated cables and opportunities for interference with other off board devices.

The solar energy harvester board is designed for communication between boards so that multiple boards may charge the same batteries, communicating between a board and a computer for data collection, and off-board auxiliary power to keep the system online at all times. All off board connections must be isolated with magnetic or optical galvanic isolation in order to prevent ground loops between boards and common panel and battery grounds. For the serial communication busses, this is accomplished with analog devices iCoupler components that use on chip transformers to achieve isolation. While the first board revision utilizes off board isolated lab power supplies, the second revision allows for a 2.1mm DC jack connection, which is designed for 12V-isolated input from a wall-wart style adapter. It is the users responsibility to assure that this supply is indeed isolated, and that all other connection though the auxiliary IO and power terminals do not create additional grounding connections.

4.3.7 Communication

The Revision 2 Solar Energy Harvester Boards each have two off board serial connections to facilitate communication between multiple boards, and between a single board and a computer. These connections are located on the left middle side of the board. There is one isolated RS232 Serial connection, and one isolated I2C connection. Both of these connections need power on the off board

side, but this power source can be shared among all boards and can be between 3-5V. RS232 Isolation is accomplished with the Analog Devices ADUM3211 general-purpose isolator and ADUM1250 I2C isolator.

4.3.8 Load Control and Auxiliary IO

Revision 2 of the Solar Energy Harvester board has eight microcontroller ports broken out on the right side of the board, as well as each voltage supply rail and four ground terminals. It is important to understand the purpose and limitations of these ports. The purpose of these ports it to allow for the interfacing of additional functionality, especially concerning the driving of relays for loads. The availability of these ports means that wide variety of possible solutions for integration with loads and other devices such as sensors and switches can be accomplished with the Solar Energy Harvester.

Any load attached to the battery terminals should be controlled for two reasons: to provide an over-current protection, and to shut the load off when the batteries become discharged to prevent over-discharge. More complex load control may be added in future projects, such as regulated voltage rails, isolated outputs, integrated overcurrent protection, switching, and so on. The simplest way to achieve control of a load is with a simple transistor controlled relay. The microcontroller is not capable of driving more than 20mA at 3.3V, so the actuator coil of a relay should be driving with a transistor such as the ULN2803 Darlington NPN Transistor Array. The 12V rail had 60mA of current budgeted for driving relays. It is important that when making these connections, the ground of the transistor or relay should not be tied to the battery ground, only to the designated ground pins on the board, in order to prevent ground loops.

4.4 Software Design

The code running on the microcontroller was written in C with Code Composer Studio and loaded onto the MSP430F2616 via a MSP-FET430UIF JTAG interface. The code was written to accomplish the following functions:

1. Using the SPI to the ADC, trigger the ADC to sample each channel, and transfer the data from the ADC to the microcontroller memory.
2. Enable or disable the converter based on the input voltage required to startup the converter.
3. Calculate the input power from the ADC measurements.
4. Use the current and previous power measurements to calculate the maximum power point tracking algorithm output.
5. Update the digital to analog converter channel that controls the converter duty cycle with the output of the maximum power point tracking algorithm.
6. Report all ADC measurements over the PC serial communication bus for logging.

Each of these functions was executed sequentially in the main loop of the program with the MPPT algorithm update rate controlled by a delay at the end of the loop.

5 Measurements and Results

With the groundwork for the system design laid out, first a variable load was created and tested for a proof-of-concept of the system. Once realized an initial PCB iteration of the panel manager board was developed and tested for its functionality. The following subchapters document the findings.

5.1 Variable Load for Panel Interrogation

Before the completion of the first PCB based prototype, a dynamic load system was developed to interrogate some of the characteristics of the solar panels. This allowed for the confirmation of the solar panel characteristics and the development of the panel voltage and current measurement systems.

The system consisted of a series of five air-core resistors connected in parallel through power MOSFETs to allow the resistors to be switched in and out of parallel connection with the panel. A sixth MOSFET short-circuited the panel. This resulted in a crude variable load for the solar panel. These MOSFETs were then controlled by a general-purpose input/output port that a MATLAB script, running on a PC, would use to switch each of the MOSFETs in a binary counted fashion. For each combination of resistors (including open-circuit and short-circuit configurations), the MATLAB script recorded the voltage across the solar panel, and the current output of the panel using two HP 34401A multi-meters connected to the computer via a General Purpose Interface Bus (GPIB). The multi-meter measuring the voltage was connected directly across the solar panel leads, while the multi-meter measuring the current was connected to the voltage output of an Allegro Microsystems ACS712 Hall-Effect current sensor evaluation board, which was connected in series between the panel and the switchable resistor load.

Once the load was verified to work with a current limiting power supply, it was connected to the first of the 230W Sun Power Panels (SPR-230-WHT-U) installed on the Atwater Kent Laboratories Roof. The MATLAB script took a measurement through the entire range of the load every few seconds for the duration of a day. The resultant family of I-V curves plotted over time can be seen in Figure 36.

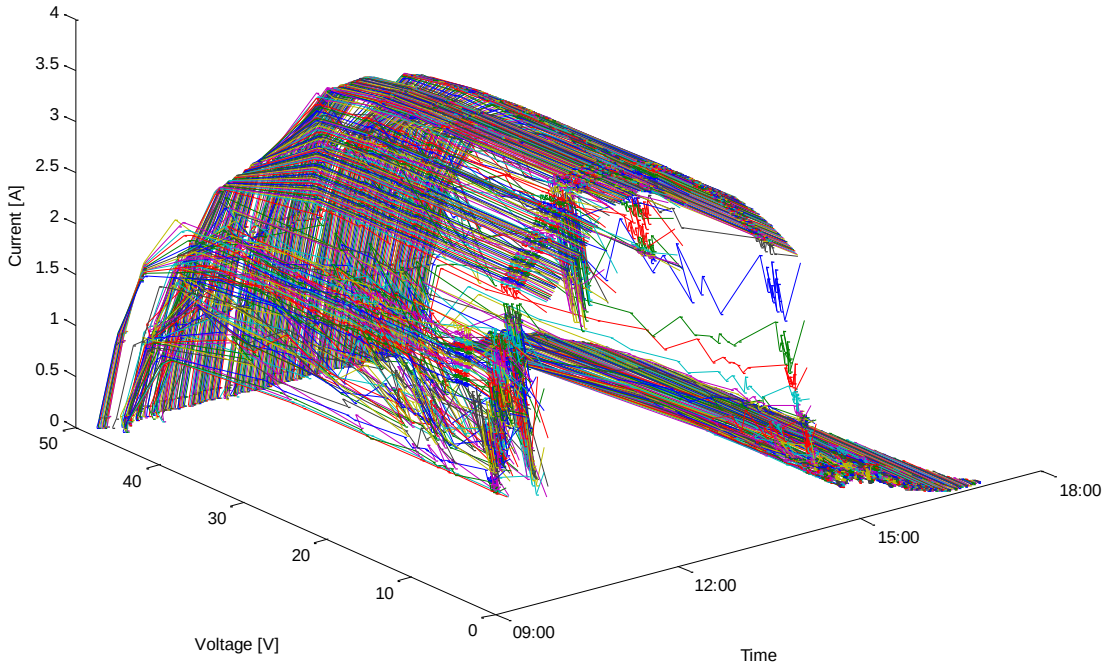

FIGURE 36: SOLAR PANEL CURVES OVER ONE DAY

While the system was not perfectly matched to the solar panel characteristics, it produced usable results. Mainly, the resistors that were available to use in the system were not matched in a way that interrogated the solar panel I-V characteristic in an even fashion. Additionally, the digital multimeters and general purpose interface bus (GPIB – IEEE-488) used to communicate with the multimeters was particularly slow. Several minutes were required to acquire the 64 different data points taken for each I-V curve, and seemingly random jagged data points are most likely because the points were not taken in an orderly fashion along the I-V curve and because cloud cover was obstructing the panel at a frequency higher than that to interrogate the whole I-V curve.

5.2 Converter Circuitry

5.2.1 PCB Revision 1

The first PCB revision was nearly identical to the second PCB revision in terms of the converter with the exception of the input LC filter, which was omitted from the second revision, and the ideal diode controller to prevent reverse current, which was included in the second PCB revision. The first revision was successfully tested when configured in constant voltage mode at a power of 200W. At this power, and efficiency of 93% was measured using current and voltage meters on the input and output terminals.

5.2.2 PCB Revision 2

The second PCB revision contained minor design and layout changes so improve the grounding and efficiency of the converter. The input voltage, output voltage, switch node voltage, high side gate drive, and low side gate drive waveforms were all studied and recorded. Figure 37 and Figure 38 show the input and output voltage waveforms respectively, with the input waveform yielding ripple voltage of less

than 200mV and the output waveform yielding a ripple voltage of less than 20mV. There is some switching raining in these nodes, but this noise is of little consequence as the battery and the solar panel are nearly ideal current sources and sinks and are not negatively impacted by the waveforms.

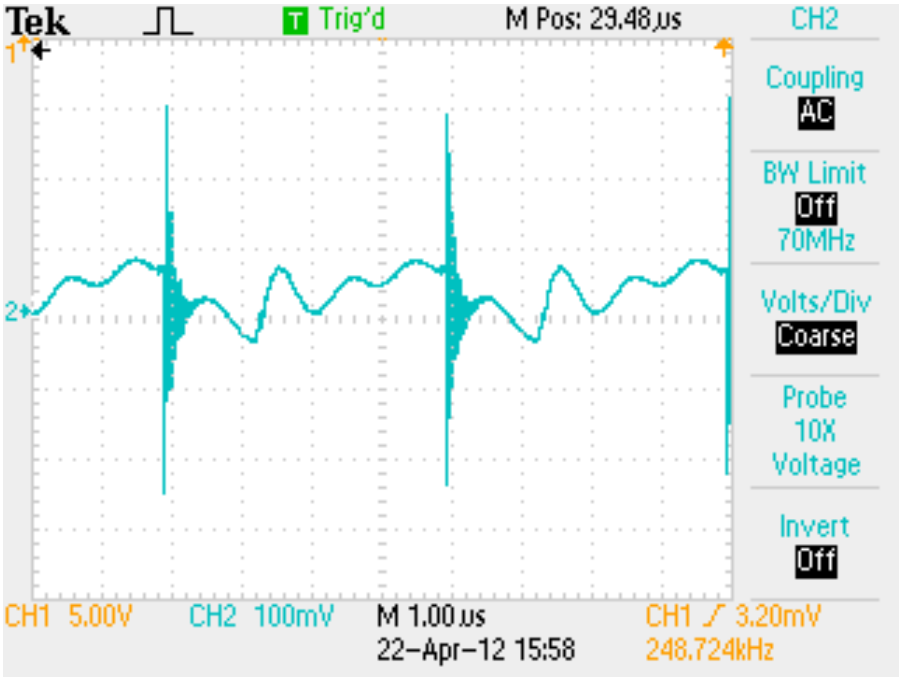

FIGURE 37: INPUT VOLTAGE RIPPLE

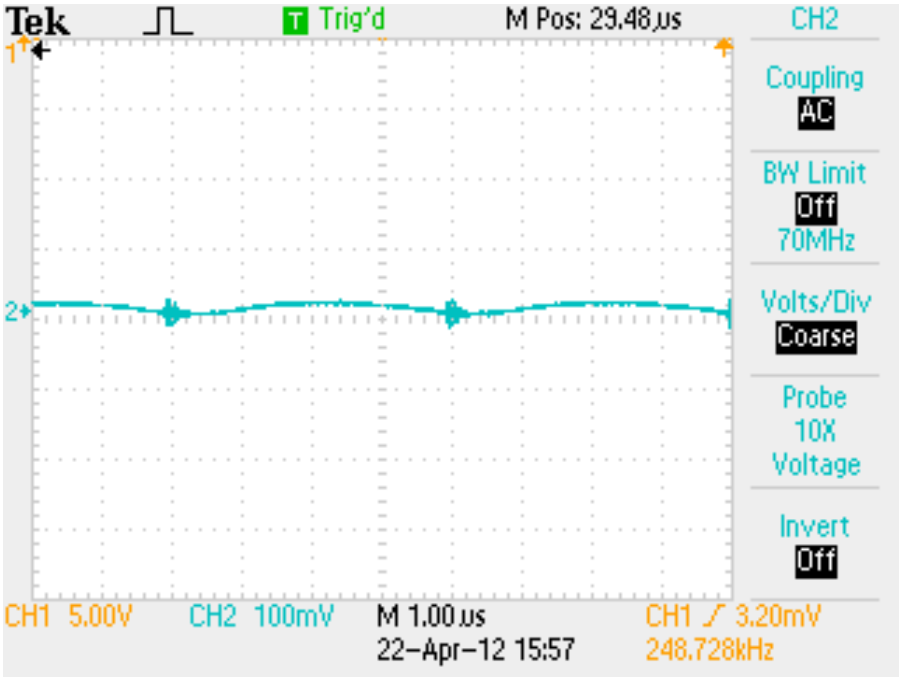

FIGURE 38: OUTPUT VOLTAGE RIPPLE

The switch node swings from 0V to the 40V input (see Figure 39. In this instance, the converter is being tested at 100W. The node exhibits a small second order ringing transients, which can result in greater switching losses. Footprints are available for creating an RC snubber to damn these transients, but the footprints were not large enough and the additional parts values necessary to design the snubber could not be ordered in time. Future revisions should address these issues in order to mitigate losses.

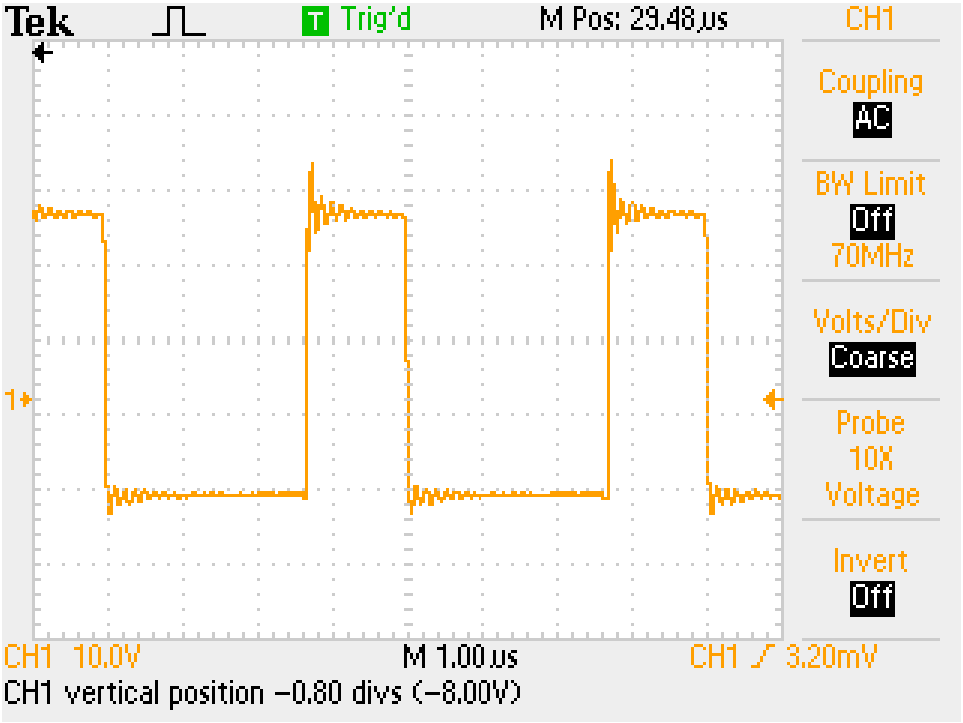

FIGURE 39: SWITCHING NODE WAVEFORM

Figure 40 and Figure 41 show the low side and high side MOSFET drive, and the dead time between low side and high side gate switching can be seen when comparing the two images. The high side has significant gate ringing which may be able to be addressed by placing a small resistance before the MOSFET gate.

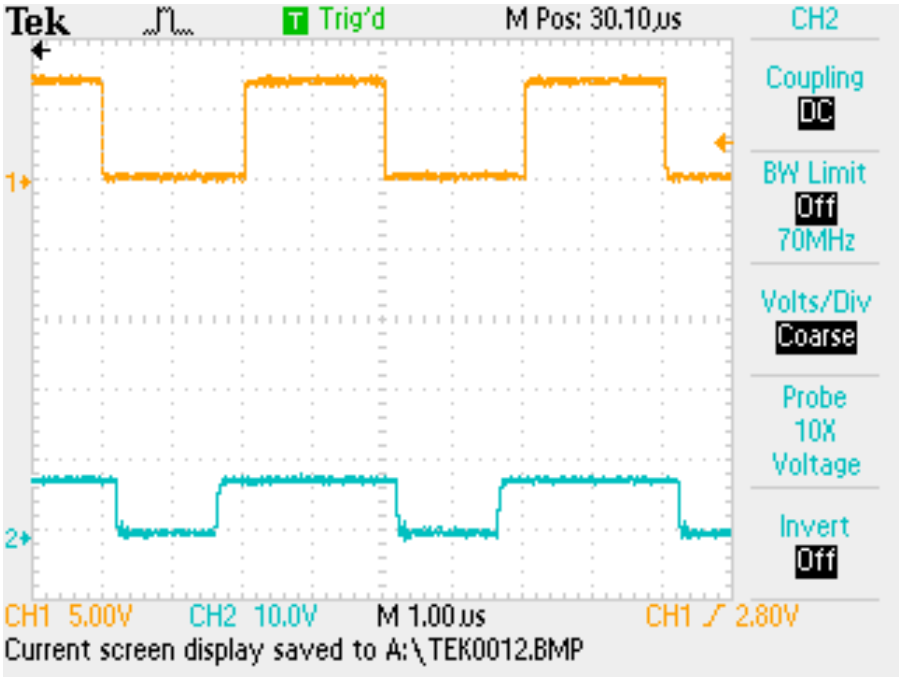

FIGURE 40: LOW SIDE MOSFET DRIVE

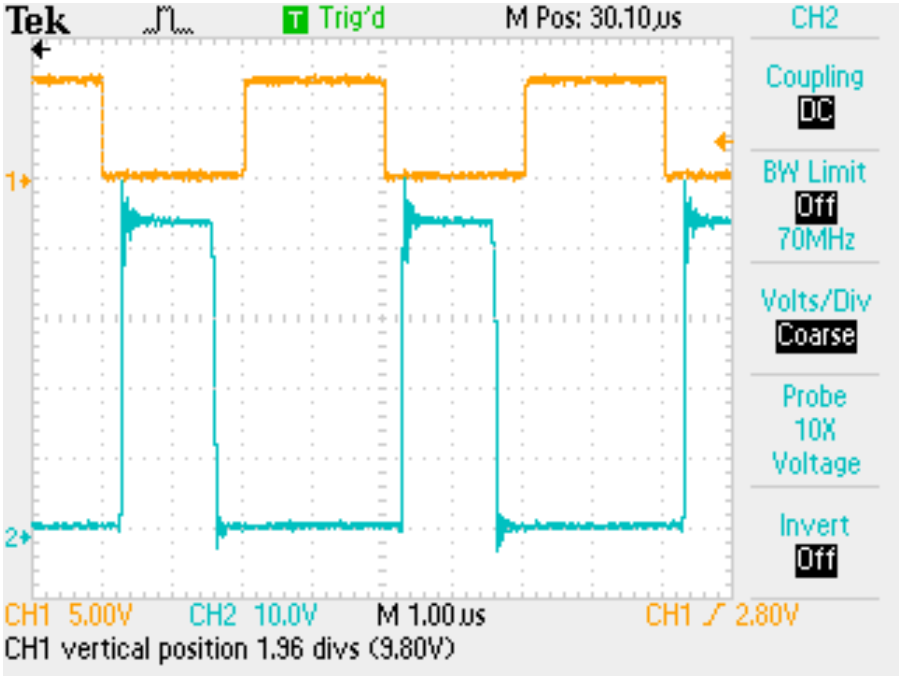

FIGURE 41: HIGH SIDE MOSFET DRIVE

5.3 Measurement Circuitry

Once tested for individual functionality, simulated voltages and currents were inputted to the measurement circuitry and the output ADC codes were recorded.

5.3.1 PCB Revision 1

The following subsections pertain to the measurement results of the two PCBs created from the first layout design.

Voltage Measurement, Calibration, and Error

Voltage calibration involved connecting a Data Precision 8200 voltage supply directly to the op-amp circuitry (see Figure 30 for reference). Rather than record the voltage displayed on the power supply, an HP3458A digital multi-meter would record the input voltages. To automate the calibration process, MATLAB's instrument control toolbox controlled the power supply and multi-meter were over a GPIB connection and the ADC codes were transmitted to a computer over a serial connection via a microcontroller. The calibration procedure would set the voltage source record the voltage reading on the meter, take 100 samples from the ADC, and repeat. All of the data collected was stored in a MATLAB variable file. A polynomial fit between the input voltage and the average of the 100 output codes for that voltage extracted calibration parameters that would be stored and later used to translate any ADC code to a specific voltage level.

Figure 42, Figure 43, Figure 44, and, Figure 45 depict the results of the voltage calibration.

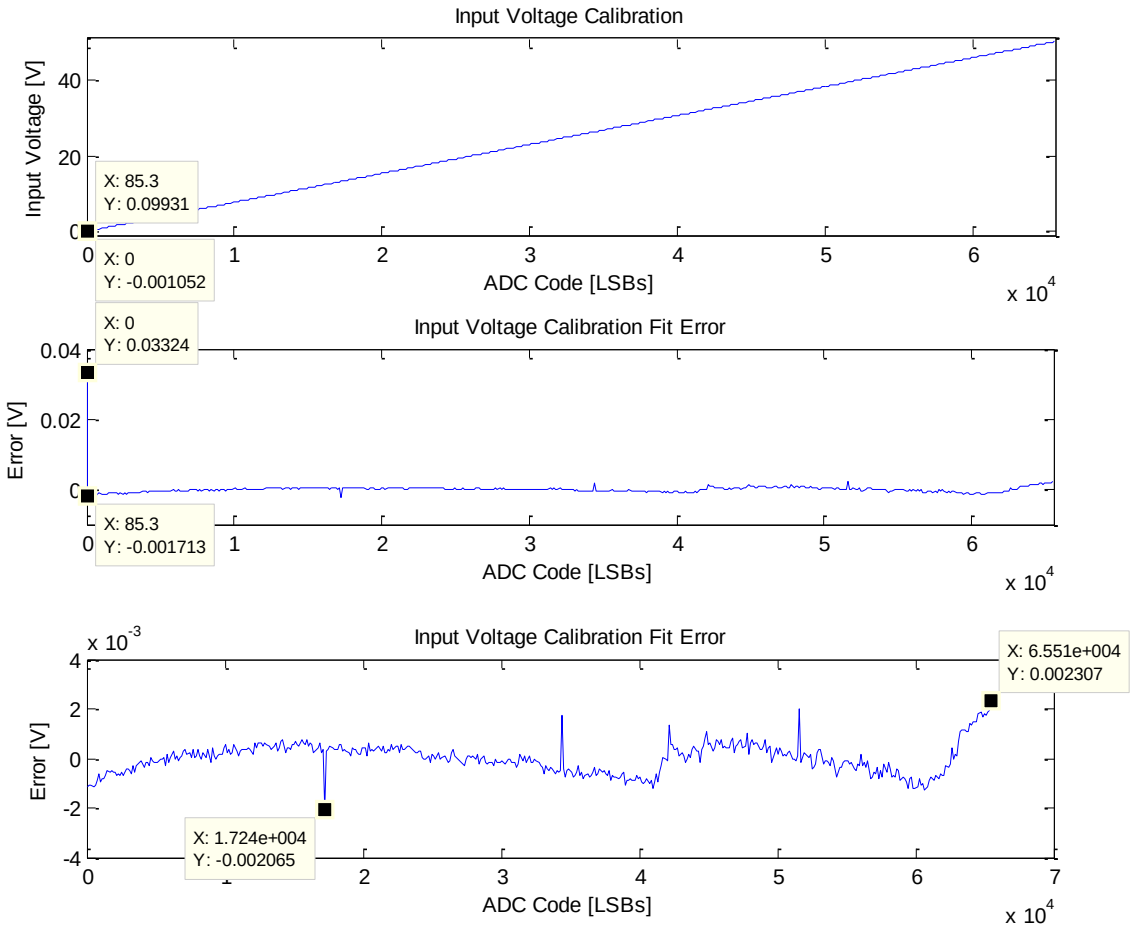

FIGURE 42: BOARD 1 INPUT VOLTAGE CALIBRATION

The top plot depicts the polynomial fit line between the input voltages and the ADC codes. The middle plot shows the difference between the polynomial fit line and the recorded measurements. It was noticed that the 0V output of the power source was in actuality a negative voltage. Since the ADC chosen only has a 0V reference, any value below 0V will always produce a 16-bit zero code. Because of this actual measured negative voltage, the error in calibration would be great at this point. The next value of input voltage was measured at approximately 0.1V (the stepping voltage for the input calibration). There is orders of magnitude difference between the voltage errors of these two points. Since ideally, the panel will never output exactly 0V, and the system will not be operational at such a low panel voltage, it was decided to remove the first data point and generate a new line of best fit. The new fit line was practically identical to the line in the upper plot. However, the error in calibration was then bounded between ±2.5mV. Similar results were observed in calibrating the input of the second PCB (see Figure 43)

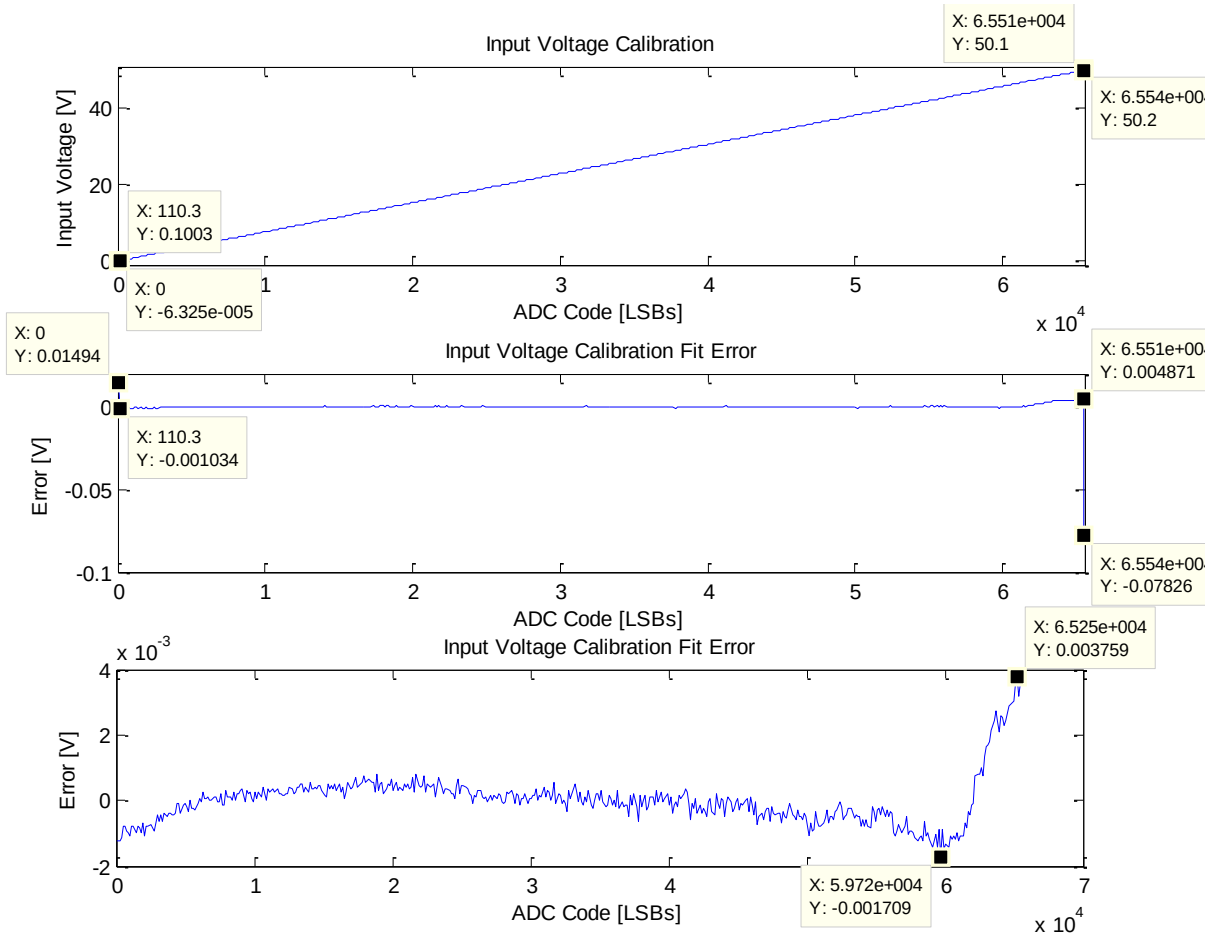

FIGURE 43: BOARD 2 INPUT VOLTAGE CALIBRATION

As with the first board, calibrating the second board produced the same behavior at a measurement of 0V. In addition, there was an error two orders of magnitude greater than a majority of the errors seen when measuring 50V, as seen in the second plot. This was due to the voltage mapping of the op-amp circuitry. The input voltage at that point was measured at 50.2V at which the differential amplifier circuit would output 4.102V, higher than the ADC's voltage reference. At a voltage of 4.096V or higher

the ADC would output binary 65,535. Since the maximum output voltage of any of the voltage panels was approximately 48V, it was decided to eliminate both the first and final measurements in the data set and produce a new polynomial fit line. The third plot reflects that error after calibration is bounded between ±4mV.

Figure 44 and Figure 45 depict the results of the output voltage calibration.

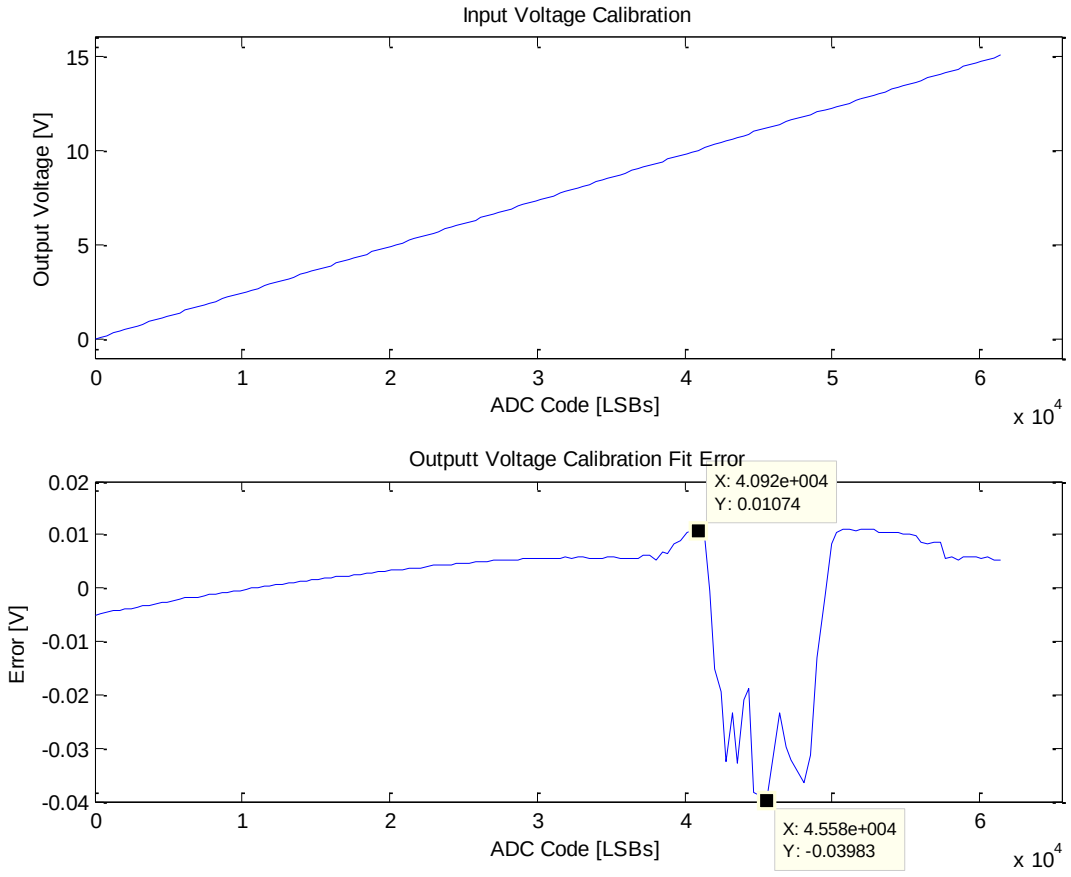

FIGURE 44: BOARD 1 OUTPUT VOLTAGE CALIBRATION

A majority of the error in the output voltage calibration was approximately 1-2 orders of magnitude greater than what was recorded on each board's input measurement. It was noticed that a 0V input (-0.001468V measured) did not output zero on the ADC, rather the average value of the samplings was about 21 LSBs. An interesting phenomenon occurred when measuring 9-12V, observable when looking at the error in calibration. The amount or error spiked within voltage domain. The error in was bounded between ±40mV. Assuming that this may have been a property of the output circuitry, the second board was tested for comparison (see Figure 45).

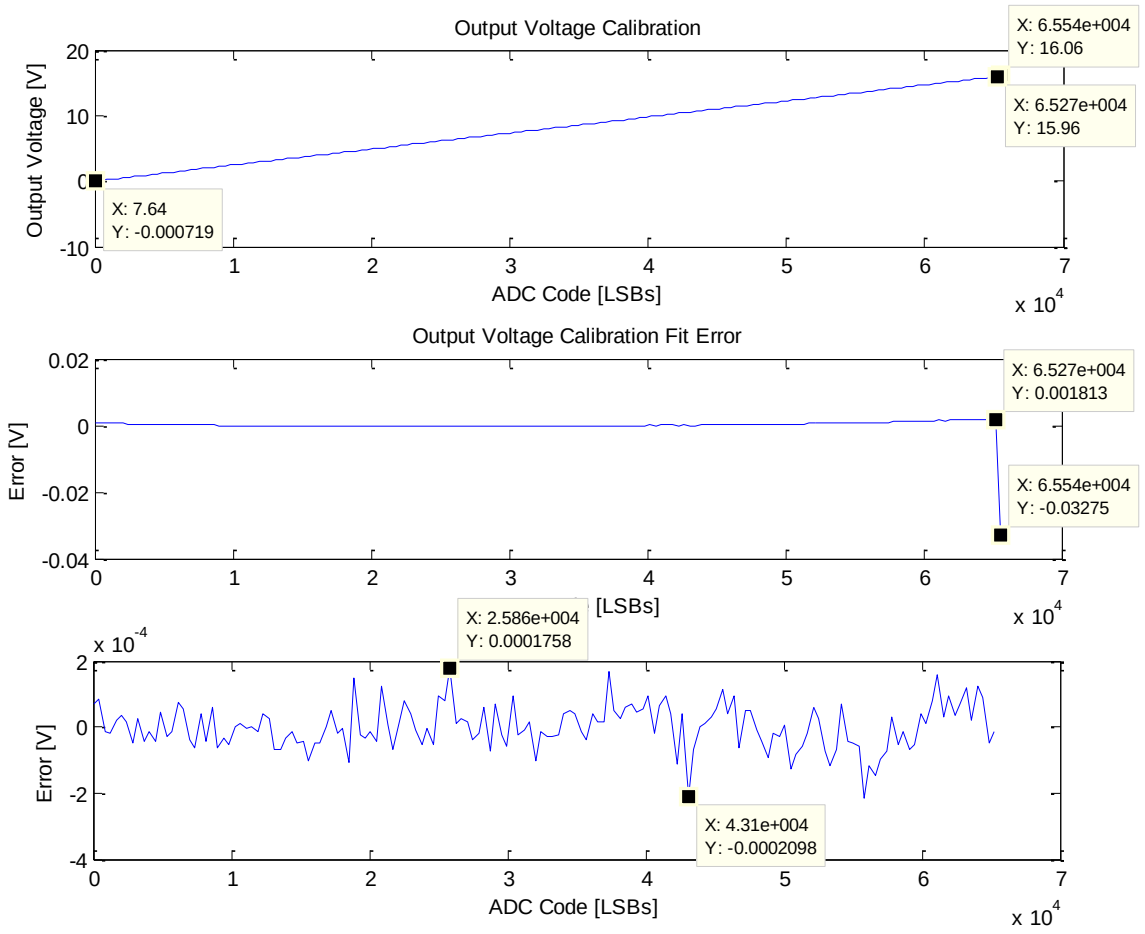

FIGURE 45: BOARD 2 OUTPUT VOLTAGE CALIBRATION

In calibrating the second board's output circuitry, an error spike occurred at a final measurement voltage outside of the range specified for this circuitry. It was also noted that a value below 0V did not output zero on the ADC. After fitting a refined data set, the error was bounded within ±250μV.

Current Measurement, Calibration, and Error

Calibrating the current measurement circuitry proved the most difficult task mainly because it was difficult to find a power source that would output large currents accurately to serve as something to calibrate against. For each of the boards, a power source was shorted to supply a current to the measurement circuitry. The measurement circuitry was designed to measure currents from 0A-26A but the supply could output a maximum of 5A. It was decided to calibrate to 5A by taking numerous data points (500) and then extrapolate the data outwards. The current was passed through a wire and the voltage drop across the wire was measured. An initial polynomial fit was calculated between the voltage measured across the wire and the current as displayed on the power source. The extracted coefficients were evaluated over the voltage measurement range to attain a higher accuracy of the actual amount of current passing through the circuitry. Next, a polynomial fit was taken between the ADC codes recorded and the newly calibrated source current. The polynomial fit coefficients were to be later used to translate the ADCs codes to specific values of current. An error analysis between the polynomial fit

and the measured current was carried out to analyze the error that would be made in the translation. The following figures detail the current calibration results.

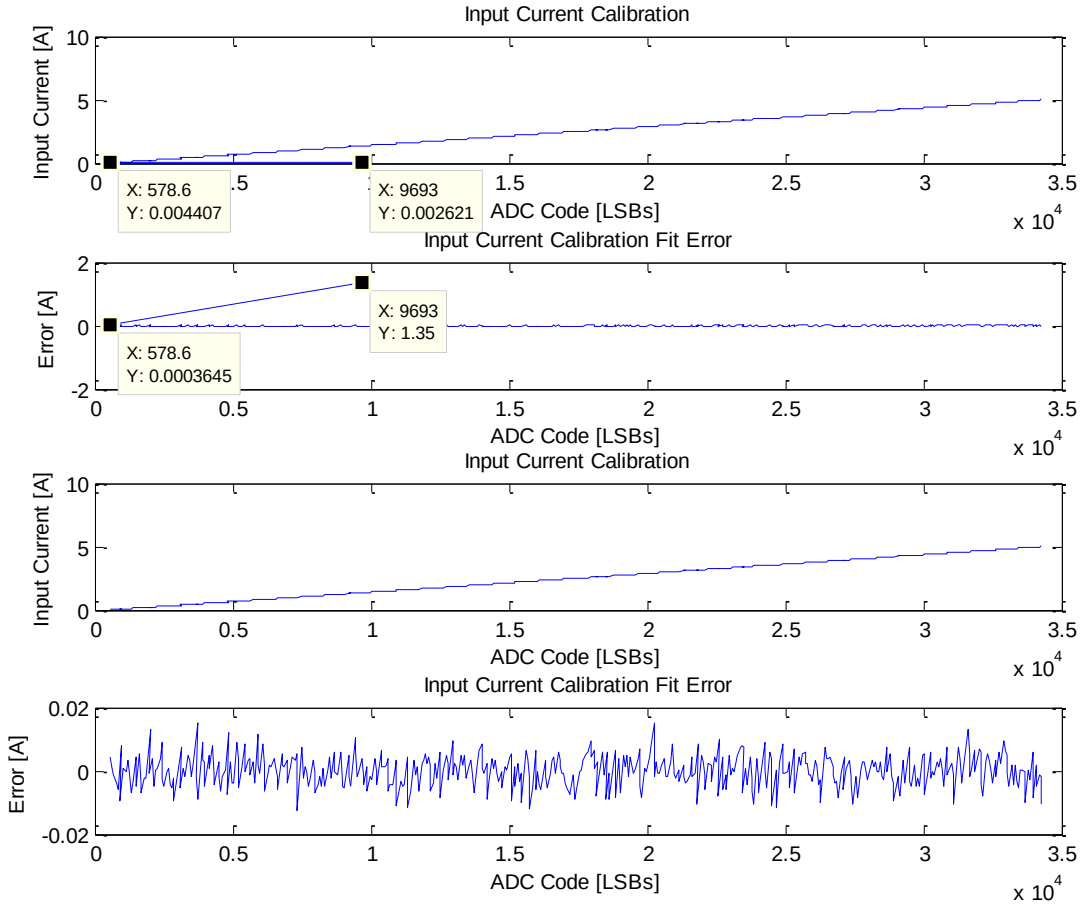

FIGURE 46: BOARD 1 INPUT CURRENT CALIBRATION

The first data point collected at 0A produced a significant amount of error. It was again noticed that the ADC did not output zero as it should. Since the system will not be operational at such a current, the data point was removed from the set and a new polynomial fit was taken with the amount of error ranging between ±20mA. Figure 47 depicts the input current calibration of the other PCB for comparison.

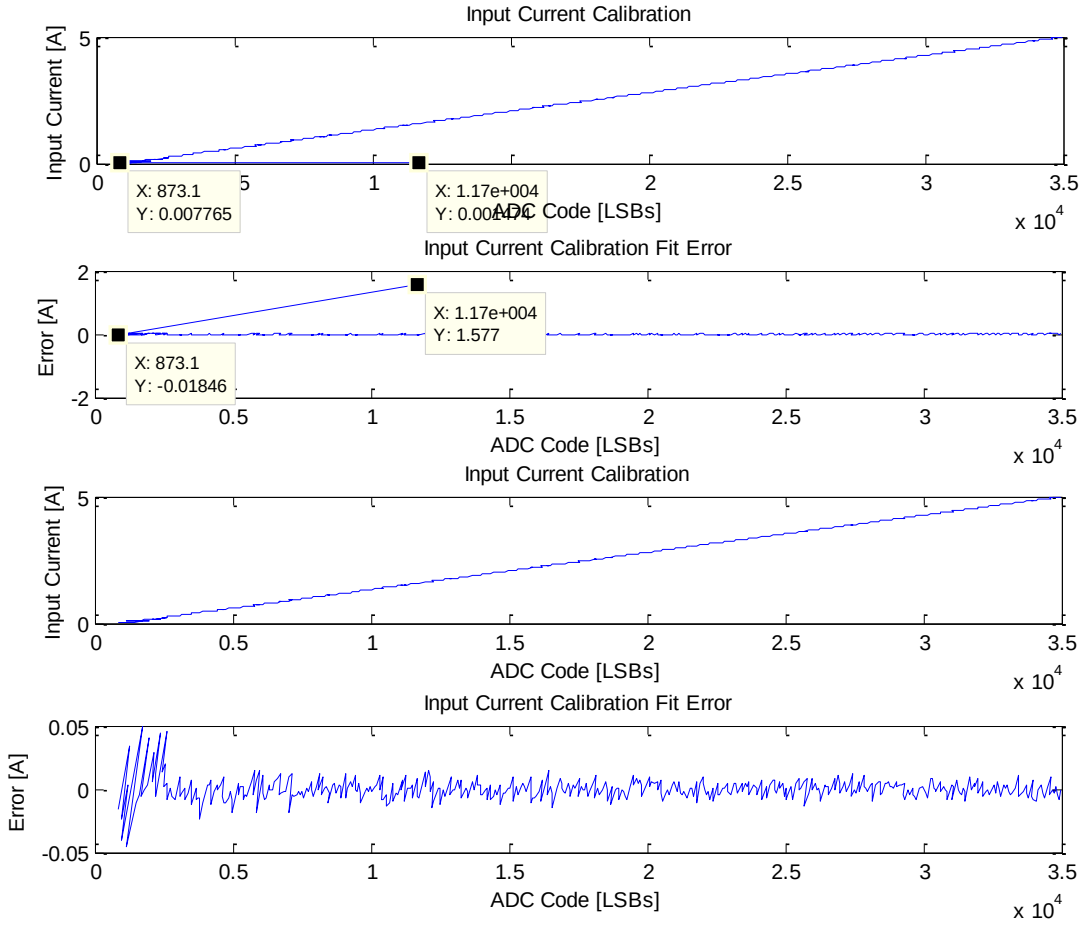

FIGURE 47: BOARD 2 INPUT CURRENT CALIBRATION

Similar to the results of the first board's calibration, the second board exhibited the same behavior upon calibration with the only cause for concern was measuring 0A. Refitting the data resulted in error fluctuating between ± 50mA at currents below 250mA and between ±20mA at higher values of output current. It was interesting to note that the measurement of low currents caused the error to spike.

With the calibration of the input current measurement circuitry exhibiting similar behavior across both boards, the output current measurement circuits were then calibrated. One point to be made was that the input plots relative to the output plots have one major difference. That being the range of the ADC output codes. Since the simulated current source can only output a maximum of 5A, not all the ADC codes can be tested and the percentage of the codes tested differ between input and output calibration because the input was designed to measure 0A-10A, while the output was designed to measure 0A-26A. Figure 48 displays the calibration results of the first board.

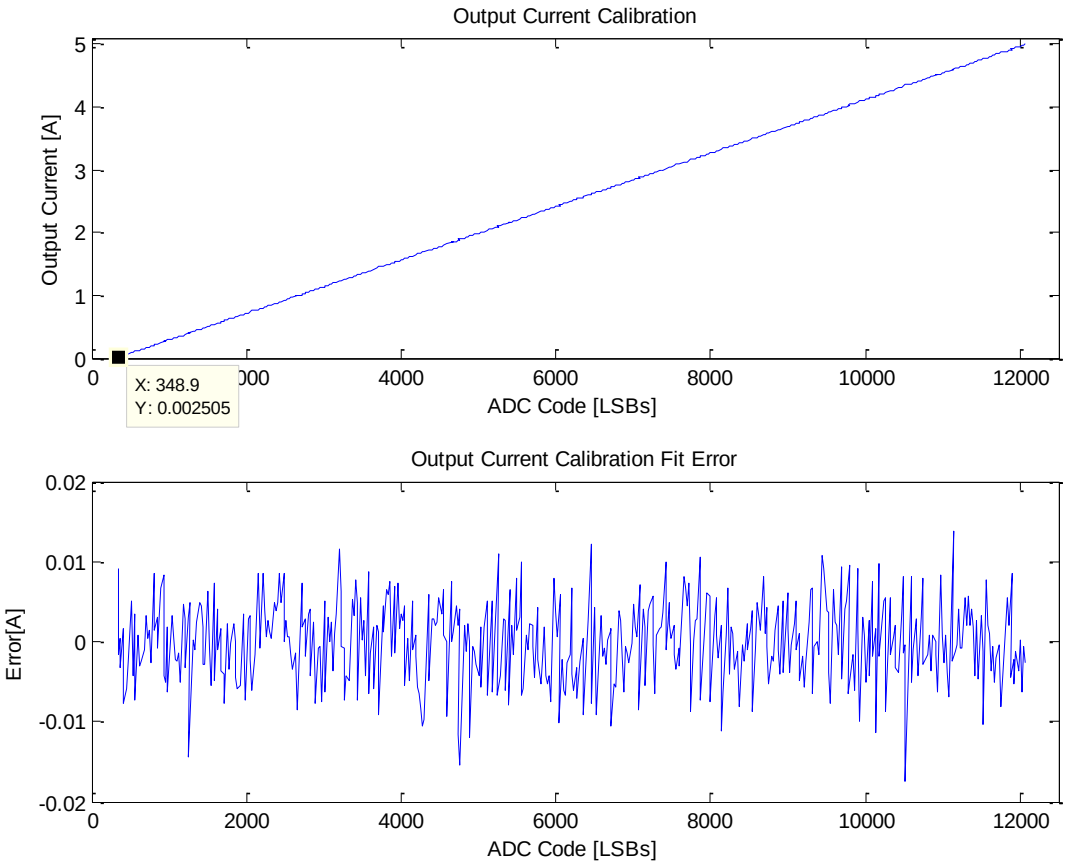

FIGURE 48: BOARD 1 OUTPUT CURRENT CALIBRATION

It was interesting to note that there was no significant error spikes in the calibration and that again 0A in did not result in an ADC code of zero. The calibration error rendered was bounded between ±20mA. The second board's calibration results are shown in Figure 49 for comparison.

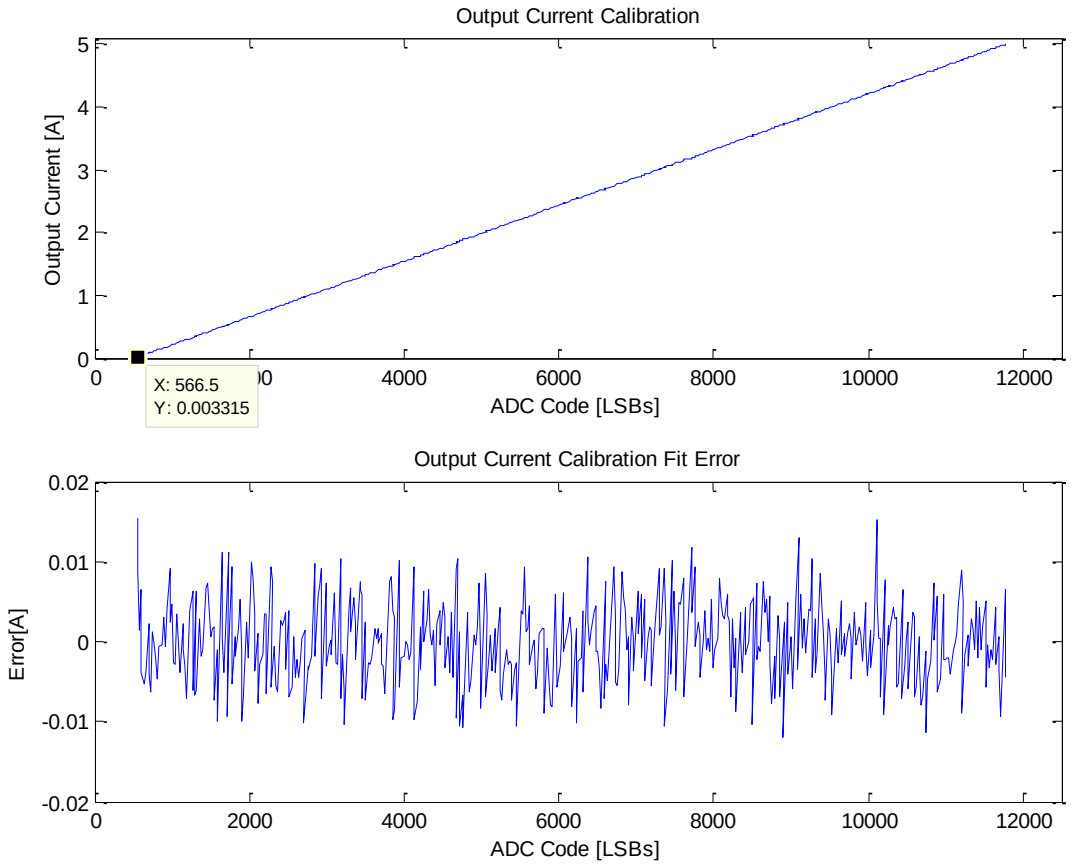

FIGURE 49: BOARD 2 OUTPUT CURRENT CALIBRATION

Again, the same behavior was recorded after calibration. An input current of 0A did not output a binary zero. The resulting calibration error was bounded between ±20mA. It was reasoned that the cause for a non-zero output with an essential zero input may be due to the output voltage of the ACS712 Hall Effect sensor. It was assumed when designing the circuitry that it would output 2.5V with no current input and the op-amp mapping circuitry was designed around this assumption. If this assumption were not correct, the overall current mapping from Hall Effect Sensor to ADC output would be off.

Power Calculation and Error

After observing the error bounds in the input and output measurements the following derivation was used to analyze the error bounds in the resulting power calculations.

$$P_{CALCULATED} = (V_{ACTUAL} \pm \Delta V)(I_{ACTUAL} \pm \Delta I)$$

$$= V_{ACTUAL}I_{ACTUAL} \pm V_{ACTUAL}\Delta I \pm I_{ACTUAL}\Delta V \pm \Delta V\Delta I$$

$$= V_{ACTUAL}I_{ACTUAL} \pm \frac{V_{ACTUAL}I_{ACTUAL}\Delta I}{I_{ACTUAL}} \pm \frac{I_{ACTUAL}V_{ACTUAL}\Delta V}{V_{ACTUAL}} \pm \frac{V_{ACTUAL}I_{ACTUAL}\Delta V\Delta I}{V_{ACTUAL}I_{ACTUAL}}$$

$$= V_{ACTUAL}I_{ACTUAL}\left(1 \pm \frac{\Delta I}{I_{ACTUAL}} \pm \frac{\Delta V}{V_{ACTUAL}} \pm \frac{\Delta V\Delta I}{V_{ACTUAL}I_{ACTUAL}}\right)$$

$$= P_{ACTUAL}(1 \pm \Delta P)$$

Using the equation above and the appropriate error bounds, contour plots (see Figure 50) were plotted to observe the behavior of the error in power calculations.

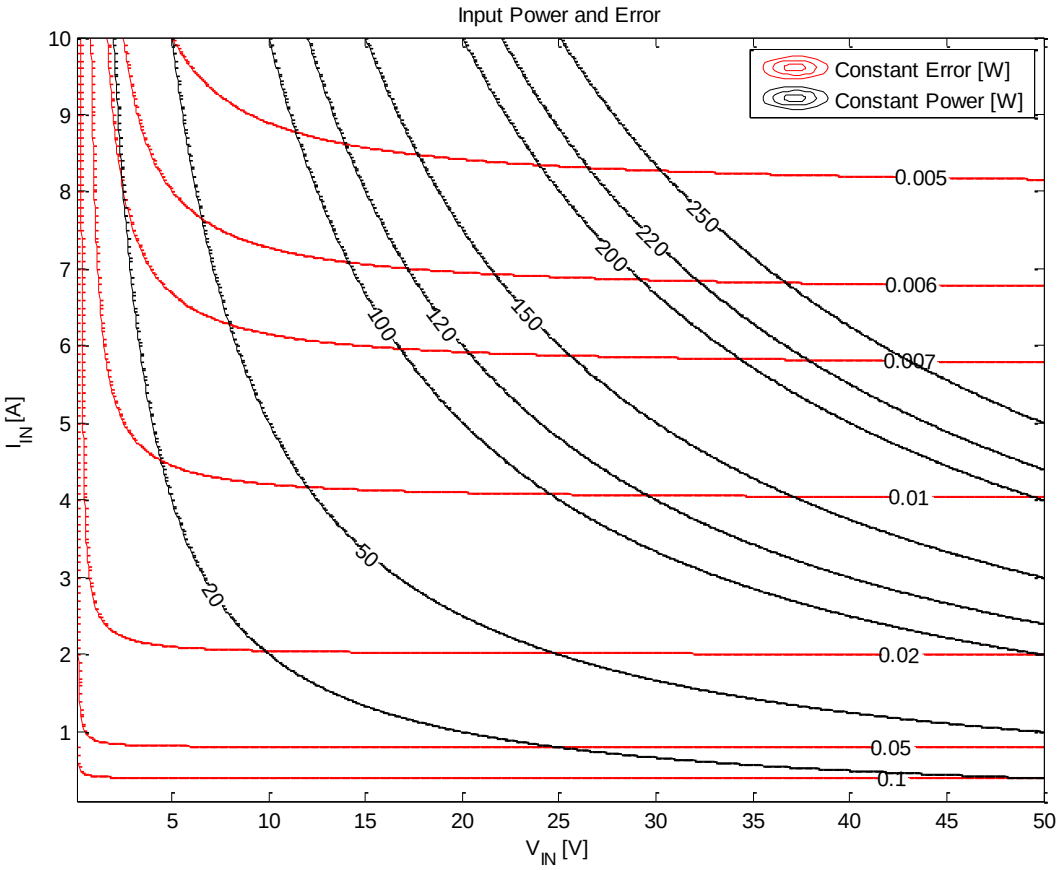

FIGURE 50: BOARD 1 INPUT POWER CONTOURS

The ΔP term in the previous equations is shown graphically by the red contour lines and as indicated by the mathematical model indicated the error term grows as the currents and voltages measured decrease. The black contour lines represent lines of constant power calculated by multiplying various currents and voltages. As the amount of power calculated increases, the error will decrease. Figure 51 shows the input power calibration contours for the second board.

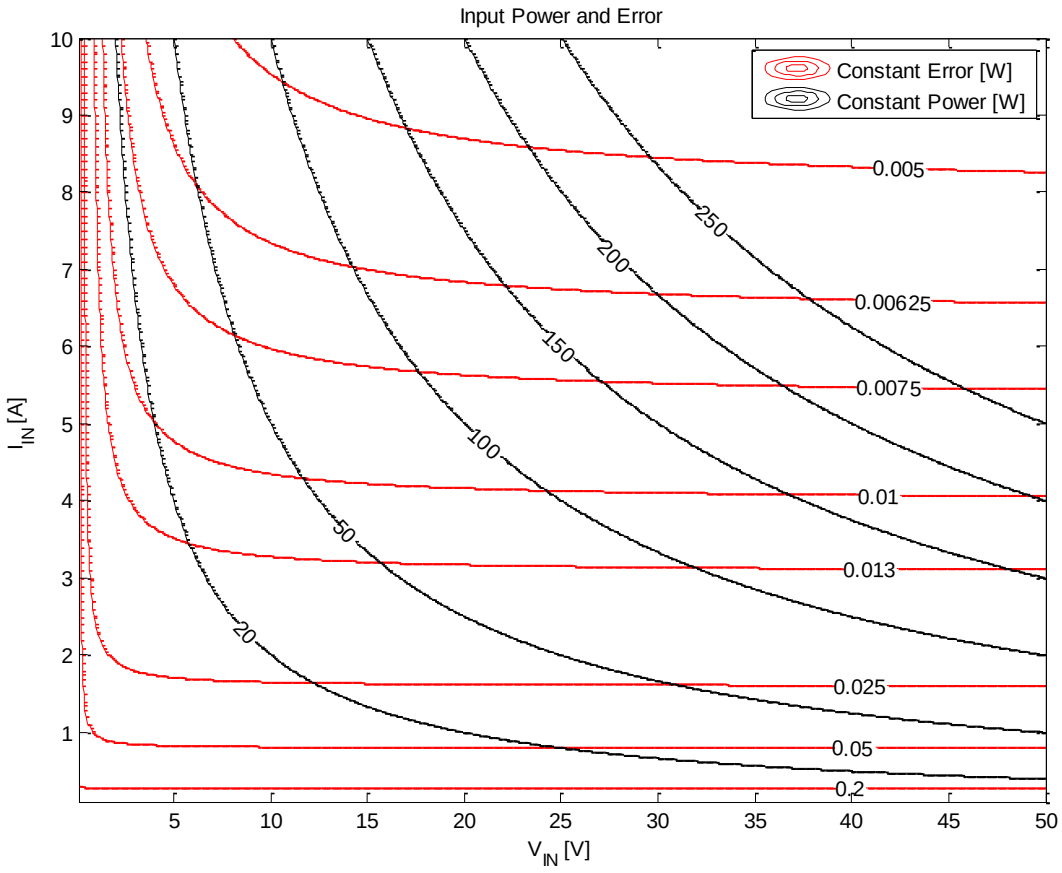

FIGURE 51: BOARD 2 INPUT POWER CONTOURS

The second board's error had the same general curvature as the first board that is the error is mostly constant with the voltage and heavily dependent upon the current. Rather, the ΔI relative to the current range (see Figure 47) dominates the ΔV relative to its voltage range (see Figure 43). In addition, the second board exhibited larger bounded errors in the voltage and current measurements when compared to the first board, which explains the larger contour magnitudes. Figure 52 shows the error in the output power calculation.

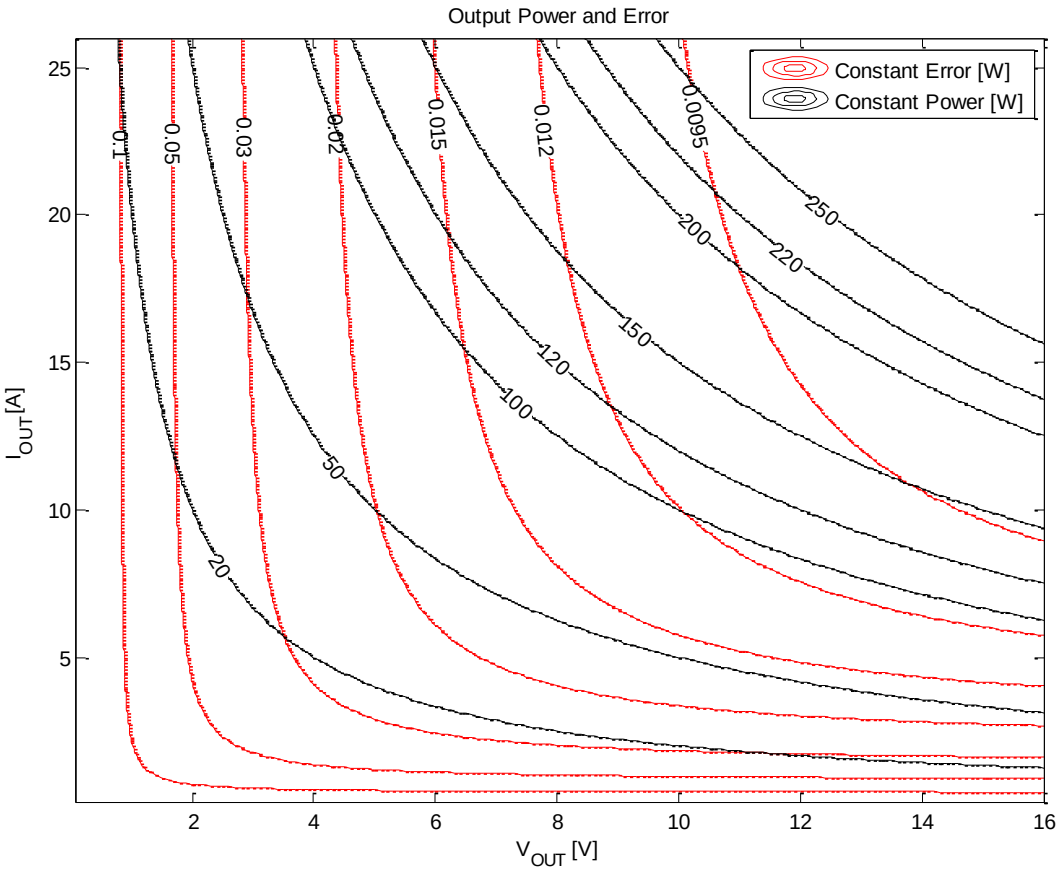

FIGURE 52: BOARD 1 OUTPUT POWER CONTOURS

There is a significant difference in the shape of this plot when compared to the previous error plots because the ΔV and ΔI terms relative to their domains contribute equally to the error. This is a resultant of the increase in voltage calibration error for this board's output voltage measurement circuitry (see Figure 44). For comparison, the error in the output power calculation is depicted in Figure 53.

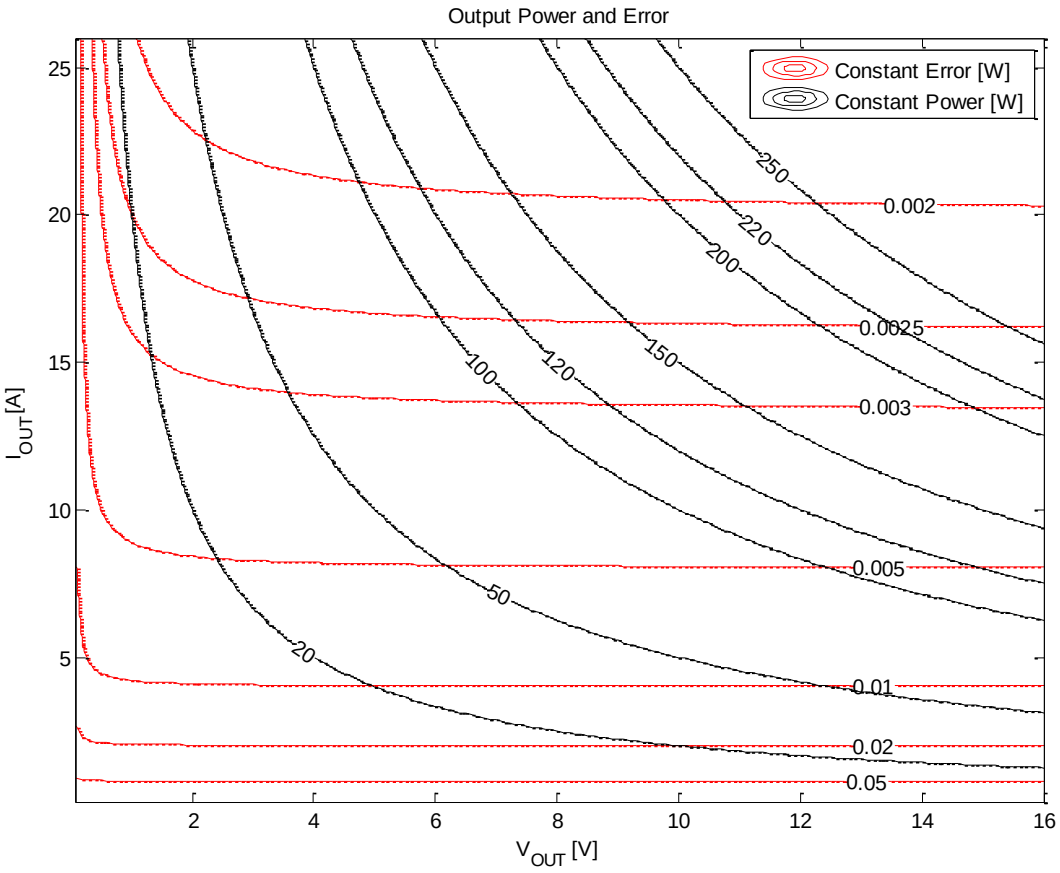

FIGURE 53: BOARD 2 OUTPUT POWER CONTOURS

The general shape of this plot resembled both input power error plots with the ΔI term dominating. The error introduced in the output power calculation by this board is much less than the other power calculations because of the small ΔV term in the output voltage calibration (see Figure 45). In all four cases, it is an ideality of the system to be operating at maximum power, which would limit the amount of error in the power calculations. Reemphasizing the fact that amount of power is governed by the amount of irradiance, daily and seasonal changes in sunlight would move the power errors about the surfaces reflected by the contour plots. With this error modeling being severely dependent upon the amount of voltage and current being measured, it was decided to report all power calculations with an appropriate error in the following form:

$$P_{ACTUAL}(1 \pm \Delta P) = P_{ACTUAL} \pm P_{ACTUAL}\Delta P \rightarrow P_{ACTUAL} \pm \varepsilon_{POWER}$$

Efficiency Calculation and Error

Modeling the power as stated in the previous chapter the bounds on the error in the efficiency can be modeled as follows:

$$\eta_{CALCULATED} = \frac{P_{OUT\ CAULCULATED}}{P_{IN\ CALCULATED}} \rightarrow \frac{P_{OUT}(1 \pm \Delta P_{OUT})}{P_{IN}(1 \pm \Delta P_{IN})} = \frac{P_{OUT}}{P_{IN}} * \frac{(1 \pm \Delta P_{OUT})}{(1 \pm \Delta P_{IN})}$$

$$= \eta_{ACTUAL} * \frac{(1 \pm \Delta P_{OUT})}{(1 \pm \Delta P_{IN})} = \eta_{ACTUAL}\left(1 \pm \frac{\Delta P_{OUT} \mp \Delta P_{IN}}{1 \pm \Delta P_{IN}}\right) = \eta_{ACTUAL}(1 \pm \Delta\eta)$$

Notice that the input error is destructive if both errors are of the same sign. The most error would occur when the error terms were of opposite signs. Since it was decided to report the error in power with each power calculation, the efficiency would also be reported each time with an error in efficiency as follows:

$$\eta_{ACTUAL}(1 \pm \Delta\eta) = \eta_{ACTUAL} \pm \eta_{ACTUAL}\Delta\eta \rightarrow \eta_{ACTUAL} \pm \varepsilon_{EFFICIENCY}$$

Taking the range of voltages and currents to be at the maximum values defined by all system specifications, Figure 54 depicts the contour curves of the error in efficiency computations alongside the power computations over those ranges.

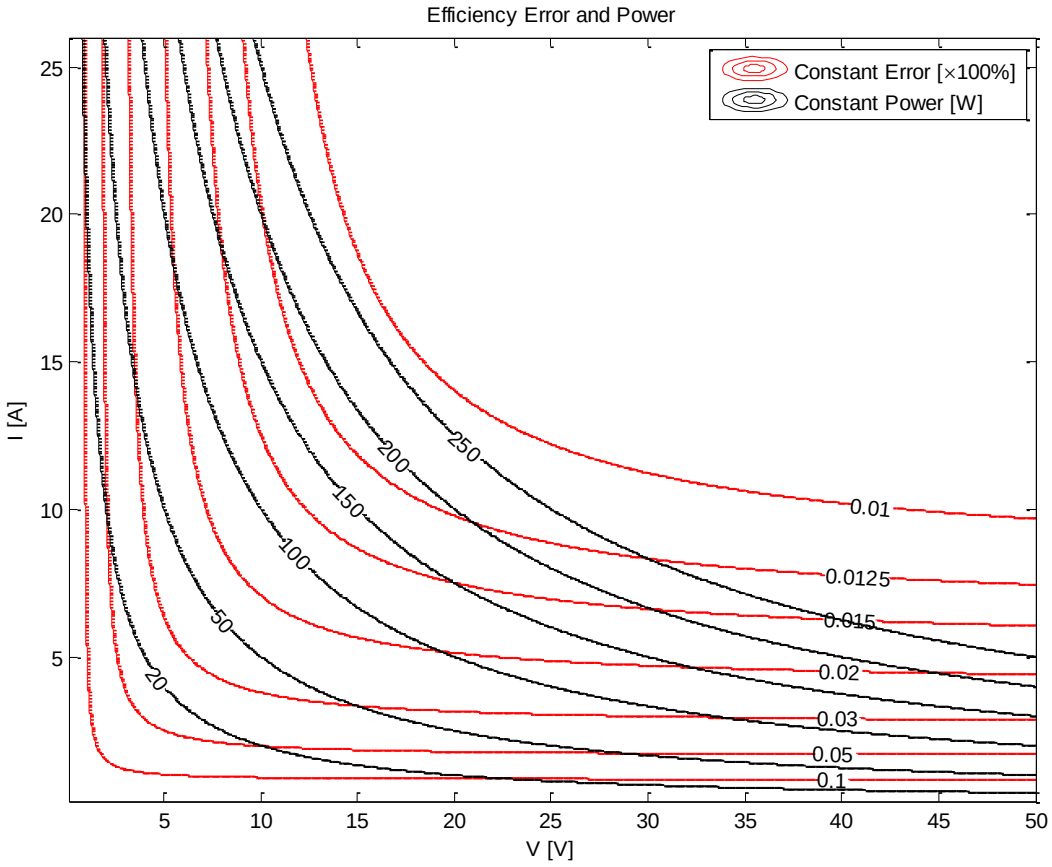

FIGURE 54: BOARD I EFFICIENCY CONTOURS

Since the ranges of the input voltage and current measurements differ from the respective output ranges, the voltage ranged from 0V-50V due to the high panel output voltages and the current ranges from 0A-26A due to the converter output current range. It should be noted that the maximum power ever seen in the system would be 250W so the power contour lines provide limits of the current with respect to a particular voltage, or vise-versa. The red lines depict the $\Delta\eta$ terms as the measurements

vary in magnitude. Again, it should be reemphasized that these terms reflect when the ΔP terms differ in sign and therefore add to one another. As expected from the previous plots, the error in efficiency was smaller when measuring power values at low voltages and high currents rather than at high voltages and low currents because of how the calibration error terms dominated. Figure 55 depicts the error contours for the second board.

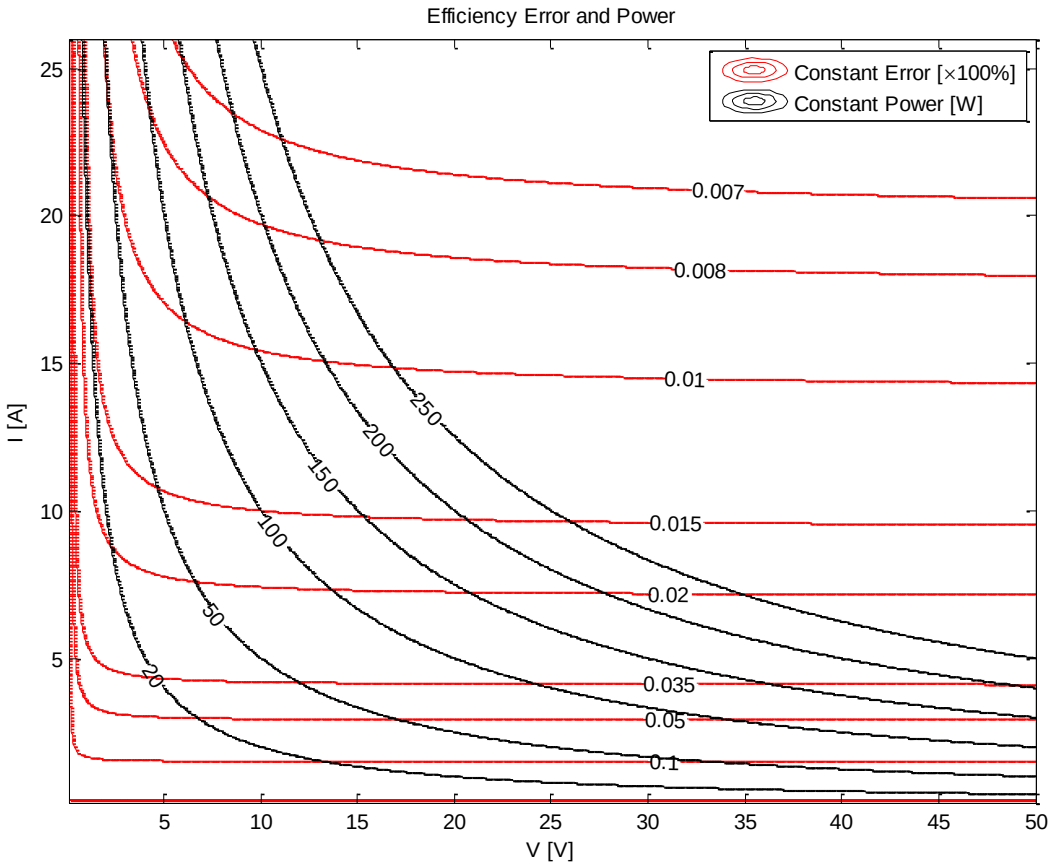

FIGURE 55: BOARD 2 EFFICIENCY CONTOURS

The general shape of the two plots differs due to the differing magnitudes of each of the voltage and current error terms for each boards input and output. The first board proved to be more accurate when computing efficiency, which was expected because of the nature of the mathematical modeling. The error in the input power measurement dominated the error term in the output measurement namely because it appears twice.

5.3.2 PCB Revision 2

The following subsections pertain to the measurement results from one of the PCBs created from the second design revision.

Voltage Measurement, Calibration, and Error

Figure 56 displays the result of calibrating the input voltage measurement circuitry.

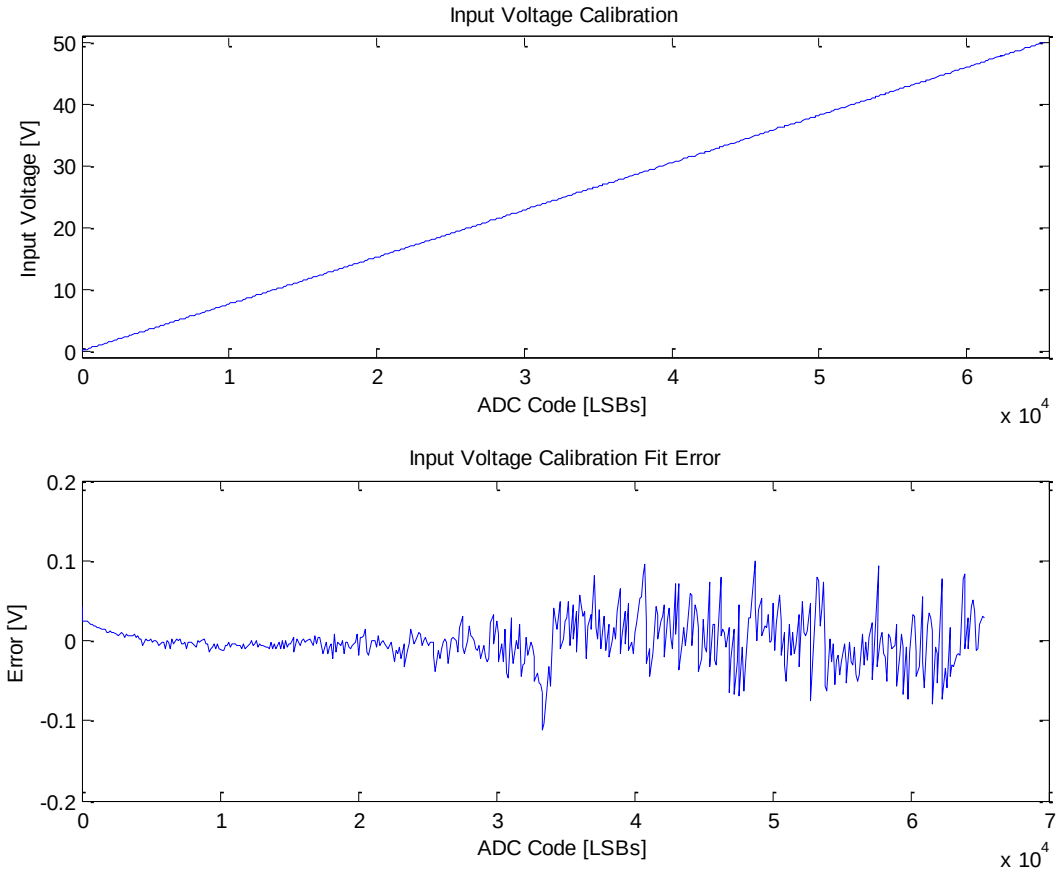

FIGURE 56: INPUT VOLTAGE CALIBRATION

The error after calibration differs greatly in the second PCB revision as it grows with the magnitude of the measurement. The bounded error term was orders of magnitude greater when compared to the first board's design. The output calibration seen in Figure 57.

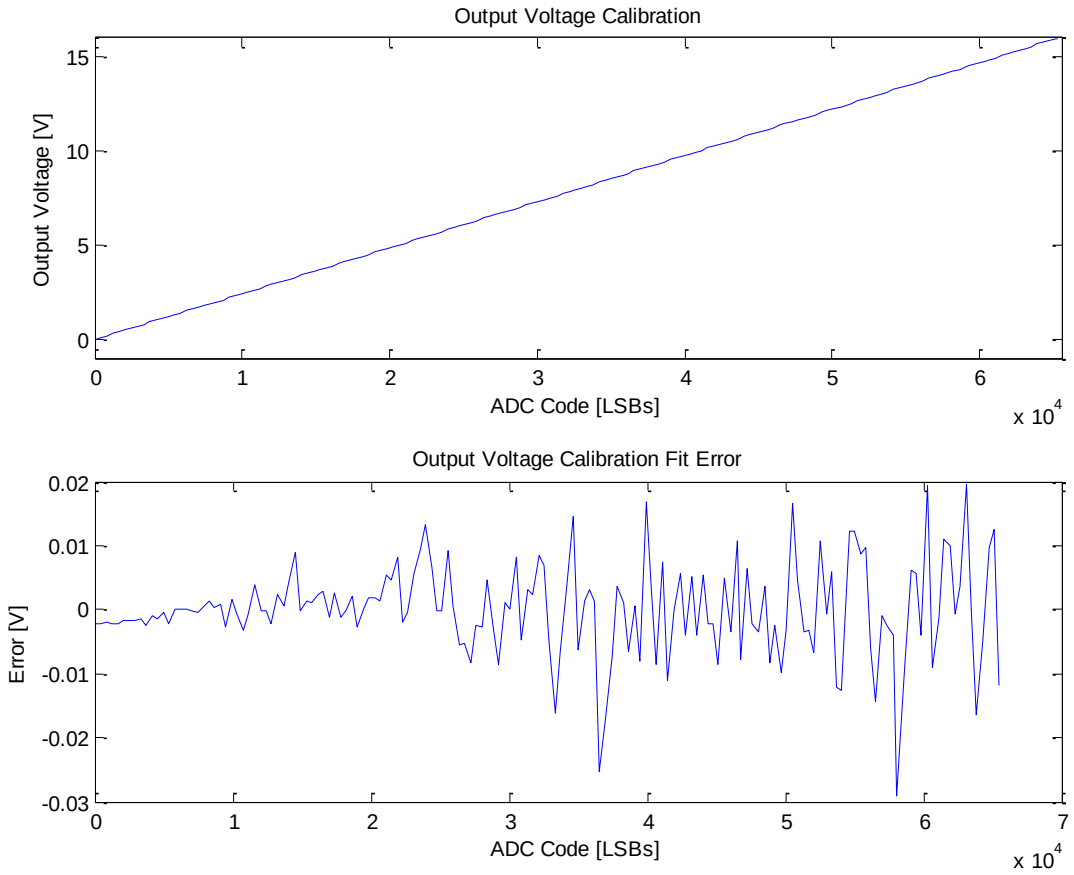

FIGURE 57: OUTPUT VOLTAGE CALIBRATION

The same behavior was observed in the calibration of the output voltage measurement circuitry. Additional analyses to determine the source of this behavior was left for future endeavors.

Current Measurement, Calibration, and Error

Encountered when trying to calibrate the current measurements was a phenomena that corrupted the output current measurement data, therefore only the input current calibration was executed (see Figure 58).

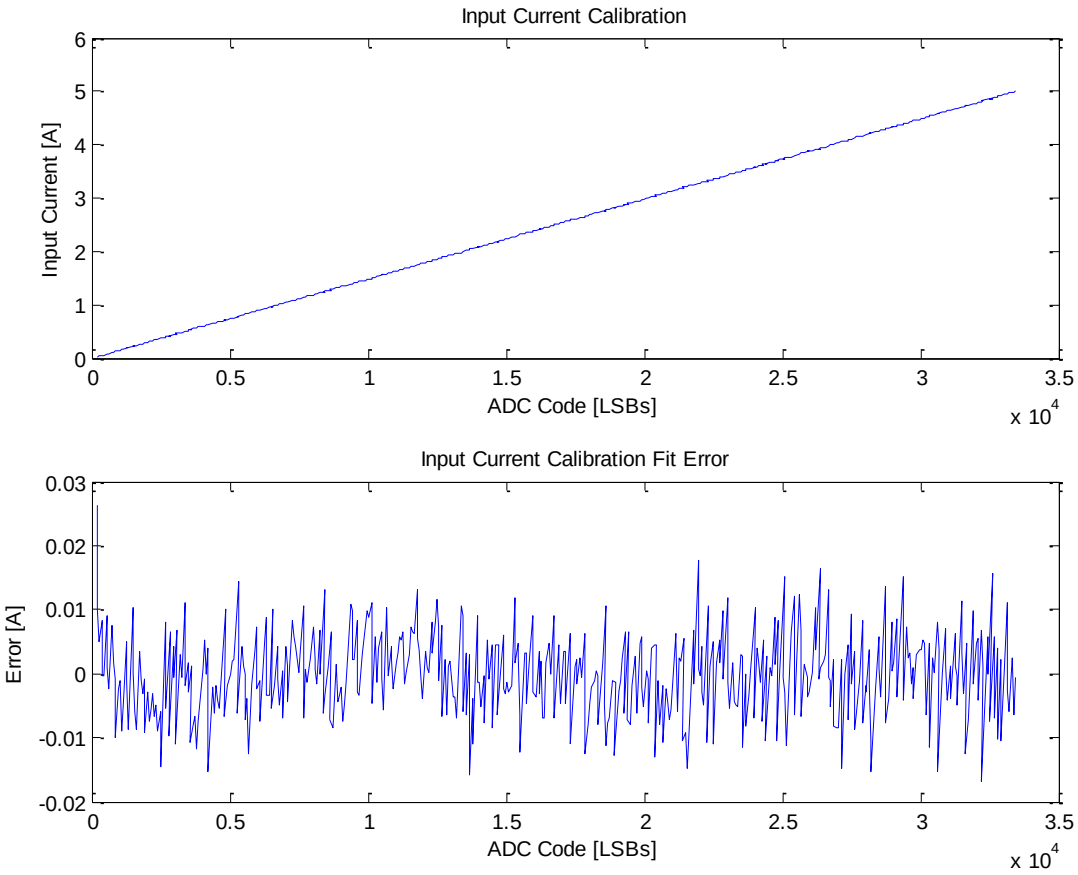

FIGURE 58: INPUT CURRENT CALIBRATION

Aside from the error spike in the 0A measurement the current measurement circuitry exhibited the same behavior when comparing it to the first board. The bounded error over the measurement range remained relatively constant and similar in magnitude to the results from the first board. Again, in the interest of time, the output current measurement issues were left for future work.

Power Calculation and Error

With only the input circuitry giving data for both current and voltage only the input power calculations were analyzed for error. Figure 36

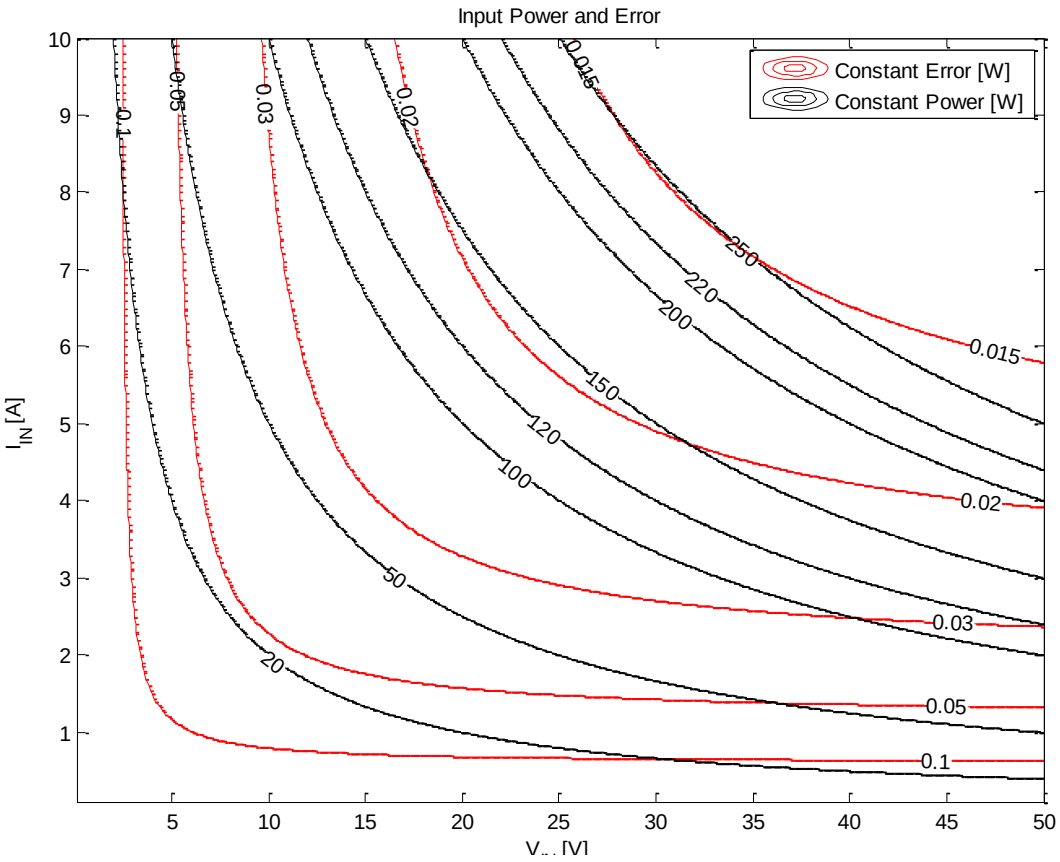

FIGURE 59: INPUT POWER AND ERROR

As expected, the error in the power measurement is approximately dependent as much on the voltage error as it is the current error, seen by how the constant error lines are roughly square to the voltage-current plane.

6 Future Work

The original goals for this project were highly ambitious and dynamic, ultimately comprising more work that could be reasonably accomplished in one MQP. The hardware developed and the panels installed will provide new MQP opportunities for teams to explore renewable energy. Future MQP groups will be able to contribute new work and build towards the original vision for this venture.

6.1 Final Installation

At this time, there are two solar panels on the roof of the Atwater Kent building. These panels are temporarily installed utilizing hardware that allowed the project to stay within budget. One desirable goal would be to work with WPI's facilities department to achieve a permanent install of at least the six panels donated, possibly more with future donations or purchases. The installation would include adequate cabling rated for the specific application, circuit breakers for safety, and possibly conduits to run the cabling to the Power Panel Lounge. Another aspect of the permanent install would be to find places to store the batteries being charged, install the converting/measurement PCBs, and hook-up a computer to gather, process, and transmit the data to a display. There is conversation of renovating the roofing and HVAC systems in AK in the near future and permanent installation may be more fiscally reasonable if performed in conjunction with the renovations.

6.2 Second PCB Revision Testing

As the deadline for project, completion was approached, testing and debugging the measurement circuitry of the second board was left incomplete. Conclusions as to whether the second revision improved upon the initial design were not made. Future project teams could test the remaining functional block of the systems to conclude the any improvements or drawbacks of the second design to arrive at this conclusion.

6.3 Design Improvements

Future circuit revisions could be explored to increase the accuracy in the measurements of power and converter efficiency. One major component of increasing the measurement accuracy would be to explore different current measuring topologies or utilizing higher accuracy integrated circuits. Alternate converter designs should be developed to increase the efficiency of the power extraction from the panel. One interesting avenue would be to redesign the board into multiple modular boards to accept a wide array of converters to allow WPI to become a test bed for converters developed in the renewable energy industry if the accuracies in measurement can be further increased.

The converter topology used did not prevent current from flowing back into the converter when the converter sets a voltage lower than the battery voltage. It was necessary to use an "Ideal Diode" Controller which turns on a MOSFET in the forward bias direction and shuts it off in the revers bias direction in order to prevent current from flowing into the low side MOSFET. This problem can be corrected through the use of a converter topology that supports current sense and prevents reverse current.

Finally, it would be ideal if the board could remotely communicate with either a display medium or a computer that also talks to a display. With an initial design concept developed and working it should be

scrutinized in every aspect to improve design especially when considering circuits that deal with renewable energy conversion.

6.4 System Interface and Integration

Additionally, the panels and their associated circuitry would have to be configured to charge a single battery bank without interfering with one another. Protocols would need to be developed to allow the panel specific circuitry to communicate with one another to operate and make system level decision such as whether or not to charge a battery, or whether to drive loads with the battery or another source. The system would also have to incorporate load controlling to satisfy dissipating energy once the battery is charged. Individual batteries may also need current monitoring in order to balance each battery in the system. Finally, a display medium would be constructed and programs written to display the data quantitatively and qualitatively.

7 Conclusion

The renewable energy discipline requires substantial technical and logistical effort to produce efficient and reliable systems. New developments in commercial and residential energy collection, storage, and distribution platforms are made every day. From the onset of this project, the complexity of this changing industry and the challenges it faces over traditional energy became very clear. Producing solar energy is still expensive because of the cost of panels, systems, and installation, but as fossil fuel prices rise there is a sense of urgency in bringing the cost of these new technologies down. This MQP tackled the problem from many of the different angles reflecting real world scenarios, from the application of circuit theory and analysis to the logistical challenge installation and siting.

The fundamentals of power electronics, microelectronics, signal processing, embedded computing, and communications were all applied to the power and measurement systems developed in the project. Industry practices were emphasized in circuit design, component selection, and circuit testing. The final circuit is a fully functional platform that delivers on its original goals. However, features such as measurement accuracy, converter efficiency, and implementation of a data display system can be improved upon. Future work and innovation will allow WPI to play an important part in a rapidly developing industry that still has plenty of room for new, bright ideas.

8 References

[1] Jason Beliveau, Chao Lian, Yura Pyatnychko, and Muhammad Farzan Tariq, "Photovoltaization of WPI," Worcester Polytechnic Institute, Worcester, IQP Oct. 2010.

[2] Steven Fanara, Thomas Izzo, and Carmel Kozlov, "Instrumentation of the Atwater Kent Turbine," Worcester Polytechnic Institute, Worcester, MQP Nov. 2001.

[3] Maximillian Hubson-Dupont, Max Hurgin, Christopher O'Hara, and Valerie Thierry, "Monitoring Electricity Consumption on the WPI Campus," Worcester Polytechnic Institute, Worcester, MQP May 2007.

[4] Eric Benedict, Vinod John, and Shazreen Meor Danial, "An Universal Interconnection System to Connect Distibuted Generation to the Grid," *IEEE Xplor*e, 2006.

[5] (2011, September) AstrumSolar. [Online]. http://www.astrumsolar.com/

[6] (2011, September) Lowe's. [Online]. http://www.lowes.com

[7] (2011, Sept) Sharp Electronics. [Online]. files.sharpusa.com

[8] (2011, October) Sanyo North America. [Online]. us.sanyo.com

[9] (2011, September) The Energy Conscious. [Online]. http://www.theenergyconscious.com/

[10] (2011, September) Sears. [Online]. www.sears.com

[11] (2011, September) Munro Distributing. [Online]. http://www.munroelectric.com/

[12] (2011, September) atbatt. [Online]. http://www.atbatt.com

[13] (2011, September) Battery Universe. [Online]. http://www.batteryuniverse.com

[14] Alexander Emanuel, , Worcester, Oct. 2011.

[15] James O'Rourke, , Worcester, Oct. 2011.

[16] (2011, September) SparkFun Electronics. [Online]. http://www.sparkfun.com/

[17] (2011) Solectria Renewables. [Online]. http://www.solren.com/SolrenView/products.html

[18] Yuka Yoneda. (2011, November) Inhabitat. [Online]. http://inhabitat.com/photos-inhabitat-explores-sanyos-5200-solar-panel-clad-kasai-green-energy-park/

[19] (2012, January) Google Maps. [Online]. http://maps.google.com/maps?hl=en&tab=wl

[20] John M. Kusterer. (2011, October) Atmospheric Science Data Center. [Online]. http://eosweb.larc.nasa.gov/sse/

[21] Solar Pathfinder. (2011, October) Solar Pathfinder. [Online]. http://www.solarpathfinder.com/pdf/pathfinder-manual.pdf

[22] (2012, February) Future Solar Systems. [Online]. http://futuresolar.wordpress.com/

[23] (2012, April) Wikipedia. [Online]. http://en.wikipedia.org/wiki/File:Solar_cell_equivalent_circuit.svg

[24] US Sunpower Corp. (2012, April) US Sunpower Corp. [Online]. http://us.sunpowercorp.com/

[25] Texas Instruments. (2012, April) TI. [Online]. http://www.ti.com/lit/ds/symlink/tps40170.pdf

[26] National Instruments. (2010, April) NI Developer Zone. [Online]. http://zone.ni.com/devzone/cda/tut/p/id/3546#toc1

[27] Vishay Semiconductors. (2011, March) Vishay. [Online]. http://www.vishay.com/docs/83622/il300.pdf

[28] Adel S Sedra and Kenneth C Smith, *Microelectronic Circuits*. New York, United States: Oxford University Press, 2010.

[29] Avago Technologies. (2010, July) Avago Technologies. [Online]. http://www.avagotech.com/docs/AV02-1333EN

[30] Allegro MicroSystems. (2012, April) SparkFun. [Online]. http://www.sparkfun.com/datasheets/BreakoutBoards/0712.pdf

9 Appendix

9.1 Solar Calculator Input Parameters

Address: 100 Institute Road Worcester, MA 01604
County: Worcester
Utility: National Grid Bay State West
Site Quality Factor: Fair – 750
System Size: 2000W (Absolute Minimum Size Permissible)
Electricity Usage: $200/Mo.
Yearly Rate Increase: 5%

9.2 Solar Path Finder Apparatus Diagram

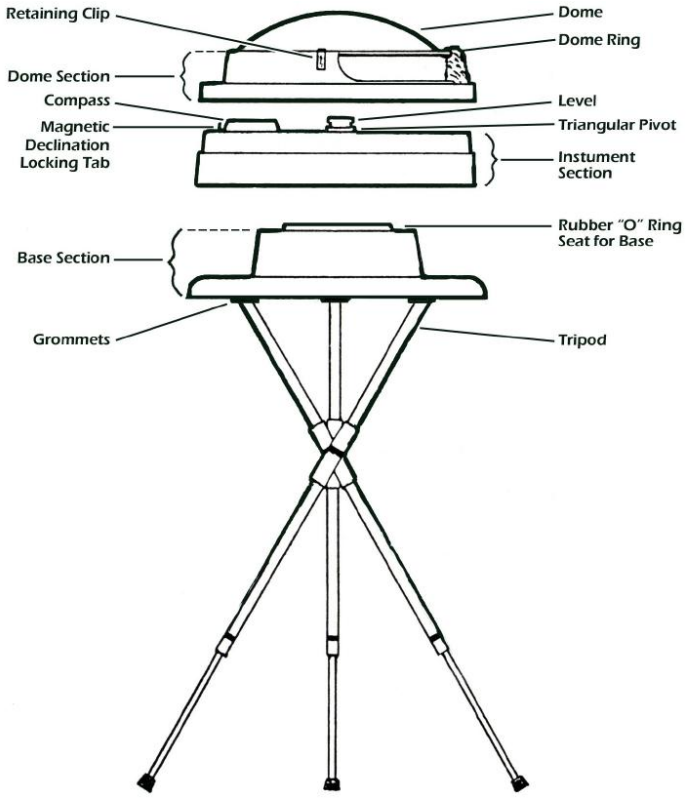

FIGURE A-1: SOLAR PATH FINDER DIAGRAM [**21**]

9.3 Solar Path Finder Charts

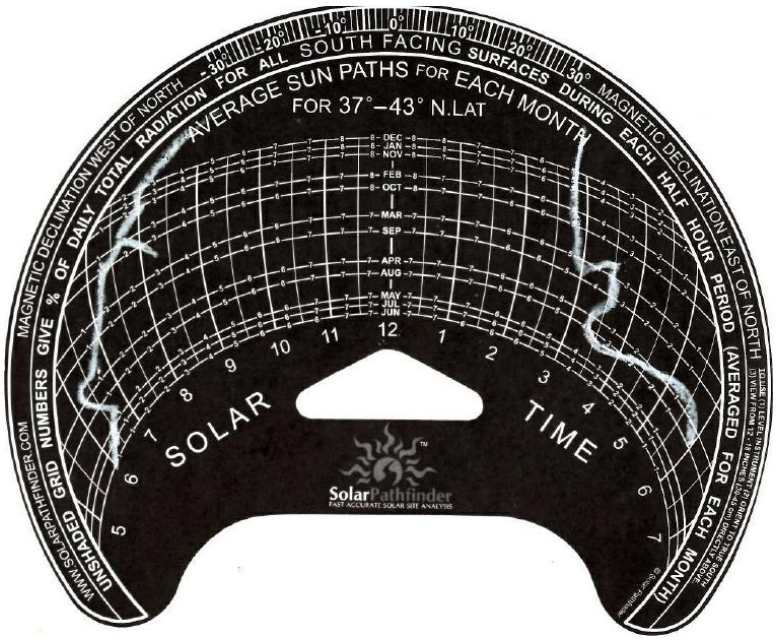

FIGURE A-2: SOLAR PATH FINDER SHADE ANALYSIS CHART, TRIAL 1, SITE 1

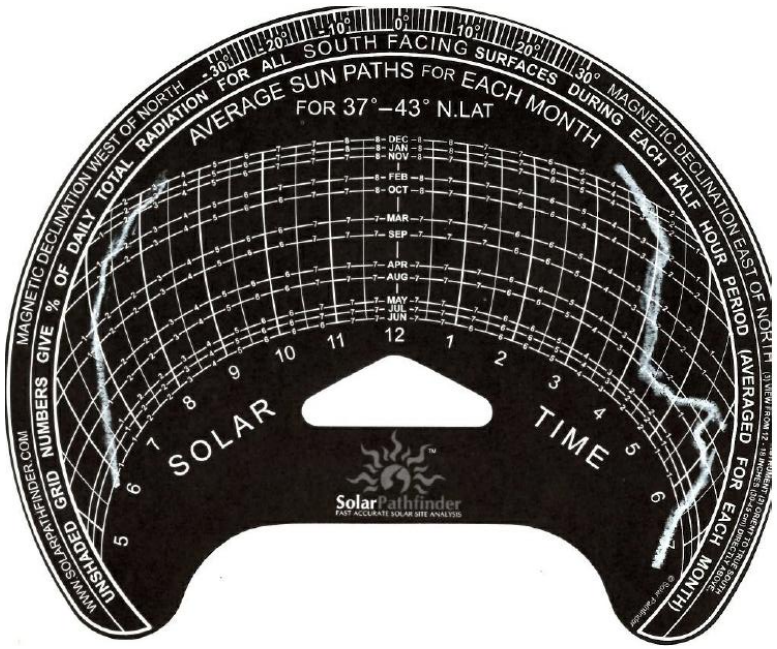

FIGURE A-3: SOLAR PATH FINDER SHADE ANALYSIS CHART, TRIAL 1, SITE 2

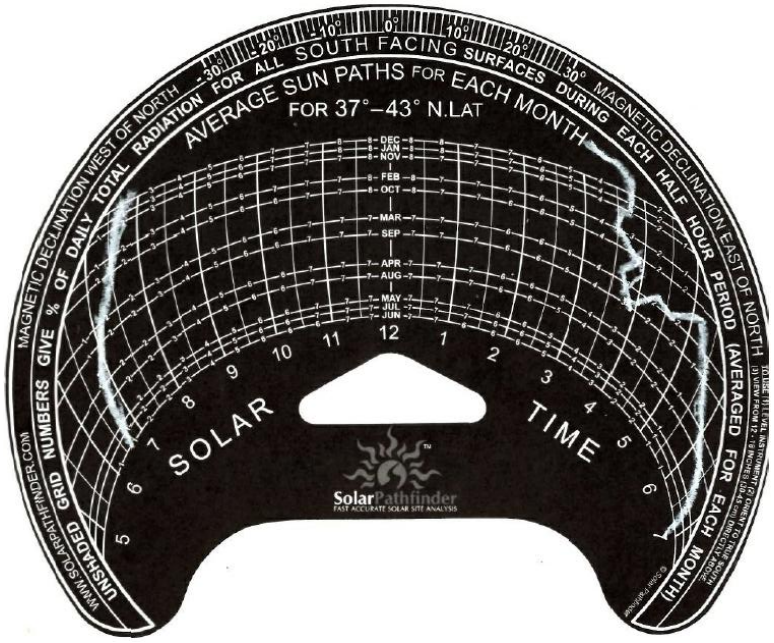

FIGURE A-4: SOLAR PATH FINDER SHADE ANALYSIS CHART, TRIAL 1, SITE 3

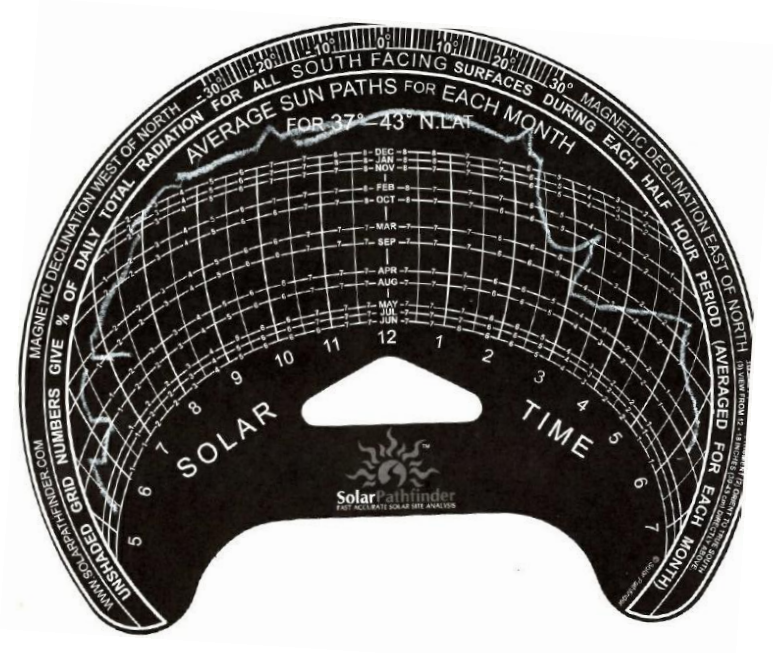

FIGURE A-5: SOLAR PATH FINDER SHADE ANALYSIS CHART, TRIAL 2, SITE 1

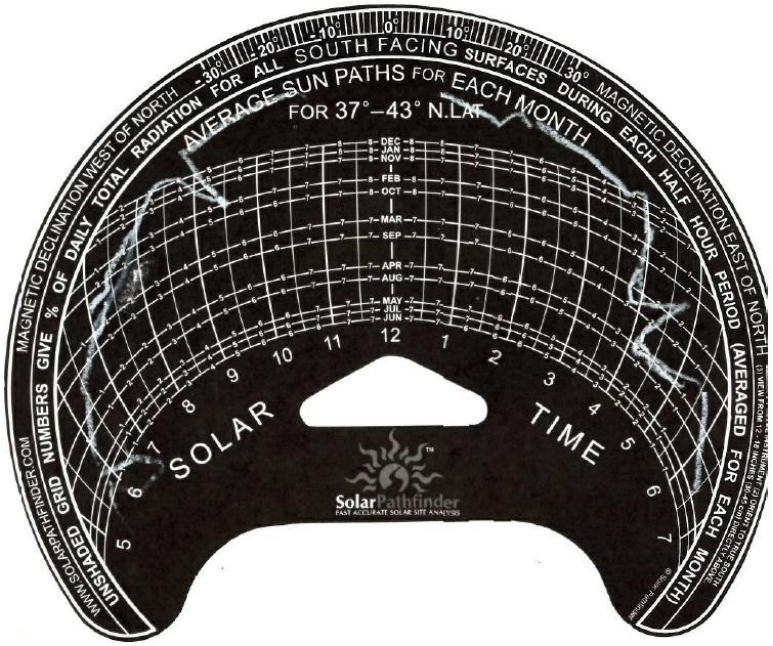

FIGURE A-6: SOLAR PATH FINDER SHADE ANALYSIS CHART, TRIAL 2, SITE 2

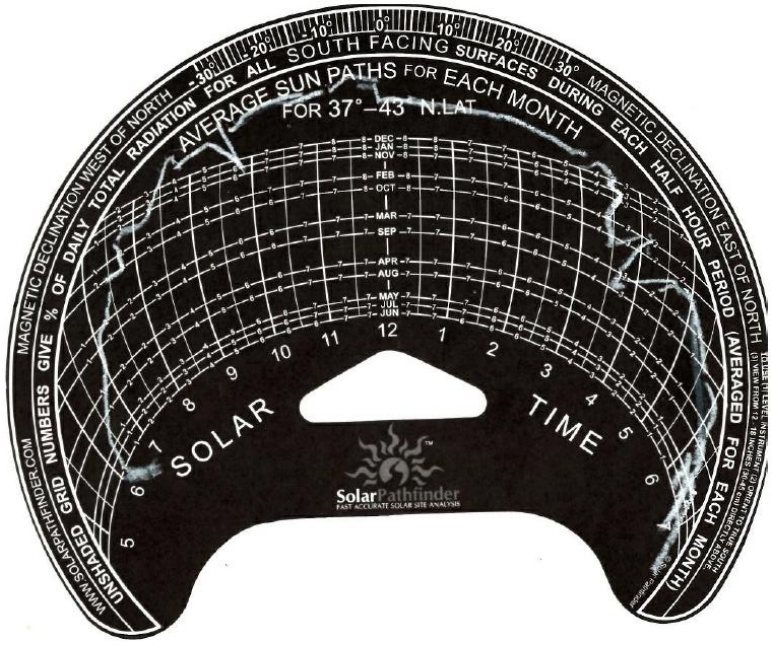

FIGURE A-7: SOLAR PATH FINDER SHADE ANALYSIS CHART, TRIAL 2, SITE 3

Ideal V_Panel [V]	V_Panel Measured [V]	V_Diff Measured [V]	V_Opto Measured [V]	Ideal V_Panel [V]	V_Panel Measured [V]	V_Diff Measured [V]	V_Opto Measured [V]	Ideal V_Panel [V]	V_Panel Measured [V]	V_Diff Measured [V]	V_Opto Measured [V]
0	-0.0043	0.00078	0.00095	17	16.99	1.392	1.37	34	33.95	2.785	2.741
1	0.9962	0.08129	0.0835	18	17.97	1.472	1.45	35	35.04	2.873	2.828
2	1.9965	0.1633	0.16104	19	19.01	1.558	1.535	36	35.99	2.952	2.904
3	2.9971	0.2454	0.2418	20	20.02	1.642	1.615	37	36.97	3.032	2.985
4	3.9974	0.3275	0.3224	21	21.02	1.723	1.696	38	37.97	3.115	3.065
5	4.9977	0.4095	0.4031	22	21.96	1.801	1.772	39	39.02	3.201	3.15
6	5.9978	0.4916	0.4838	23	23.01	1.887	1.857	40	39.99	3.281	3.228
7	6.95	0.57	0.561	24	24.03	1.971	1.939	41	40.95	3.358	3.306
8	7.98	0.654	0.644	25	25.01	2.051	2.018	42	42.02	3.448	3.393
9	9.02	0.739	0.728	26	25.96	2.129	2.094	43	42.99	3.527	3.471
10	9.99	0.819	0.806	27	26.98	2.212	2.177	44	43.97	3.608	3.549
11	11	0.902	0.887	28	27.98	2.295	2.258	45	44.97	3.69	3.631
12	11.97	0.981	0.966	29	29.02	2.38	2.342	46	45.97	3.773	3.705
13	13.01	1.067	1.05	30	30.02	2.462	2.423	47	47.02	3.859	3.796
14	13.99	1.147	1.129	31	31.01	2.542	2.503	48	48	3.939	3.874
15	15.02	1.232	1.212	32	31.96	2.621	2.579	49	49.03	4.022	3.956
16	15.96	1.308	1.288	33	32.98	2.704	2.661	50	49.99	4.103	4.036

TABLE A-1: VOLTAGE MEASUREMENT ANALYSIS DATA

9.4 PCB Revision 1 Schematics

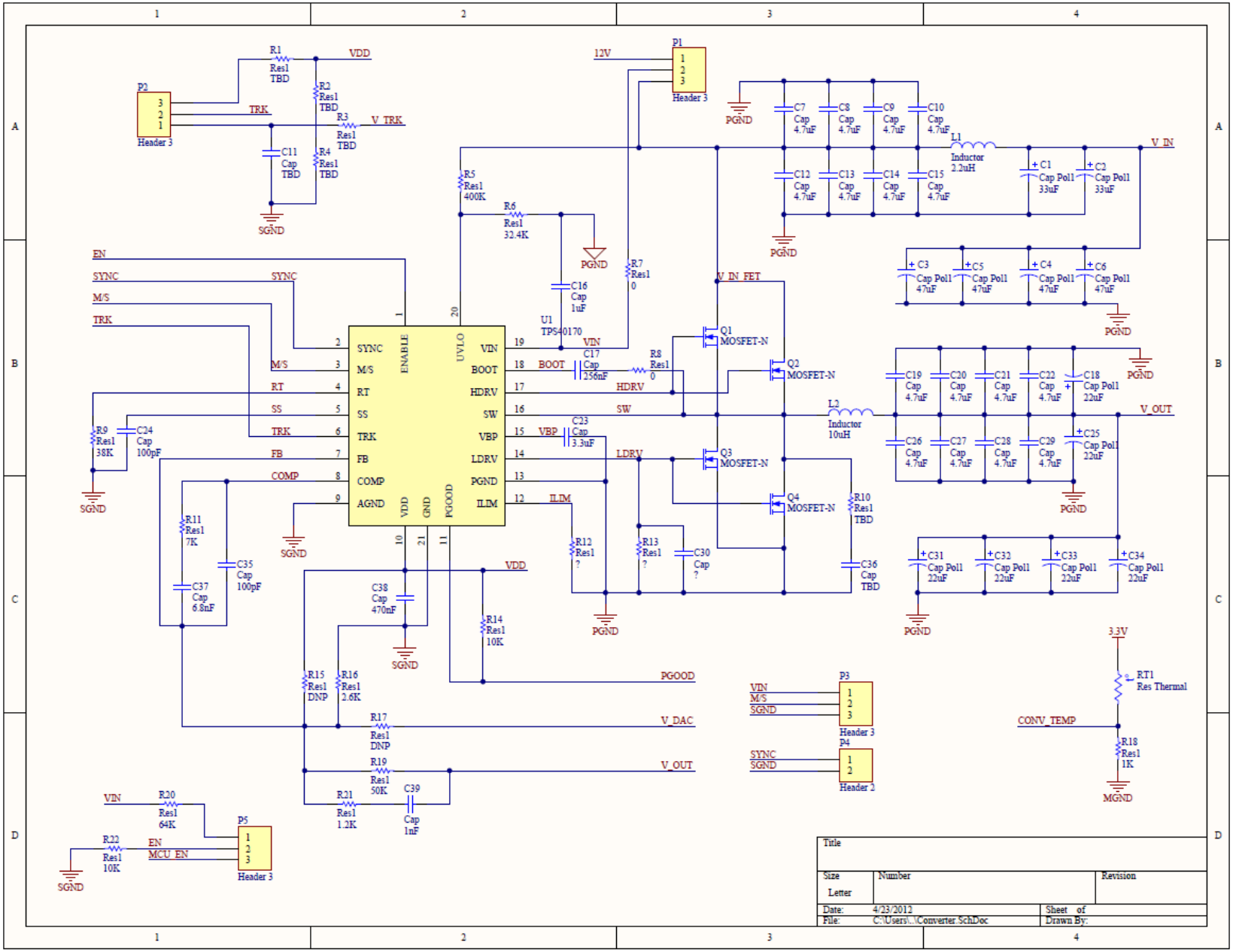

FIGURE A-8: PCB REVISION 1 CONVERTER SCHEMATIC

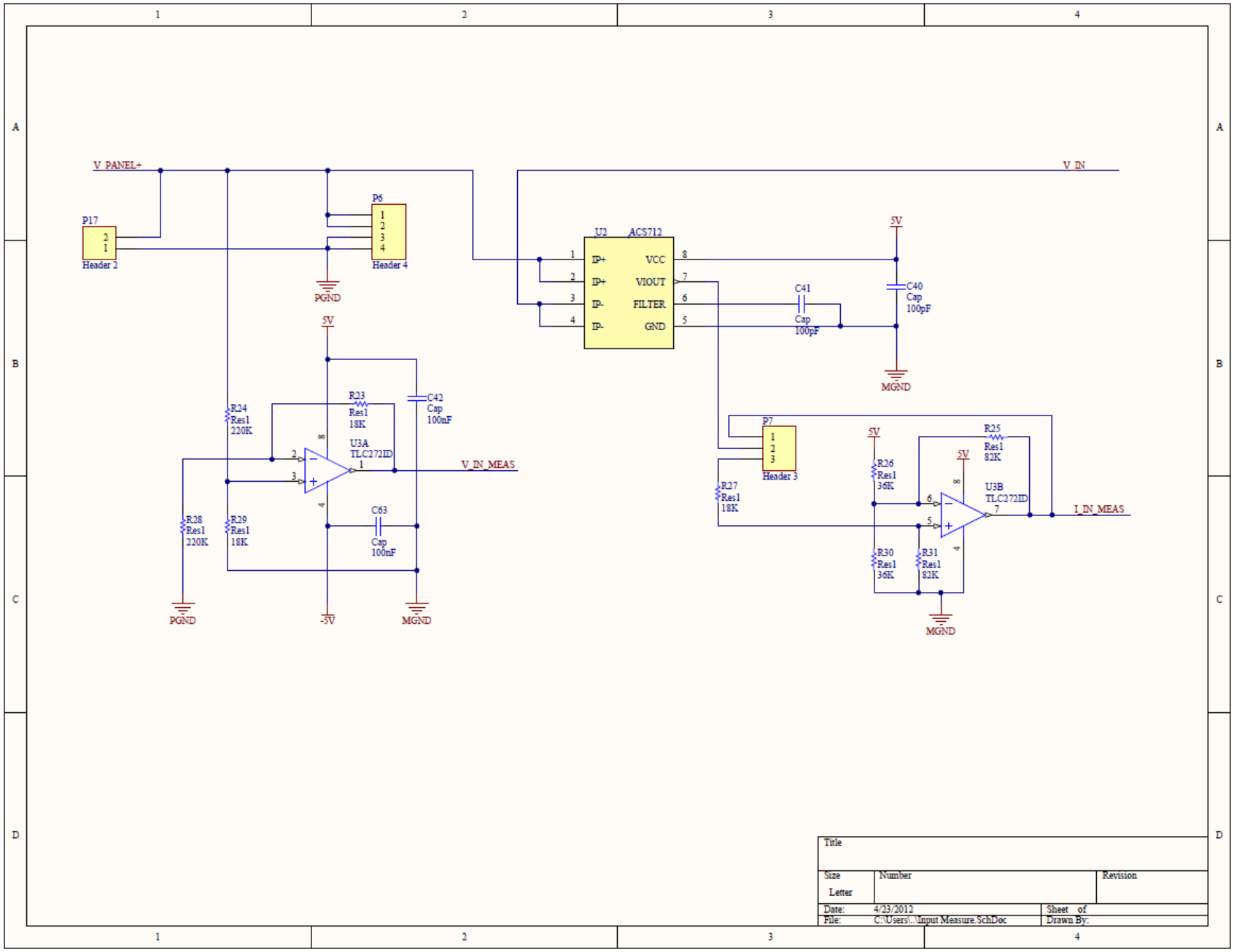

FIGURE A-9: PCB REVISION 1 INPUT MEASUREMENT SCHEMATIC

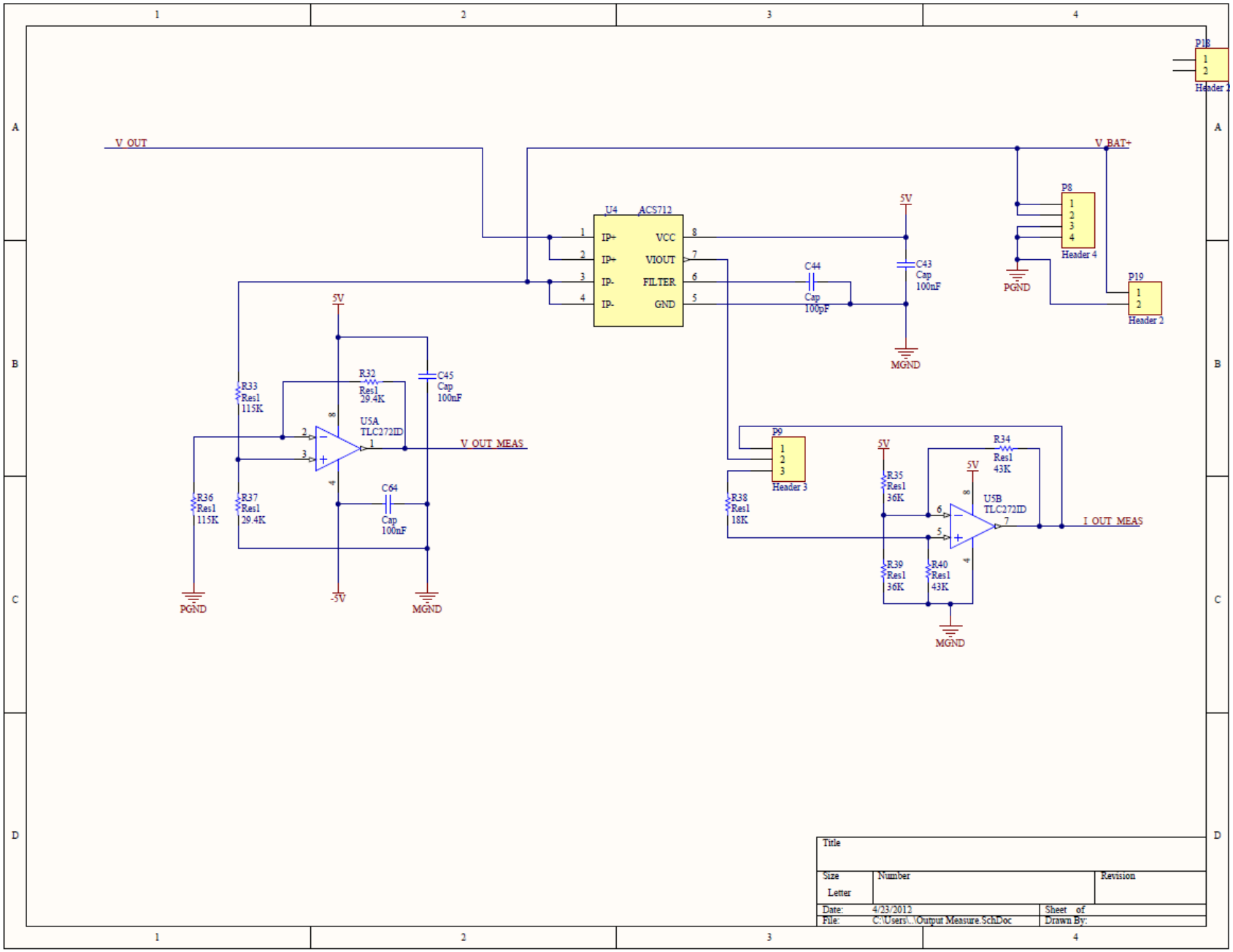

FIGURE A-10: PCB REVISION 1 OUTPUT MEASUREMENT SCHEMATIC

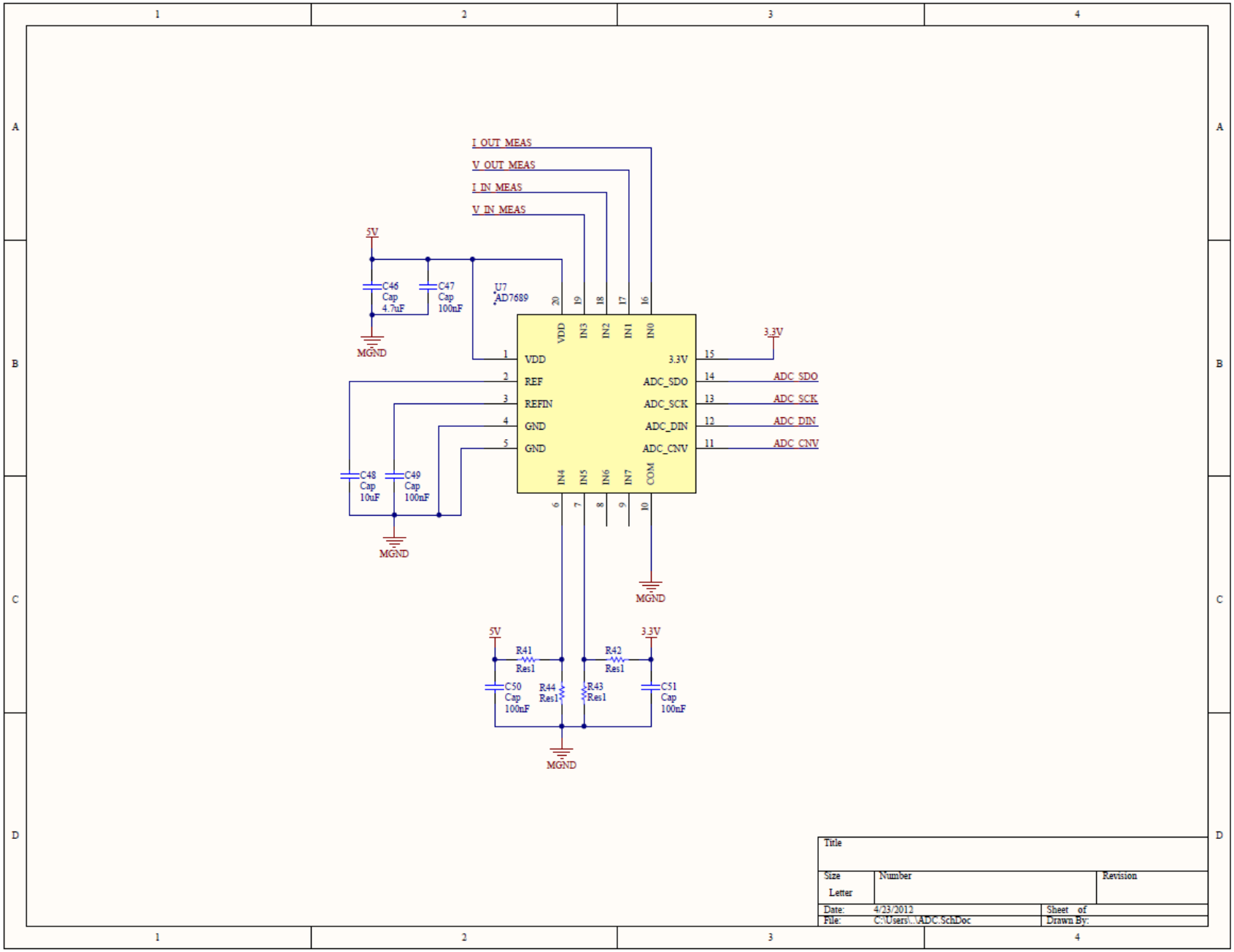

FIGURE A-11: PCB REVISION 1 ADC SCHEMATIC

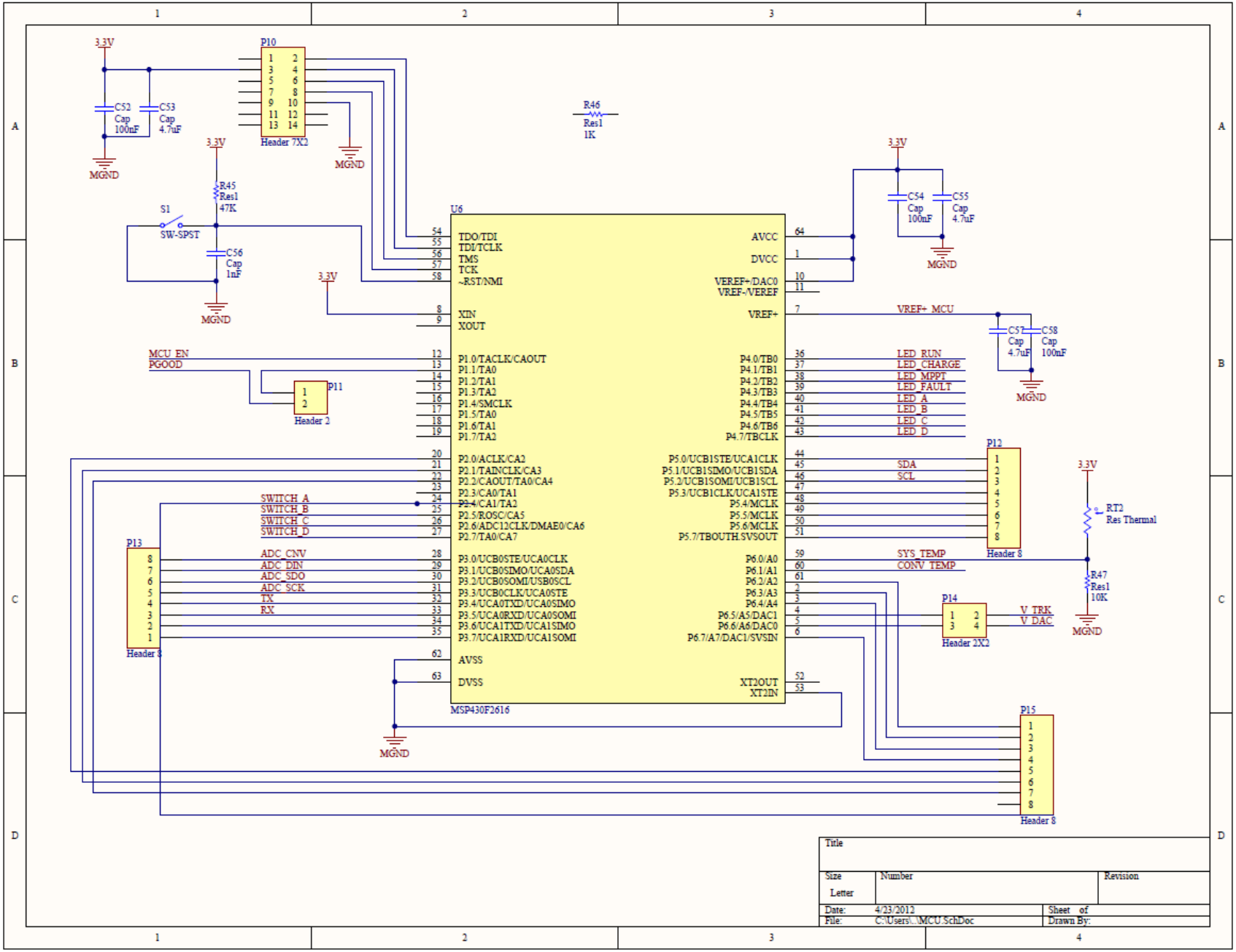

FIGURE A-12: PCB REVISION 1 MCU SCHEMATIC

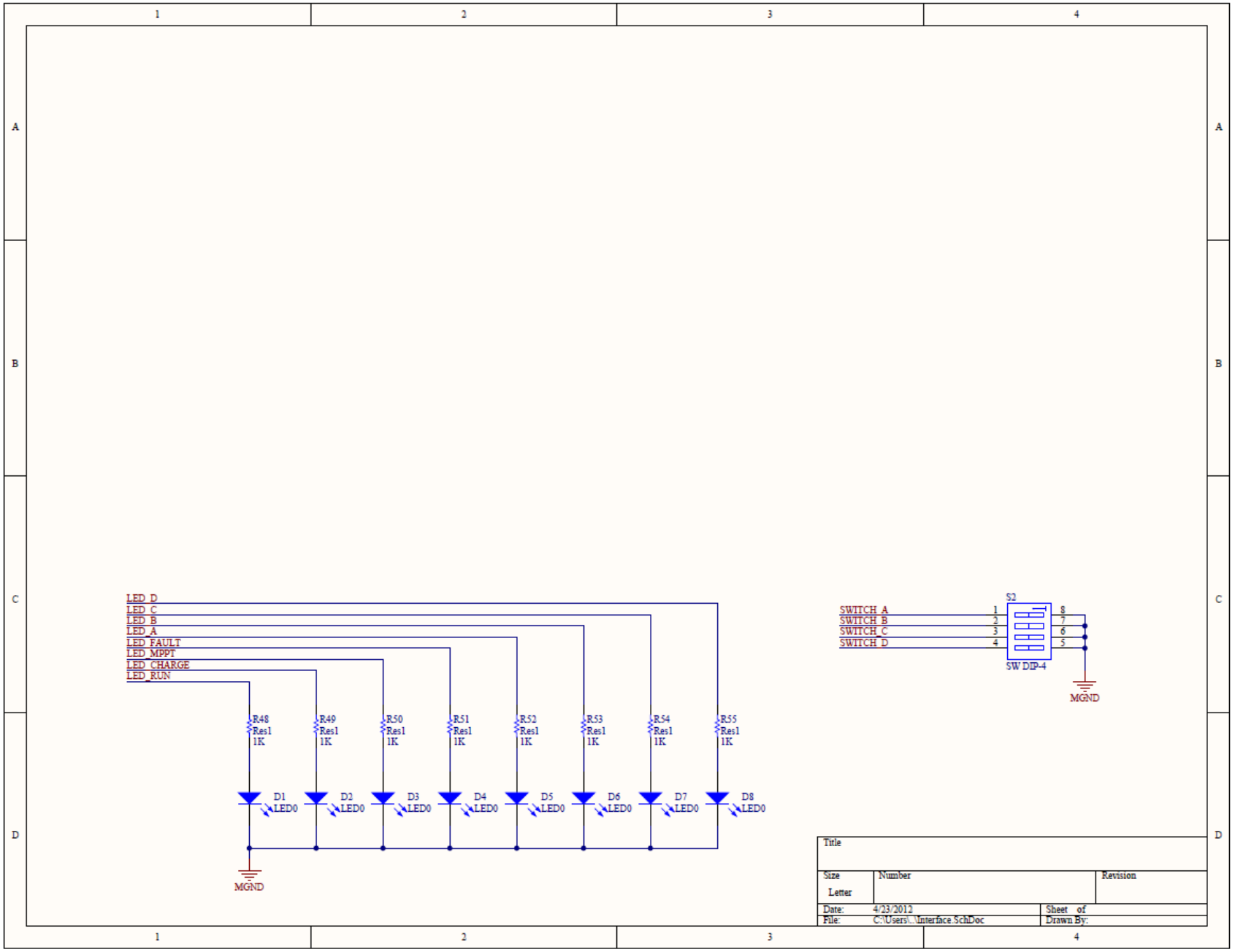

FIGURE A-13: PCB REVISION 1 BOARD INTERFACE SCHEMATIC

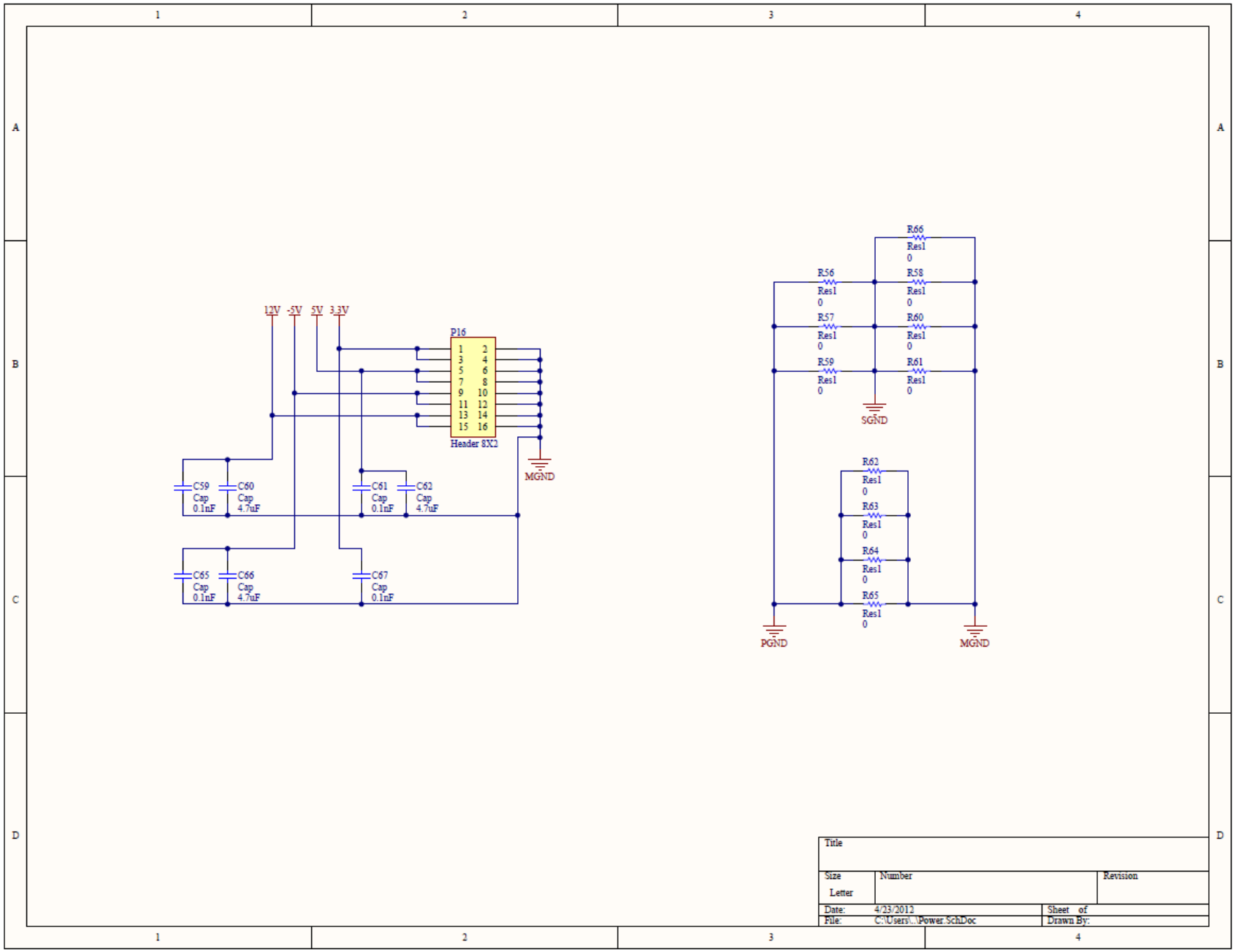

FIGURE A-14: PCB REVISION 1 OFF BOARD POWER SCHEMATIC

9.5 PCB Revision 2 Schematics

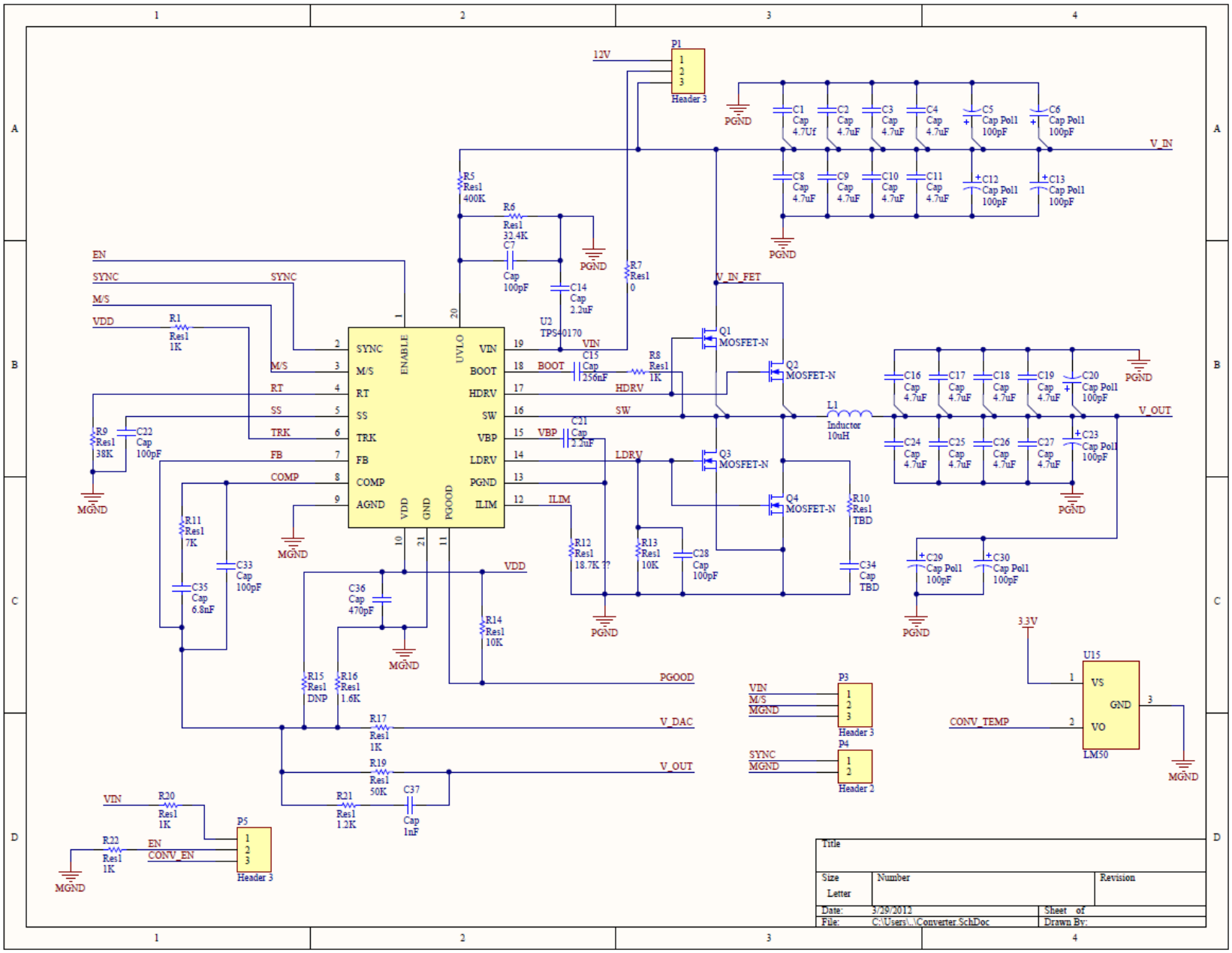

FIGURE A-15: PCB REVISION 2 CONVERTER SCHEMATIC

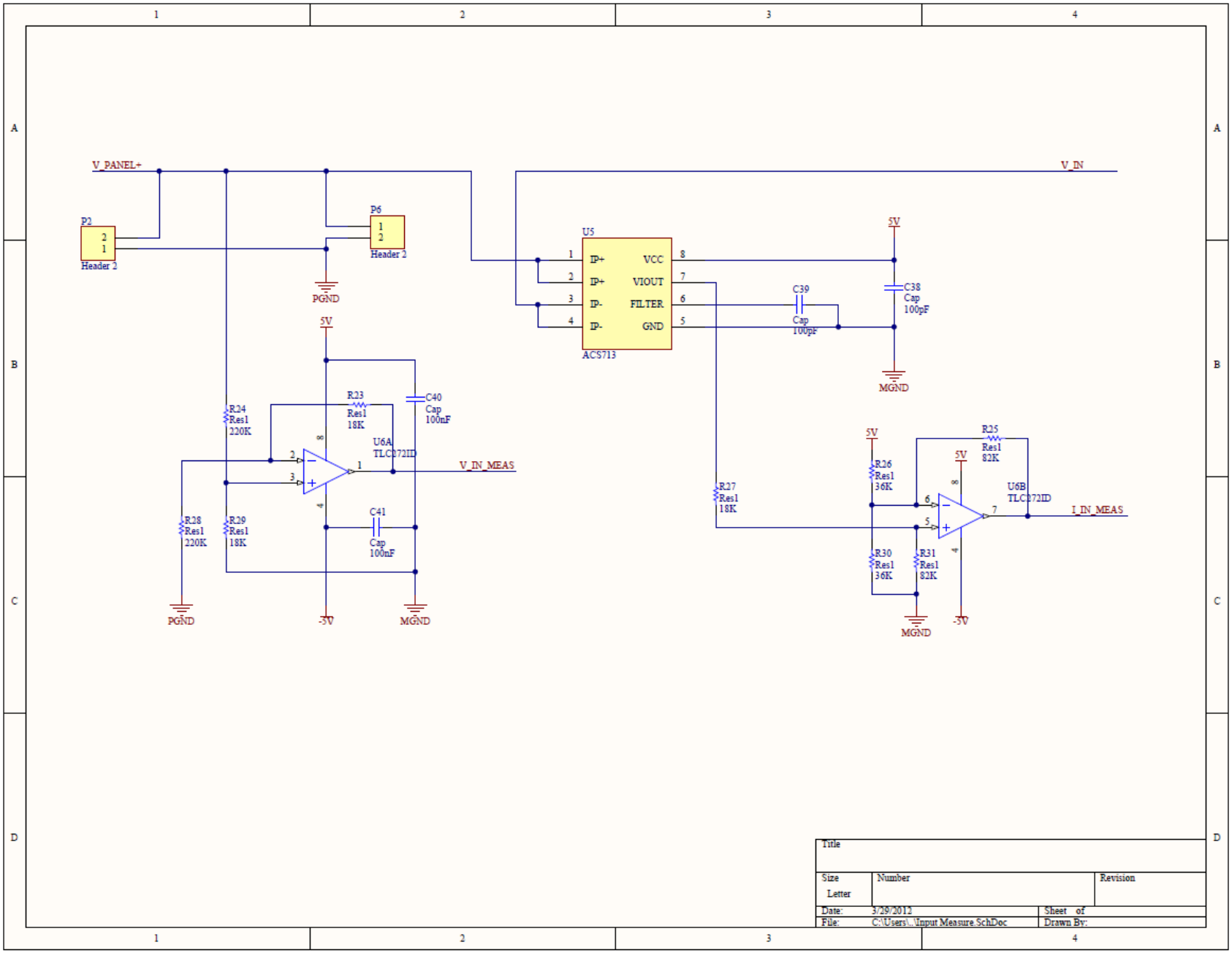

FIGURE A-16: PCB REVISION 2 INPUT MEASUREMENT SCHEMATIC

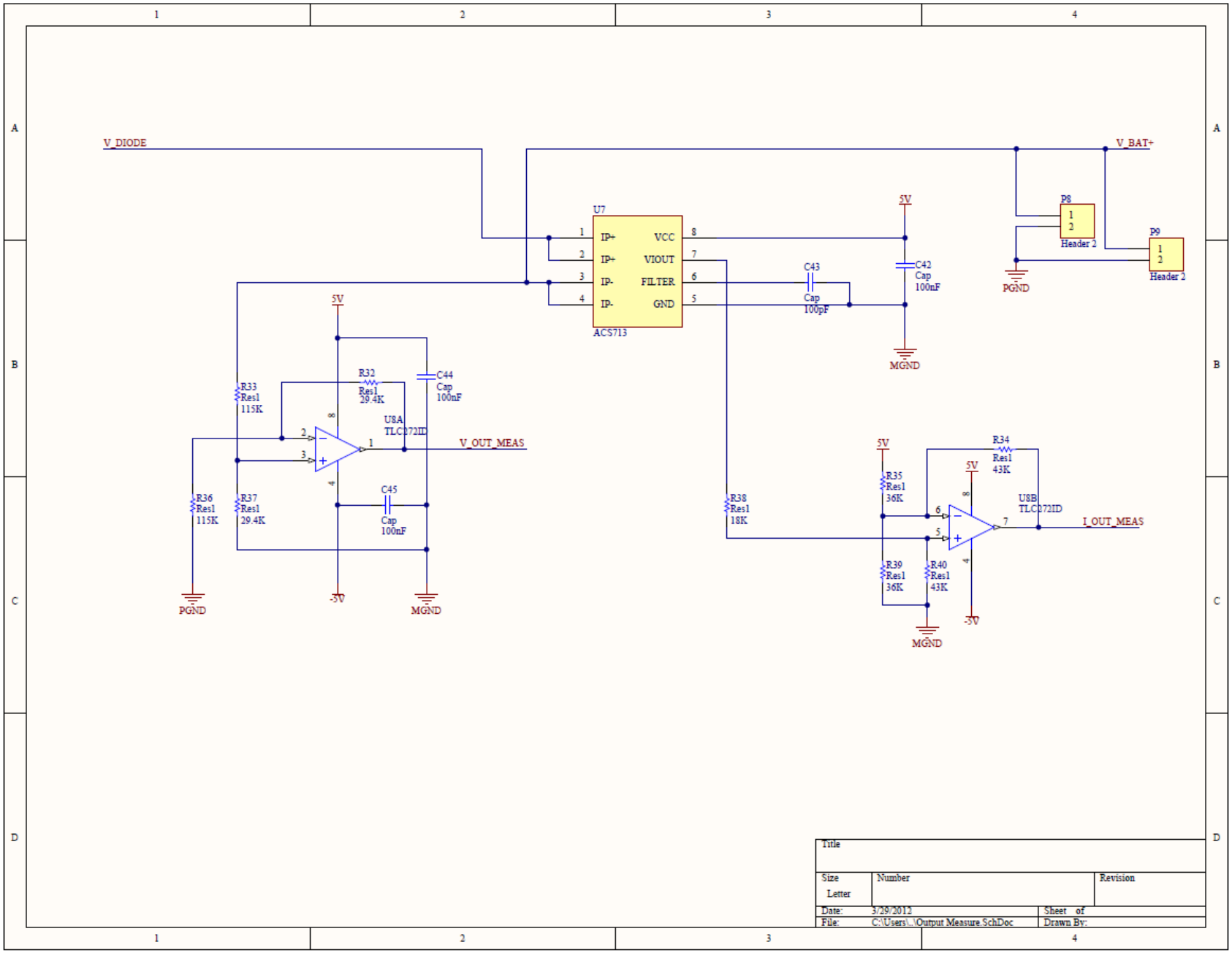

FIGURE A-17: PCB REVISION 2 OUTPUT MEASUREMENT SCHEMATIC

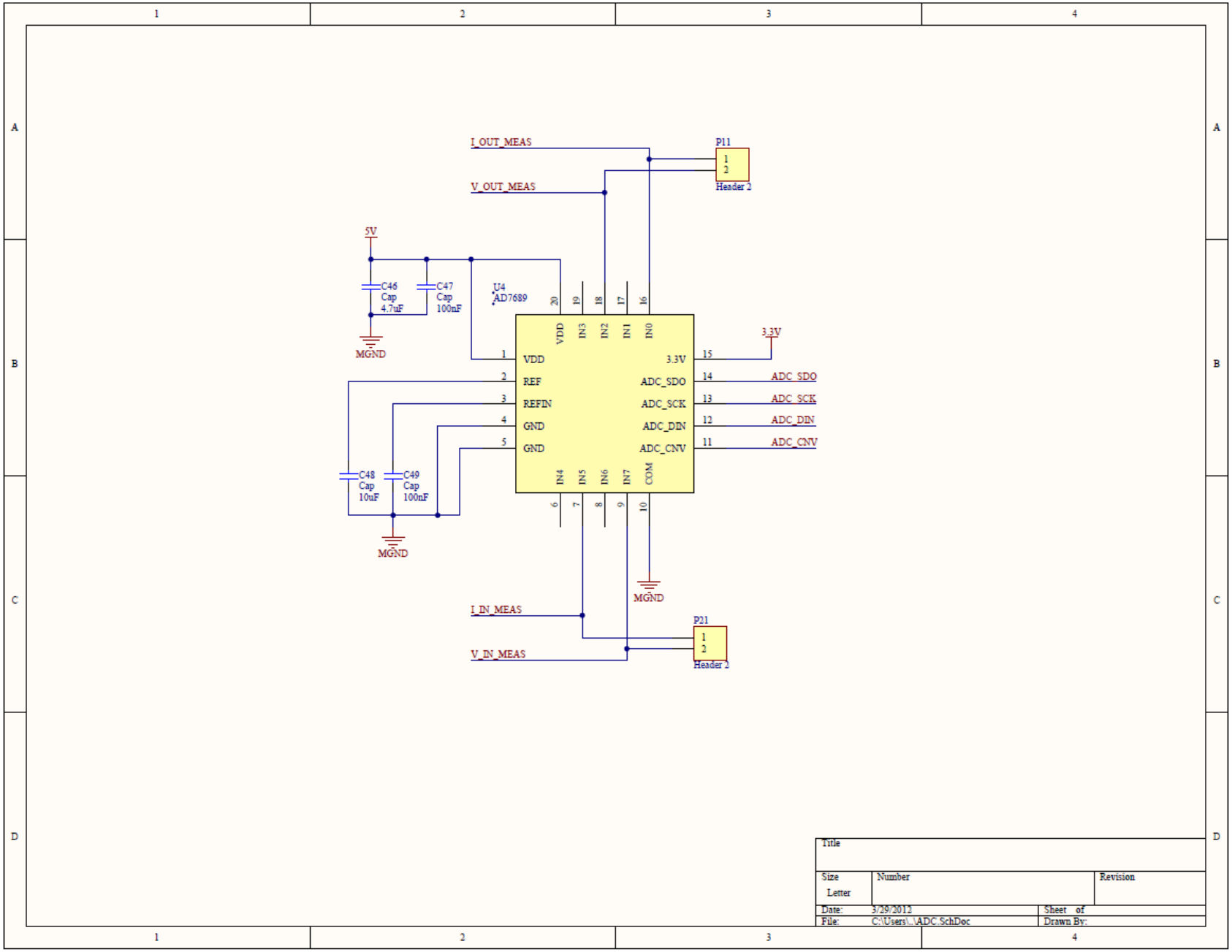

FIGURE A-18: PCB REVISION 2 ADC SCHEMATIC

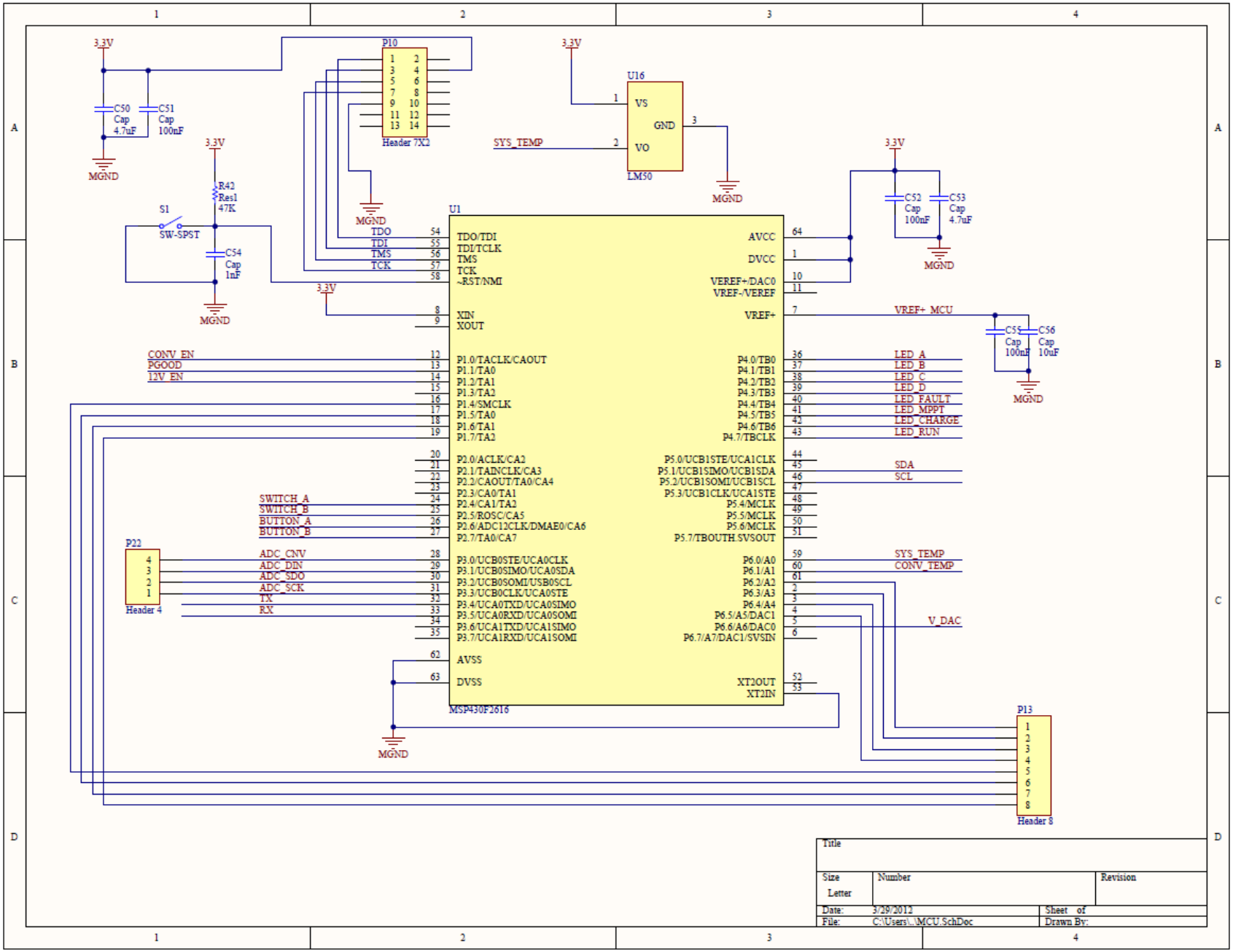

FIGURE A-19: PCB REVISION 2 MCU SCHEMATIC

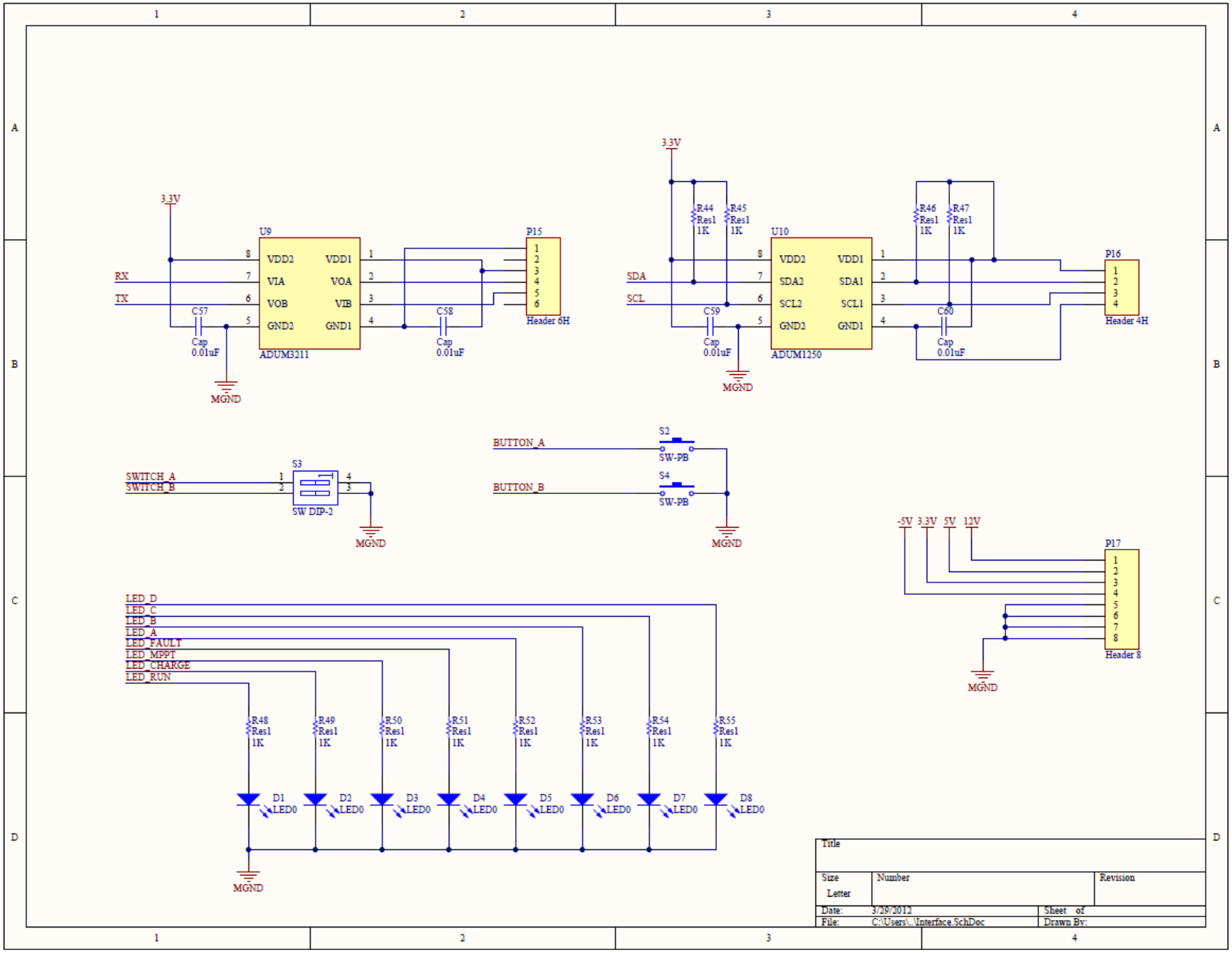

FIGURE A-20: PCB REVISION 2 BOARD INTERFACE SCHEMATIC

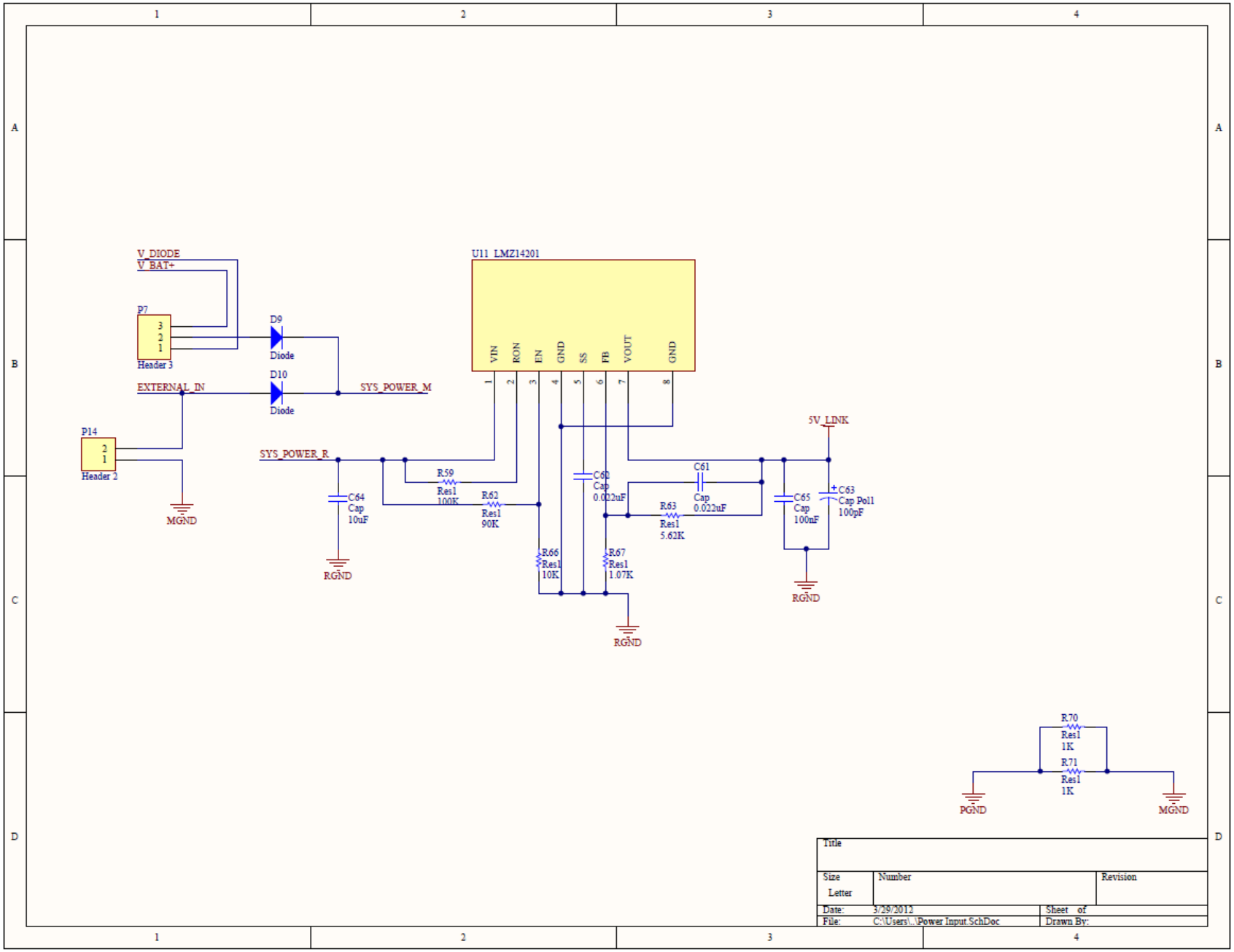

FIGURE A-21: PCB REVISION 2 BOARD POWER SCHEMATIC

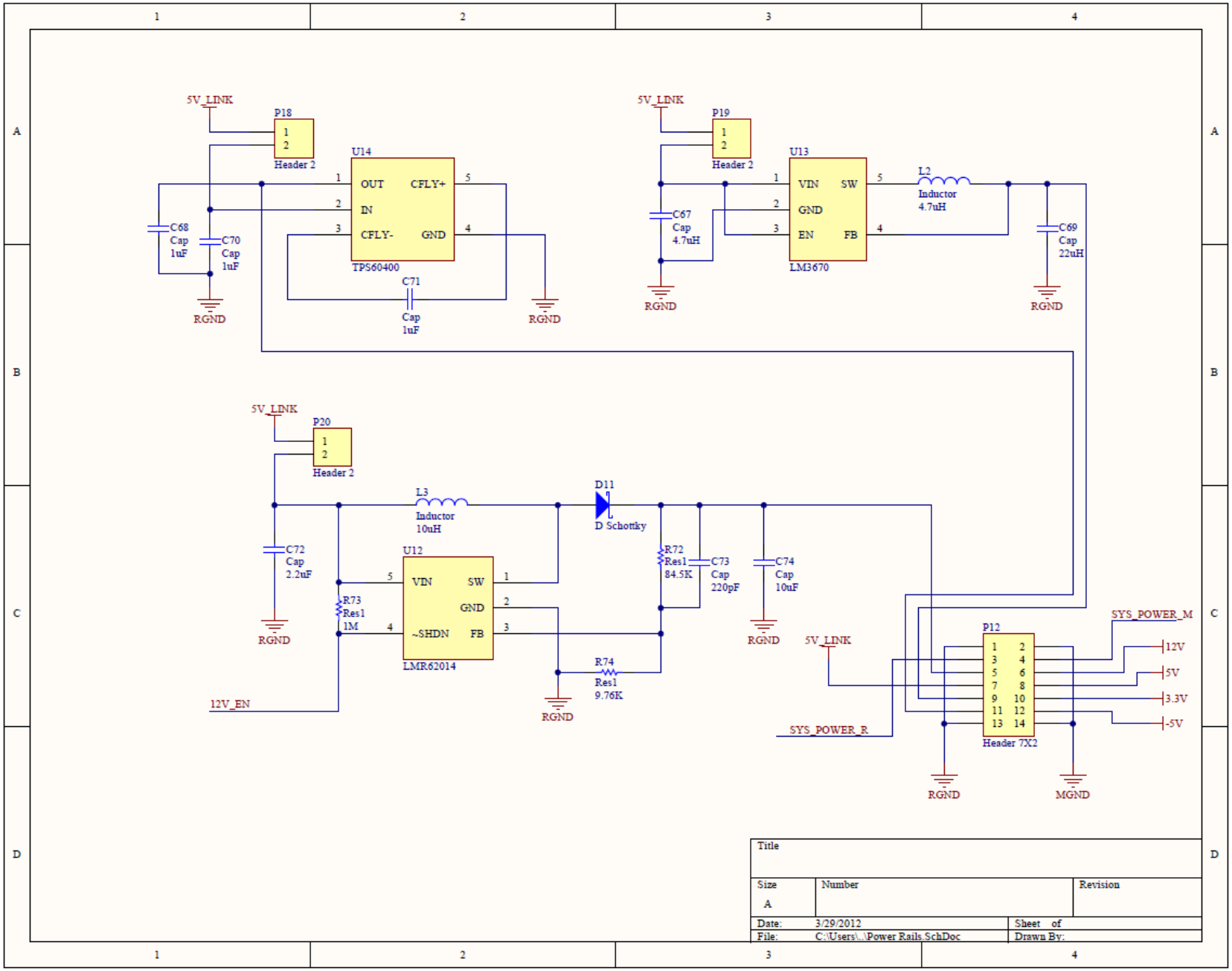

FIGURE A-22: PCB REVISION 2 SUPPLY RAILS SCHEMATIC

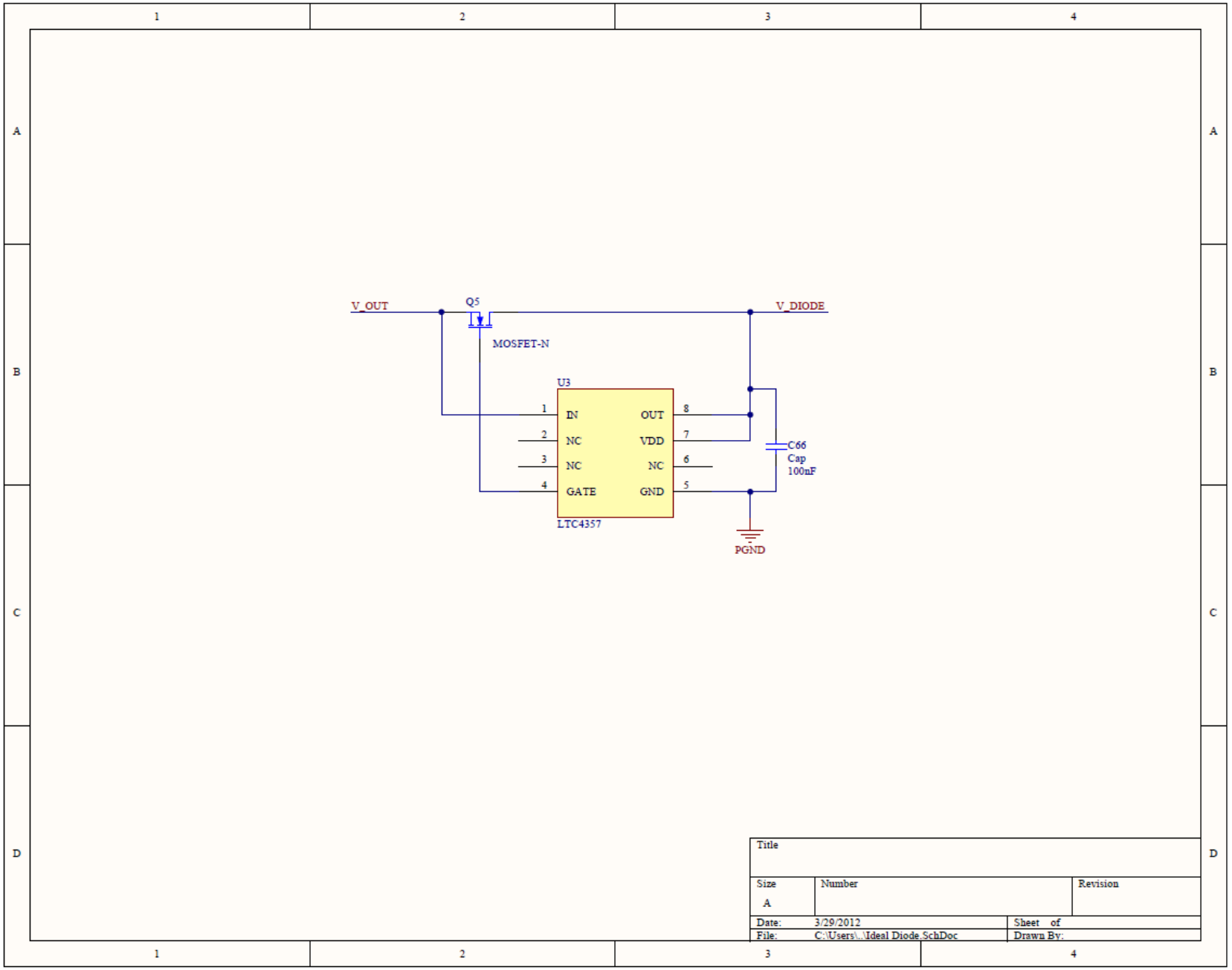

FIGURE A-23: PCB REVISION 2 IDEAL DIODE SCHEMATIC